SANDIA REPORT
SAND2019-7005
Printed Click to enter a date

Sandia National Laboratories

Assessment of the Available Drawdowns for Oil Storage Caverns at the Big Hill SPR Site – Cavern Integrity

Byoung Yoon Park

Prepared by
Sandia National Laboratories
Albuquerque, New Mexico
87185 and Livermore,
California 94550

Issued by Sandia National Laboratories, operated for the United States Department of Energy by National Technology & Engineering Solutions of Sandia, LLC.

Available to DOE and DOE contractors from
U.S. Department of Energy
Office of Scientific and Technical Information
P.O. Box 62
Oak Ridge, TN 37831

Telephone: (865) 576-8401
Facsimile: (865) 576-5728
E-Mail: reports@osti.gov
Online ordering: http://www.osti.gov/scitech

Available to the public from
U.S. Department of Commerce
National Technical Information Service
5301 Shawnee Rd
Alexandria, VA 22312

Telephone: (800) 553-6847
Facsimile: (703) 605-6900
E-Mail: orders@ntis.gov
Online order: https://classic.ntis.gov/help/order-methods/

ABSTRACT

This report updates the estimated values of the baseline available drawdowns for the caverns at the Big Hill storage facility, and an updated table listing the available drawdowns. A new finite element numerical analysis model was constructed that consists of a realistic mesh capturing the sonar-measured geometries of Big Hill SPR site and used the daily data of actual wellhead pressures and oil-brine interfaces. The number of available drawdowns for each of the Big Hill SPR caverns is estimated using the new model. All caverns are predicted to have five available drawdowns remaining from a geomechanical perspective. BC-101, 105, and 110 have a region of concern at the floor edge and/or sloping floor, where tensile and dilatant stresses are predicted to occur during each workover. The tensile state is predicted to occur because of the geometries of the edge and floor. Therefore, geomechanical examination for three caverns would be recommended after a drawdown leach. The well integrity of each cavern is not investigated in this report. The estimate of the number of baseline available drawdowns for the Big Hill caverns in this report will be incorporated in future assessments of the available drawdowns for all the SPR caverns. The estimates for the number of baseline available drawdowns are subject to change in the future as the knowledge of physical phenomena at the sites, and the further development of the models of geomechanical behavior at the sites, evolve over time.

ACKNOWLEDGMENTS

This research is funded by SPR programs administered by the Office of Fossil Energy of the U.S. Department of Energy.
The author would like to thank Steven R. Sobolik of Sandia provided technical reviews and valuable comments, and Sandia department manager Donald Conley and Sandia SPR project manager Anna C. Snider Lord who supported this work. As always, the support of Diane Willard of DOE is greatly appreciated. Paul Malphurs of DOE also is greatly appreciated, as is his comprehensive review of this report. This report has been improved by these individuals.

CONTENTS

Abstract 3
Acknowledgments 4
Contents 5
List of Figures 6
List of Tables 8
Executive Summary 9
Acronyms and Definitions 10
1. Introduction 11
2. Model Description 13
   2.1. Finite Element Model 13
   2.2. Internal Pressure Change 14
3. Salt Damage Criteria 25
4. Cavern Integrity 27
   4.1. BH-101 27
   4.2. BH-102 34
   4.3. BH-103 36
   4.4. BH-104 41
   4.5. BH-105 43
   4.6. BH-106 48
   4.7. BH-107 50
   4.8. BH-108 52
   4.9. BH-109 54
   4.10. BH-110 56
   4.11. BH-111 59
   4.12. BH-112 61
   4.13. BH-113 63
   4.14. BH-114 65
5. Conclusions - Available Drawdowns 67
References 69
Distribution 71

LIST OF FIGURES

Figure 1. Images of Big Hill salt dome and caprock obtained from the seismic, sonar and borehole survey (left), an overview of the meshes of the stratigraphy (middle), and caverns (right). The cavern ID numbers are also shown [Park, 2017a]. 13
Figure 2. Entire finite element model and boundary conditions at Big Hill. U_x=0 means no displacement in X-direction at every node [Park, 2017a]. 14
Figure 3. Field wellhead pressure histories for the seven Bayou Choctaw SPR caverns.....16
Figure 4. Individual Big Hill SPR caverns' wellhead pressure histories used in this analysis 20
Figure 5. Oil-Brine Interface depth histories to apply into the simulation for 14 Big Hill SPR caverns 24
Figure 6. BH-101 cavern cavity with five drawdown skins (leaching layers) and extra skins 27
Figure 7. Predicted maximum σ_1 (top) and minimum dilatant damage factor (bottom) in the salt surrounding BH-101 over time 28
Figure 8. Contour plots of σ_1 on 1/19/1991 and 9/18/2017 (look up view).....29
Figure 9. Contour plots of *DF* on 9/20/1991 and 9/20/2002 (look up view).....29
Figure 10. Predicted volumetric change (top), volumetric closure normalized to initial cavern volume of BH-101 (2nd), maximum σ_1 (3rd) and minimum dilatant damage factor (bottom) in the salt surrounding BH-101 over time 31
Figure 11. Contour plots of σ_1 on specific dates. Areas in tensile state are shown in red ($\sigma_1 >$ 0). Each value of maximum σ_1 are indicated by each arrow at each specific time on the 3rd panel in Figure 10 32
Figure 12. Contour plots of *DF* on specific dates. Areas in dilatant are shown in red (*DF* < 1). Each value of minimum *DF* is indicated by each arrow at each specific time on the bottom panel in Figure 10 33
Figure 13. BH-102 cavern cavity with five drawdown skins (leaching layers) and extra skins ...34
Figure 14. Predicted volumetric change (top), volumetric closure normalized to initial cavern volume of BH-102 (2nd), maximum σ_1 (3rd) and minimum dilatant damage factor (bottom) in the salt surrounding BH-102 over time 35
Figure 15. BH-103 cavern cavity with five drawdown skins (leaching layers) and extra skins ...36
Figure 16. Predicted maximum σ_1 (top) and minimum dilatant damage factor (bottom) in the salt surrounding BH-103 over time 38
Figure 17. Contour plots of σ1 on 4/20/1998, 5/22/2001, and 5/20/2016 (look up view).....38
Figure 18. Contour plots of *DF* on 5/22/2001, 6/20/2012, and 11/20/2015 (look up view) 39
Figure 19. Predicted volumetric change (top), volumetric closure normalized to initial cavern volume of BH-103 (2nd), maximum σ_1 (3rd) and minimum dilatant damage factor (bottom) in the salt surrounding BH-103 over time 40
Figure 20. BH-102 cavern cavity with five drawdown skins (leaching layers) and extra skins ...41
Figure 21. Predicted volumetric change (top), volumetric closure normalized to initial cavern volume of BH-104 (2nd), maximum σ_1 (3rd) and minimum dilatant damage factor (bottom) in the salt surrounding BH-104 over time 42
Figure 22. BH-105 cavern cavity with five drawdown skins (leaching layers) and extra skins ...43

Figure 23. Predicted volumetric change (top), volumetric closure normalized to initial cavern volume of BH-105 (2nd), maximum σ_1 (3rd) and minimum dilatant damage factor (bottom) in the salt surrounding BH-105 over time 45
Figure 24. Contour plots of σ_1 on specific dates. Areas in tensile state are shown in red ($\sigma_1 >$ 0). Each value of maximum σ_1 are indicated by each arrow at each specific time on the 3rd panel in Figure 23Figure 10.....46
Figure 25. Contour plots of *DF* on specific dates. Areas in dilatant are shown in red (*DF* < 1). Each value of minimum *DF* is indicated by each arrow at each specific time on the bottom panel in Figure 23 47
Figure 26. BH-106 cavern cavity with five drawdown skins (leaching layers) and extra skins ...48
Figure 27. Predicted volumetric change (top), volumetric closure normalized to initial cavern volume of BH-106 (2nd), maximum σ_1 (3rd) and minimum dilatant damage factor (bottom) in the salt surrounding BH-106 over time 49
Figure 28. BH-107 cavern cavity with five drawdown skins (leaching layers) and extra skins ...50
Figure 29. Predicted volumetric change (top), volumetric closure normalized to initial cavern volume of BH-107 (2nd), maximum σ_1 (3rd) and minimum dilatant damage factor (bottom) in the salt surrounding BH-107 over time 51
Figure 30. BH-108 cavern cavity with five drawdown skins (leaching layers) and extra skins ...52
Figure 31. Predicted volumetric change (top), volumetric closure normalized to initial cavern volume of BH-108 (2nd), maximum σ_1 (3rd) and minimum dilatant damage factor (bottom) in the salt surrounding BH-108 over time 53
Figure 32. BH-109 cavern cavity with five drawdown skins (leaching layers) and extra skins ...54
Figure 33. Predicted volumetric change (top), volumetric closure normalized to initial cavern volume of BH-109 (2nd), maximum σ_1 (3rd) and minimum dilatant damage factor (bottom) in the salt surrounding BH-109 over time 55
Figure 34. BH-110 cavern cavity with five drawdown skins (leaching layers) and extra skins ...56
Figure 35. Predicted volumetric change (top), volumetric closure normalized to initial cavern volume of BH-110 (2nd), maximum σ_1 (3rd) and minimum dilatant damage factor (bottom) in the salt surrounding BH-110 over time 57
Figure 36. Contour plots of σ_1 on specific dates. Areas in tensile state are shown in red ($\sigma_1 >$ 0). Each value of maximum σ_1 are indicated by each arrow at each specific time on the 3rd panel in Figure 35Figure 10.....58
Figure 37. BH-111 cavern cavity with five drawdown skins (leaching layers) and extra skins ...59
Figure 38. Predicted volumetric change (top), volumetric closure normalized to initial cavern volume of BH-111 (2nd), maximum σ_1 (3rd) and minimum dilatant damage factor (bottom) in the salt surrounding BH-111 over time 60
Figure 39. BH-112 cavern cavity with five drawdown skins (leaching layers) and extra skins ...61
Figure 40. Predicted volumetric change (top), volumetric closure normalized to initial cavern volume of BH-112 (2nd), maximum σ_1 (3rd) and minimum dilatant damage factor (bottom) in the salt surrounding BH-112 over time 62
Figure 41. BH-113 cavern cavity with five drawdown skins (leaching layers) and extra skins ...63
Figure 42. Predicted volumetric change (top), volumetric closure normalized to initial cavern volume of BH-113 (2nd), maximum σ_1 (3rd) and minimum dilatant damage factor (bottom) in the salt surrounding BH-113 over time 64
Figure 43. BH-114 cavern cavity with five drawdown skins (leaching layers) and extra skins ...65

Figure 44. Predicted volumetric change (top), volumetric closure normalized to initial cavern volume of BH-114 (2nd), maximum σ_1 (3rd) and minimum dilatant damage factor (bottom) in the salt surrounding BH-114 over time 66

LIST OF TABLES

Table 1. Dates of initial leach completion, wellhead pressure recording started, and assumed initial leach started 16
Table 2. 2019 Updated number of available drawdowns – Big Hill 67

EXECUTIVE SUMMARY

This report updates the estimated values of available drawdowns for the caverns at the Big Hill storage facility, and an updated table listing the available drawdowns. This report follows up the comprehensive SAND report [Sobolik et al. 2018] that gave greater detail to the decisions behind the estimates for the Strategic Petroleum Reserve (SPR) caverns.

The estimates for the baseline available drawdowns for each of the Big Hill caverns have been updated based on the recently upgraded Big Hill geomechanical model [Park, 2017a]. The new estimates for Big Hill are summarized in the following table:

Cavern	Basis in 2014				Updated Geomechanics in 2019	Remarks
	2D P/D < 1	3D P/D < 1	Geomechanics	Best Estimate		
BH-101	3	3	5	3	5	Re-examine after a drawdown
BH-102	4	4	5	4	5	
BH-103	2	4	5	4	5	
BH-104	3	3	5	3	5	
BH-105	4	4	5	4	5	Re-examine after a drawdown
BH-106	4	4	5	4	5	
BH-107	3	4	5	4	5	
BH-108	2	5	5	5	5	
BH-109	4	5	5	5	5	
BH-110	4	5	5	5	5	Re-examine after a drawdown
BH-111	3	4	5	4	5	
BH-112	3	3	5	3	5	
BH-113	3	3	5	3	5	
BH-114	3	5	5	5	5	

BC-101, 105, and 110 have a region of concern at the floor edge and/or on the sloping floor, where tensile and dilatant stresses are predicted to occur during each workover. The tensile state is predicted to occur because of the geometries of the edge and floor. Therefore, geomechanical examination for three caverns would be recommended after a drawdown leach.

The well integrity of each cavern is not investigated in this report. The structural integrity of caverns is examined at this time. The estimate of the number of baseline available drawdowns for the Big Hill caverns in this report will be incorporated in future assessments of the available drawdowns for all the SPR caverns. The estimates for the number of baseline available drawdowns are subject to change in the future as the knowledge of physical phenomena at the sites, and the further development of the models of geomechanical behavior at the sites, evolve over time.

ACRONYMS AND DEFINITIONS

Abbreviation	Definition
3D	Three-Dimensional
2D	Two-Dimensional
BH	Big Hill
DF	Dilatant damage factor
DOE	U.S. Department of Energy
ECP	Engineering Change Process
E-W	East-West
FE	Finite Element
FFPO	Fluor Federal Petroleum Operations
ID	Identification
MMB	Million Barrels
N-S	North-South
OBI	Oil-Brine Interface
P/D	Pillar to Diameter
Sandia	Sandia National Laboratories
SPR	Strategic Petroleum Reserve

1. INTRODUCTION

This report updates the estimated values of available drawdowns for the caverns at the Big Hill (BH) storage facility, and an updated table listing the available drawdowns. This report follows up the comprehensive SAND report [Sobolik et al. 2018] that gave greater detail to the decisions behind the estimates for the Strategic Petroleum Reserve (SPR) caverns.

A consensus has now been built regarding the assessment of drawdown capabilities and risks for the SPR caverns. This work began in 2014, when the SPR issued an Engineering Change Process (ECP), PM-00449, Baseline Remaining Drawdowns for all SPR Caverns. It described creating a technical baseline for all available drawdowns for each cavern considering P/D ratios and other factors. These meetings led to the establishment of baseline values for available drawdowns for each cavern [Sobolik et al., 2014; Sobolik 2016]. Then in September 2017, Sandia National Laboratories (Sandia) was directed to update these reports annually to include a process to track the evolution of drawdown capacity for each cavern as operations are performed on them. This request was in response to legislation in 2015 directing the sale of SPR oil through the year 2025, to reduce the stored oil inventory at SPR from approximately 700 million barrels (MMB) to approximately 500 MMB. As a result, meetings were held between Sandia, DOE/SPR, the Fluor Federal Petroleum Operations (FFPO; the SPR M&O contractor), to define the process that will be used to track volume changes and their impact on drawdown capacity [Sobolik et al. 2018].

The 2D and 3D P/D ratios for each of the Big Hill caverns are described in detail in Rudeen and Lord [2013]. Computational results from Park and Ehgartner [2011] were used to determine the geomechanical drawdown limits. No Big Hill caverns are currently predicted to exhibit a 2D P/D < 1.0 on the first raw water drawdown. The 14 SPR caverns at this site are predicted to be structurally stable well beyond the 5th drawdown leach [Park and Ehgartner, 2011]. However, the caverns in the numerical model for Big Hill were simplified to cylindrical shapes. As a result, the 3D P/D-developed limits have been used to provide the best estimate assessment of the drawdown capacity for these caverns. A new finite element numerical analysis model is being constructed that consists of a realistic mesh capturing the sonar-measured geometries of Big Hill SPR site and using the daily data of actual wellhead pressures and oil-brine interfaces [Park, 2017a]. The number of available drawdowns for each of the Big Hill SPR caverns is estimated using the new model.

The well integrity of each cavern is not investigated in this report. The structural integrity of caverns is examined at this time. The estimate of the number of baseline available drawdowns for the Big Hill caverns in this report will be incorporated in future assessments of the available drawdowns for all the SPR caverns. The estimates for the number of baseline available drawdowns are subject to change in the future as the knowledge of physical phenomena at the sites, and the further development of the models of geomechanical behavior at the sites, evolve over time.

This page left blank

2. MODEL DESCRIPTION

2.1. Finite Element Model

A three-dimensional finite element (FE) model capturing realistic geometries of BH site has been constructed using sonar and seismic survey data obtained from field investigations [Park, 2017a]. The model contains the interbed between the caprock and salt top; and the interface between the dome and surrounding in situ rock to examine the interbed behavior in the most realistic manner available. Figure 3 shows an overview of the hexahedral finite element mesh of the stratigraphy and cavern field at BH. The element blocks in Figure 3 are combined into single FE mesh as shown Figure 4, which includes the boundary conditions for numerical analysis. The salt dome is modeled as being subject to a uniform regional far-field stress state acting from an infinite distance away. The surrounding rock block encircles the caprock and salt dome blocks. The lengths of the model's boundaries are 14,600 ft (more than two times the dome's minor diameter) in the N-S direction and 12,400 ft (more than two times the dome's major diameter) in the E-W direction. The sizes of the caverns are much smaller than the dome size. Therefore, the model boundary distances (surrounding rock) are enough to be regarded as being at infinite distance away from the caverns (i.e. fixed boundaries are applied).

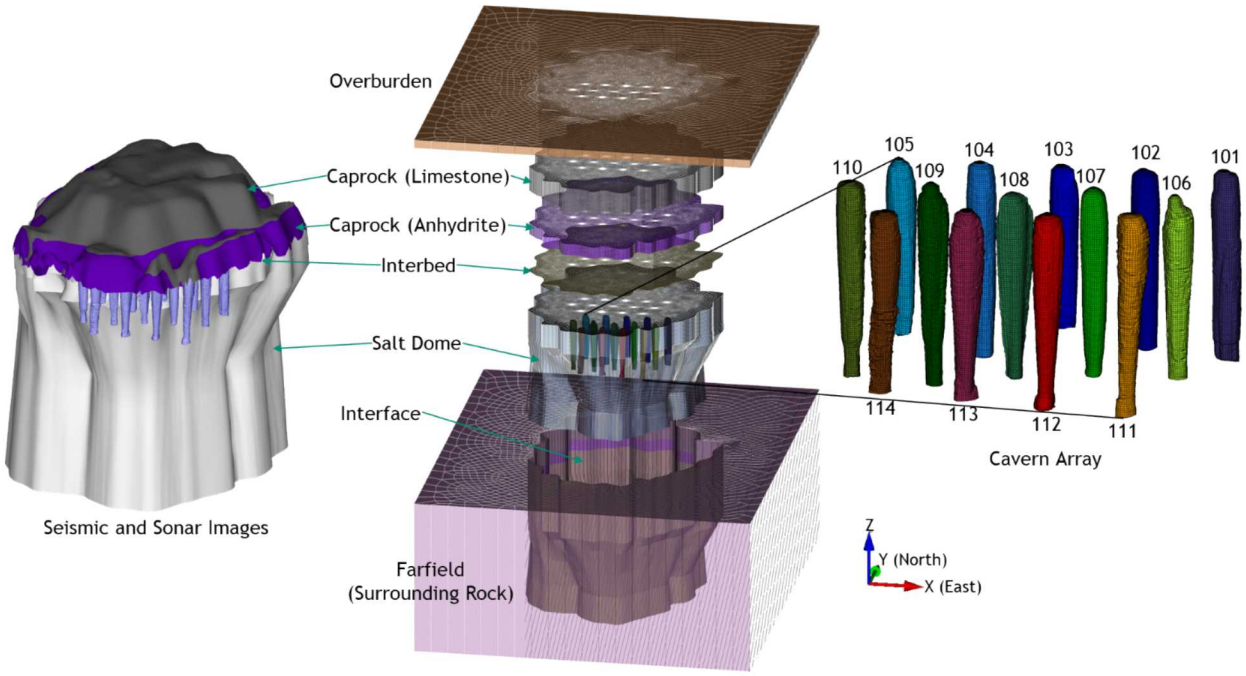

Figure 1. Images of Big Hill salt dome and caprock obtained from the seismic, sonar and borehole survey (left), an overview of the meshes of the stratigraphy (middle), and caverns (right). The cavern ID numbers are also shown [Park, 2017a].

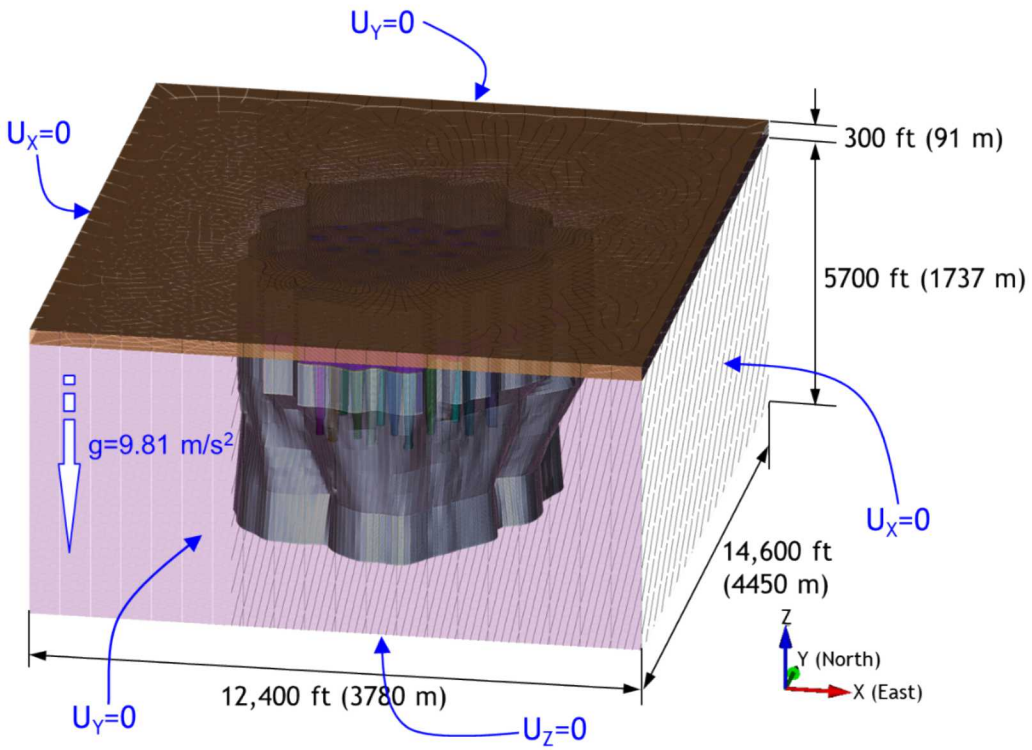

Figure 2. Entire finite element model and boundary conditions at Big Hill. U_x=0 means no displacement in X-direction at every node [Park, 2017a].

2.2. Internal Pressure Change

The modeling simulates the cavern responses forward in time from the initial cavern creation. The actual wellhead pressure histories of BH-101 through BH-114 have been recorded since the dates in Table 1 as shown Figure 3. They are recorded at the oil-side wellhead, i.e. oil-side wellhead pressure. Pressure drops occurred during workovers and fluid transfers. For the purposes of the present simulation, it is assumed that the initial leaches of the caverns started on the dates one year before the wellhead pressure recording started, i.e. they were leached to full size over a one-year period. For example, the wellhead pressure of BH-101 was recorded from 9/19/1990, so it is assumed that the initial leach of BH-101 started on 9/19/1989 with one year leaching period.

Figure 4 shows the wellhead histories, which consist of the actual (4/20/1990 - 9/18/2017) and the assumed future (9/19/2017 - 9/18/2047) pressure records used for 14 SPR caverns in the simulation. The previous approximately two-year (2/3/2007 - 2/12/2009) wellhead pressure history of each cavern as shown in Figure 3 is selected for the assumed future wellhead pressure replication. The selected period, during which no drawdowns take place, contains the typical normal operation histories. These histories are replicated one and half times for the next five-years (9/19/2017 - 9/18/2022). This five-year histories are replicated for the next five-year drawdown cycles thereafter (9/19/2022 - 9/18/2047). The first drawdown leach is assumed to

start at 9/19/2022. Note that the 1st, 2nd, etc., in the plots indicate the drawdown leach start dates (9/19/2022, 9/19/2027, 9/19/2032, 9/19/2037, and 9/19/2042, respectively).

In general, the SPR caverns are most susceptible to structural instability when a workover is in progress. In this analysis, the workover is simulated by means of an internal pressure change in the SPR caverns. Modeling of the workover processes is used to investigate the structural stability of the caverns. For simulation purposes, the pressure drop to zero psi for each cavern lasts for three months, or 5 percent of time during a 5-year period. The duration of the workover may be slightly longer than is historically encountered in the field, but is chosen to provide an adverse condition and closely simulate actual subsidence measurements [Park et al. 2005].

Rather than complicating the analyses, the following assumptions are made:

- The replicated five-year histories (7/18/2017 - 7/17/2047) are applied for the majority of the time, with pressure drops periodically included.
- For workover conditions, zero wellhead pressure is used.
- Not all caverns are in workover mode at the same time.
- BH-101 is the first cavern in the workover which starts on 1/1/2019 and lasts for three months.
- After that, workovers are performed on BH-102, BH-103 …, and BH-114 in order with three months duration as shown Figure 4.
- These workover cycles are repeated every 5 years to meet the drawdown cycles.
- The pressure due to the oil and brine in the cavern plus the wellhead is applied on the cavern inside boundary.

Before a cavern's initial leach starts, the model has a stabilization period (1/1/1900 - 4/20/1989). To avoid the numerical shock, gravity is applied gradually into the mesh for ten seconds. After that, the model is allowed to consolidate with gravity for approximately 89 years so that every element is stabilized numerically.

The analysis simulates caverns that were leached to full size over a one-year period by means of gradually switching from salt to fresh water in the caverns. Creep is permitted to occur over the entire simulation period (1/1/1900 - 9/18/2047). On 9/19/2022 and subsequently every 5 years thereafter, the SPR caverns are instantaneously leached to produce an increased volume of 15% during each leach cycle to simulate drawdowns. Modeling of the leaching process in the caverns was accomplished by deleting elements along the walls of the caverns so that the volume increased by 15% with each leach. Leaching is assumed to occur uniformly along the entire height of the cavern. However, loss of salt due to leaching in the floor or roof of the caverns is not simulated in the model. The 5-year period between each drawdown allows the stress state in the salt to return to a steady-state condition, as will be evidenced in the predicted closure rates. The simulation was run out to 9/18/2047 to investigate the structural behavior of the dome for approximately 57 years, as the process of salt creep continues to reduce the caverns' volume.

In actuality, the caverns were not always fully filled with just oil. Brine fills the bottom of the caverns, and the proportion changes with time depending on cavern operations. The difference between pressure gradients of oil (0.37 psi/ft of depth) and brine (0.52 psi/ft of depth) cannot be ignored [Park, 2017a]. So, the amount of oil and brine in a cavern over time needs to be considered. Figure 5 shows the oil-brine interface (OBI) depth history of SPR caverns used in

this analysis. The history data (1/1/1990 – 9/18/2017) were obtained from the BC field office. The previous approximately two-year (2/3/2007 - 2/12/2009), which is the same period as the wellhead history replication period for the normal operation, OBI history of each cavern is selected for the assumed future OBI replication for the rest of the simulation.

Table 1. Dates of initial leach completion, wellhead pressure recording started, and assumed initial leach started

Cavern ID	Date of Initial Leach Completion	Date of Wellhead Pressure Recording Started	Assumed Date Initial Leach Started
BH-101	09/17/1990	09/19/1990	09/19/1989
BH-102	10/19/1990	10/20/1990	10/20/1989
BH-103	11/27/1990	11/29/1990	11/29/1989
BH-104	10/21/1990	10/21/1990	10/21/1989
BH-105	05/13/1990	05/14/1990	05/14/1989
BH-106	10/15/1990	10/17/1990	10/17/1989
BH-107	04/23/1990	04/25/1990	04/25/1989
BH-108	06/13/1990	06/14/1990	06/14/1989
BH-109	07/23/1990	07/25/1990	07/25/1989
BH-110	04/18/1990	04/20/1990	04/20/1989
BH-111	07/14/1991	07/15/1991	07/15/1990
BH-112	06/17/1991	06/19/1991	06/19/1990
BH-113	04/30/1991	05/02/1991	05/02/1990
BH-114	08/26/1991	08/29/1991	08/29/1990

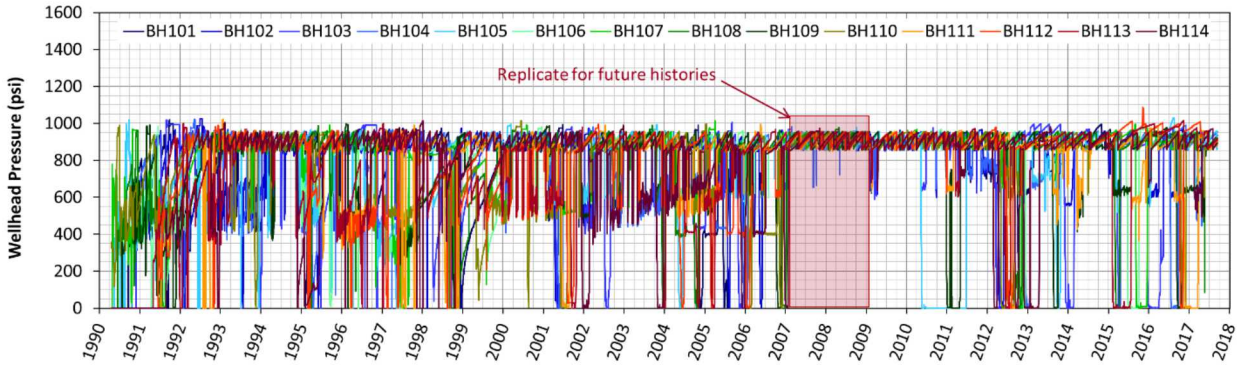

Figure 3. Field wellhead pressure histories for the seven Bayou Choctaw SPR caverns

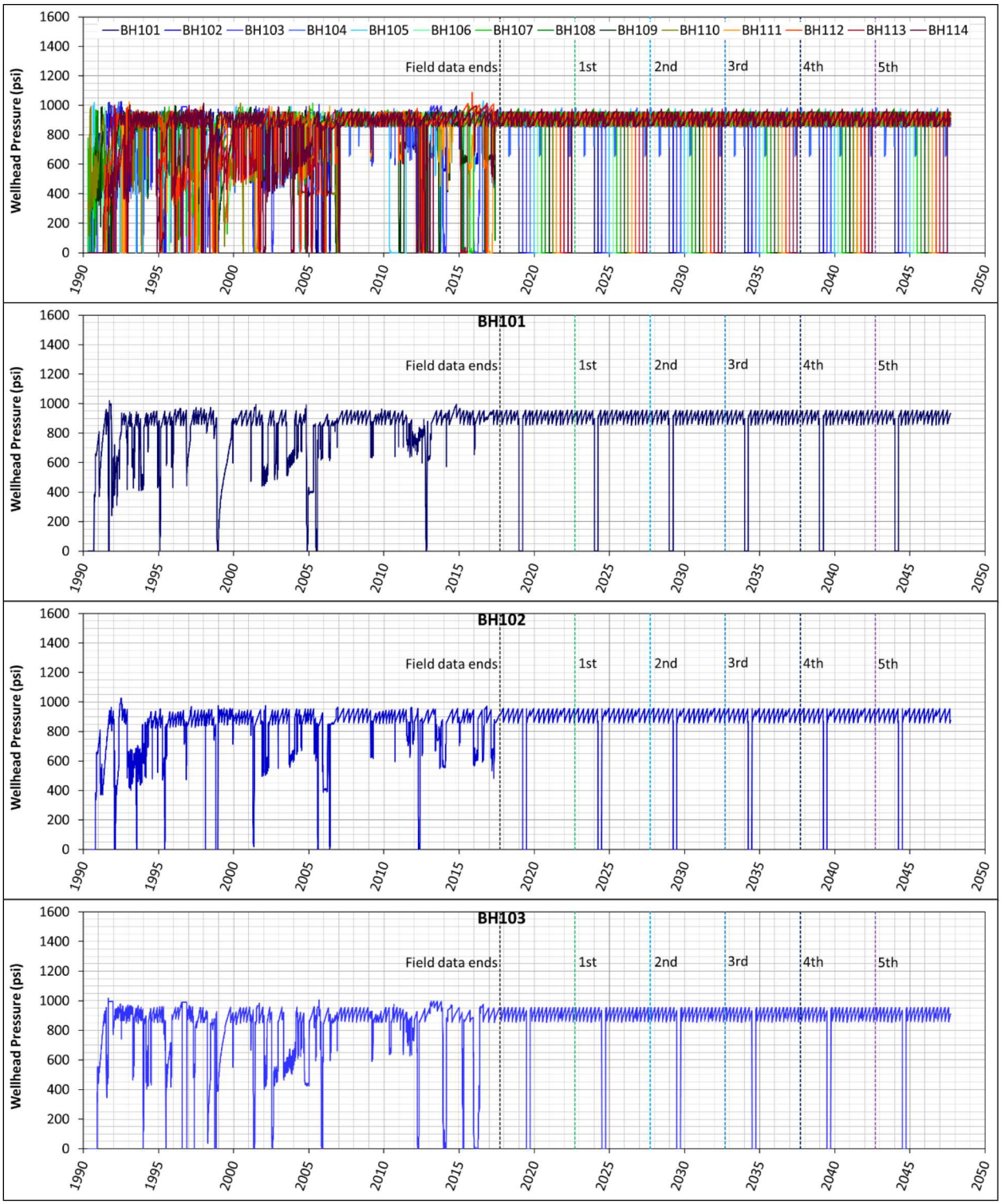
BH101 BH102 BH103 BH104 BH105 BH106 BH107 BH108 BH109 BH110 BH111 BH112 BH113 BH114
Field data ends
1st
2nd
3rd
4th
5th
Wellhead Pressure (psi)
BH101
BH102
BH103

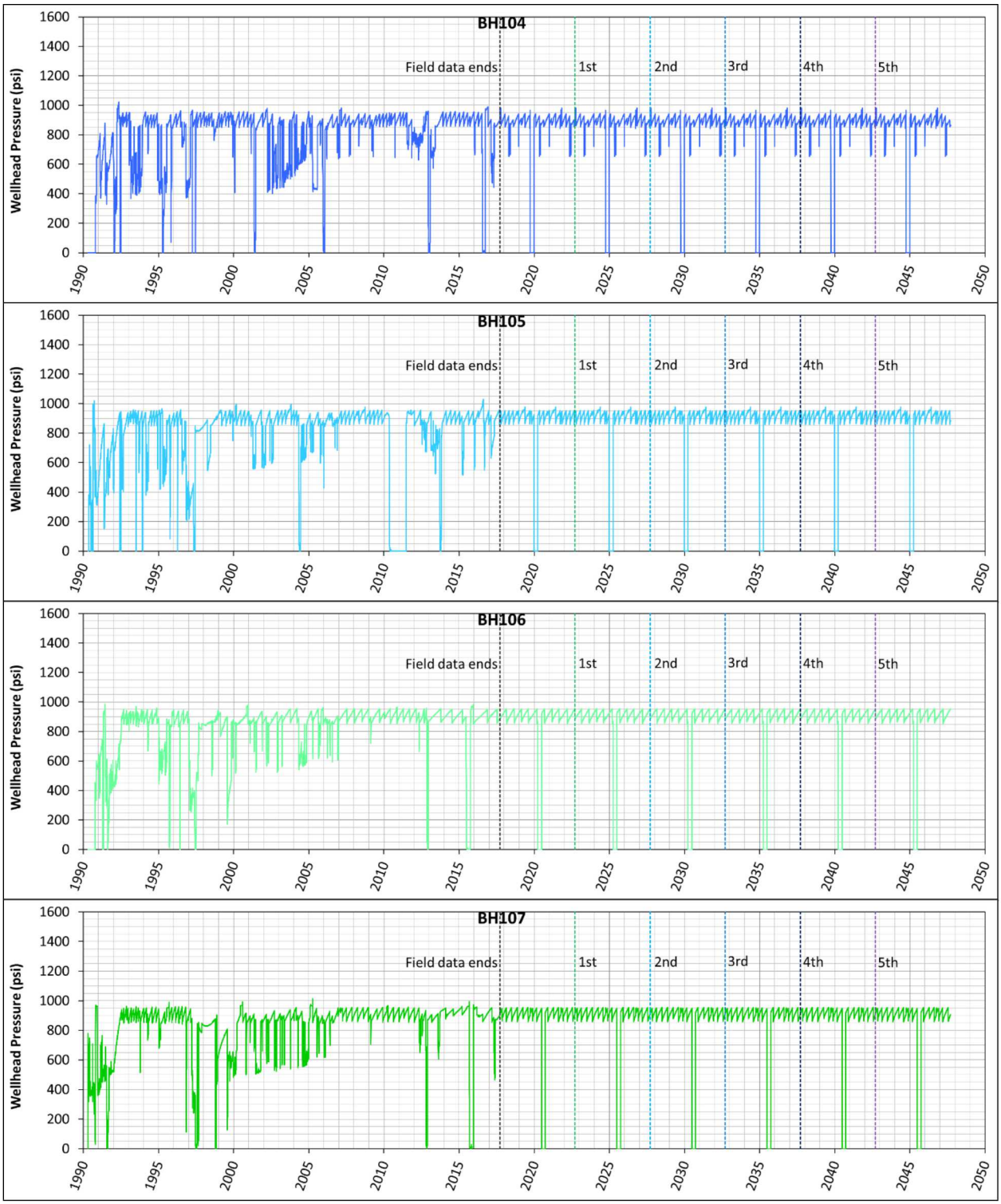
BH104
Field data ends
1st
2nd
3rd
4th
5th
Wellhead Pressure (psi)
BH105
Field data ends
1st
2nd
3rd
4th
5th
Wellhead Pressure (psi)
BH106
Field data ends
1st
2nd
3rd
4th
5th
Wellhead Pressure (psi)
BH107
Field data ends
1st
2nd
3rd
4th
5th
Wellhead Pressure (psi)

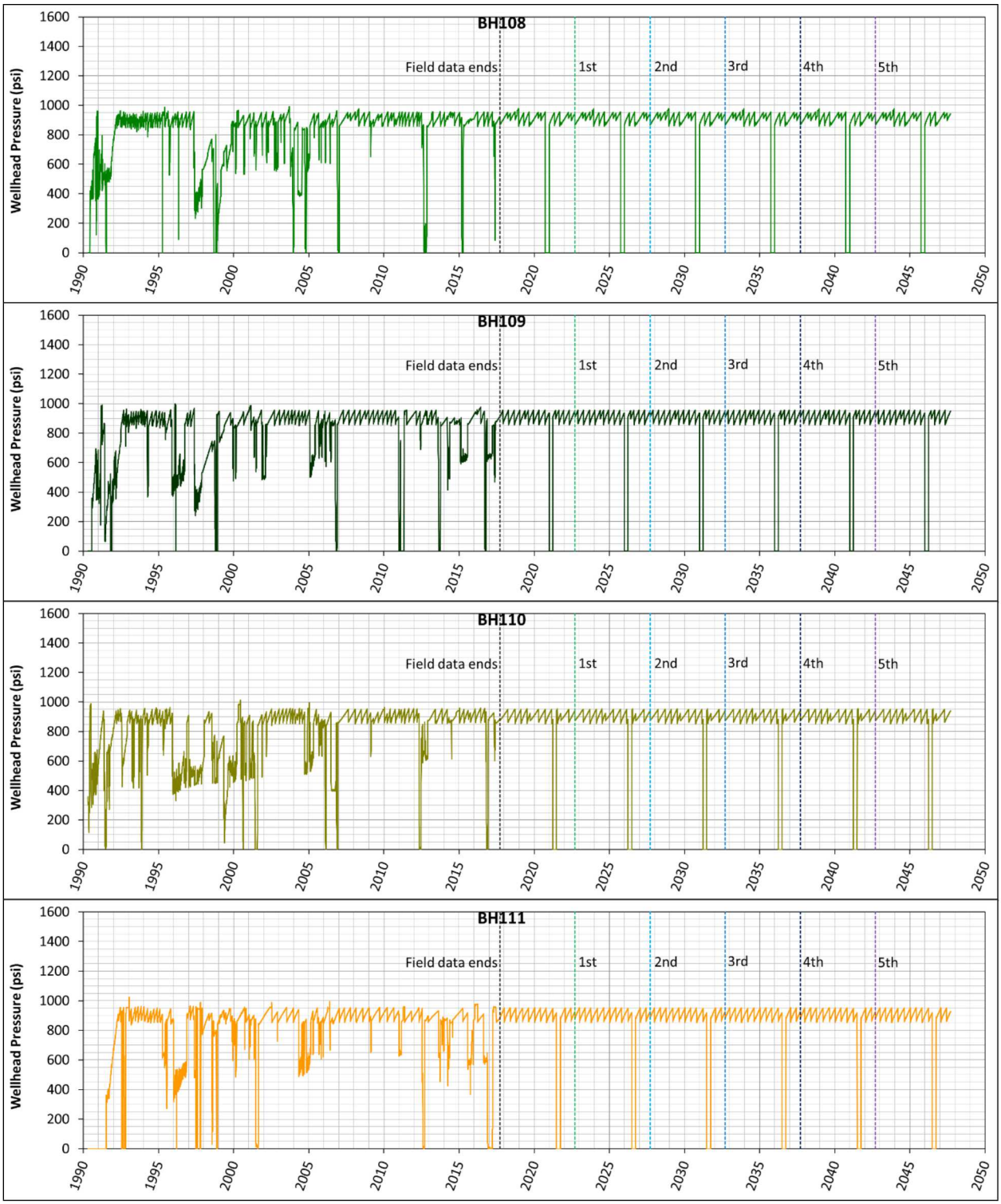
BH108
Field data ends
1st
2nd
3rd
4th
5th
Wellhead Pressure (psi)
0
200
400
600
800
1000
1200
1400
1600
1990
1995
2000
2005
2010
2015
2020
2025
2030
2035
2040
2045
2050
BH109
Field data ends
1st
2nd
3rd
4th
5th
Wellhead Pressure (psi)
BH110
Field data ends
1st
2nd
3rd
4th
5th
Wellhead Pressure (psi)
BH111
Field data ends
1st
2nd
3rd
4th
5th
Wellhead Pressure (psi)

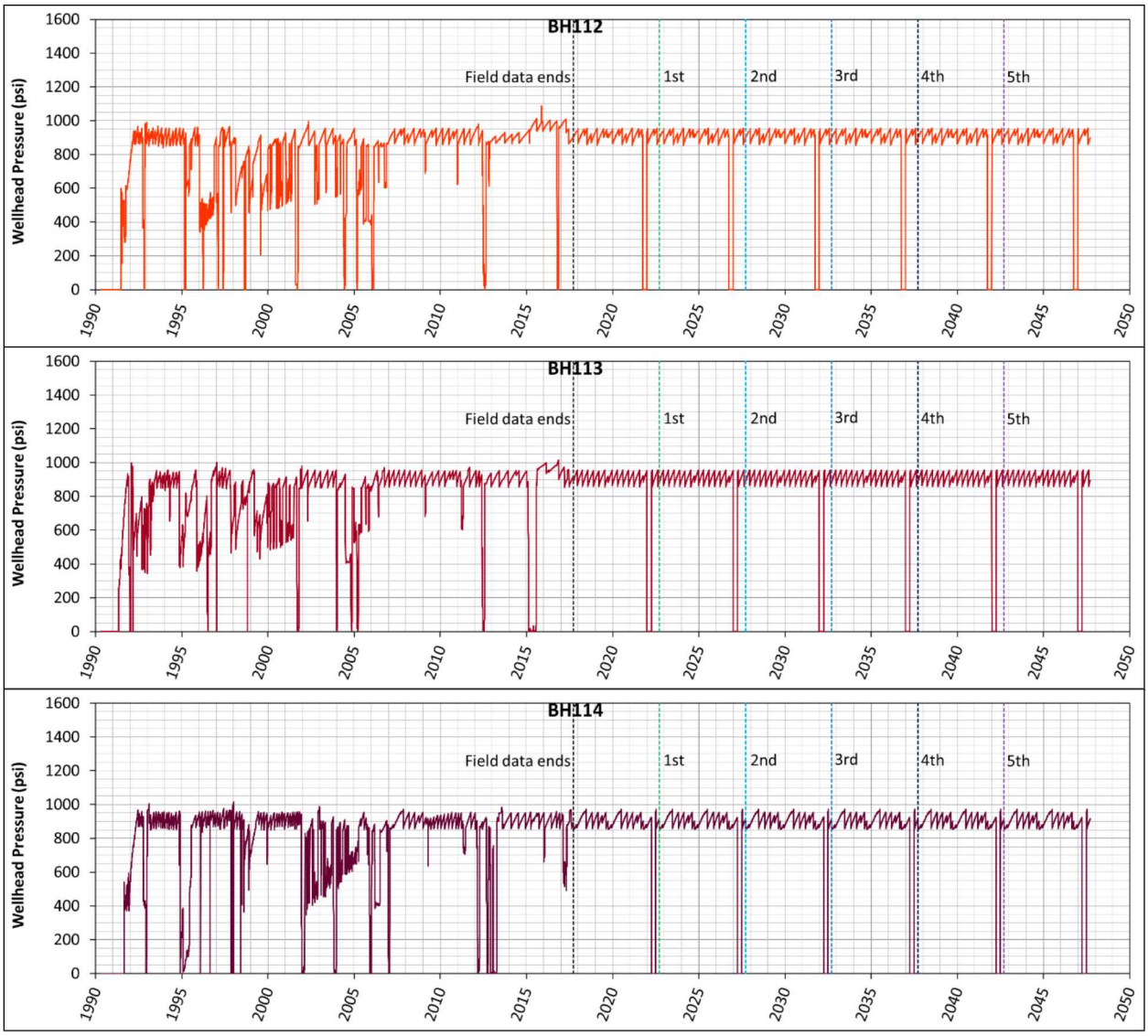

Figure 4. Individual Big Hill SPR caverns' wellhead pressure histories used in this analysis

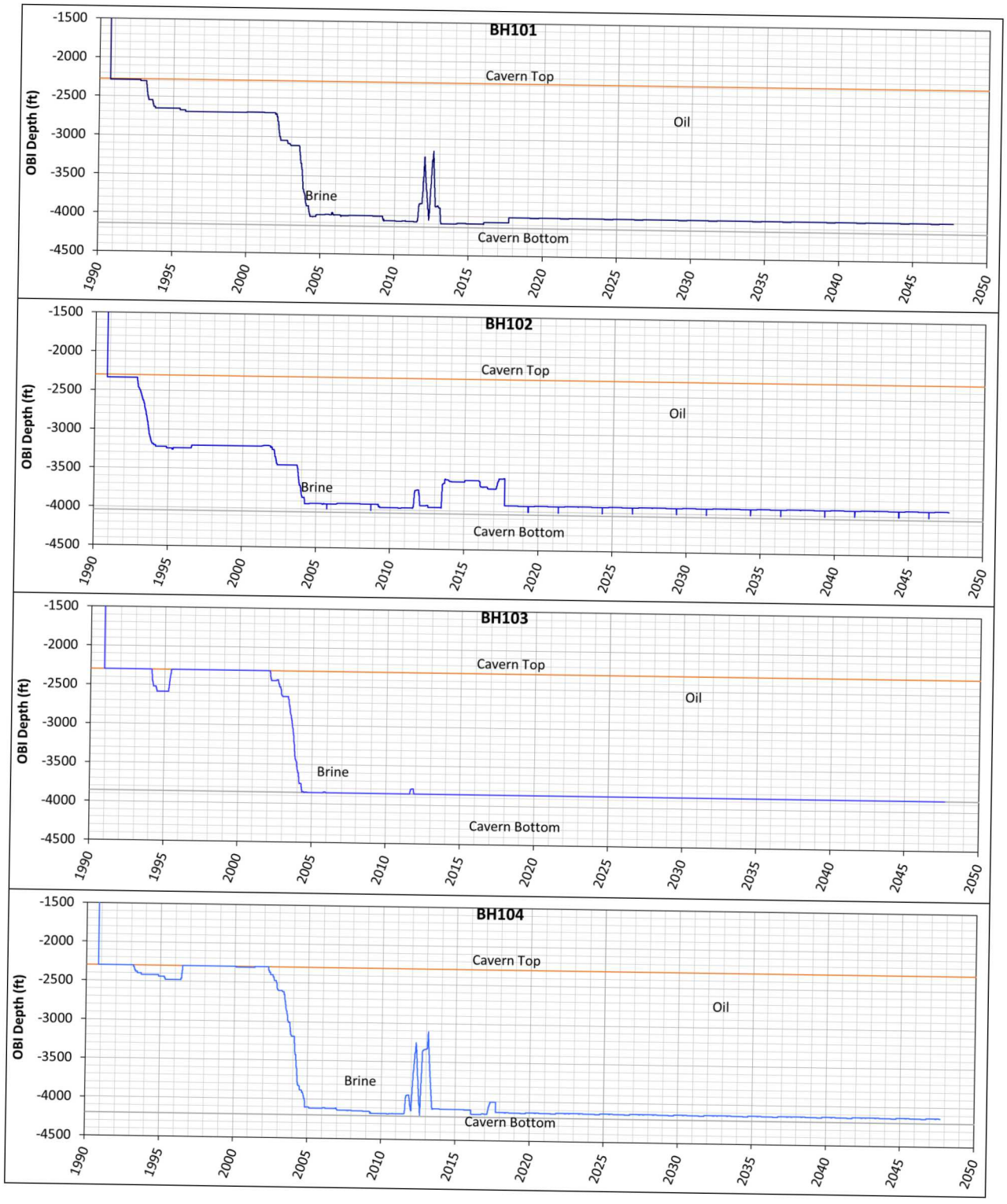
BH101
Cavern Top
Oil
Brine
Cavern Bottom
OBI Depth (ft)
-1500
-2000
-2500
-3000
-3500
-4000
-4500
1990
1995
2000
2005
2010
2015
2020
2025
2030
2035
2040
2045
2050
BH102
Cavern Top
Oil
Brine
Cavern Bottom
OBI Depth (ft)
BH103
Cavern Top
Oil
Brine
Cavern Bottom
OBI Depth (ft)
BH104
Cavern Top
Oil
Brine
Cavern Bottom
OBI Depth (ft)

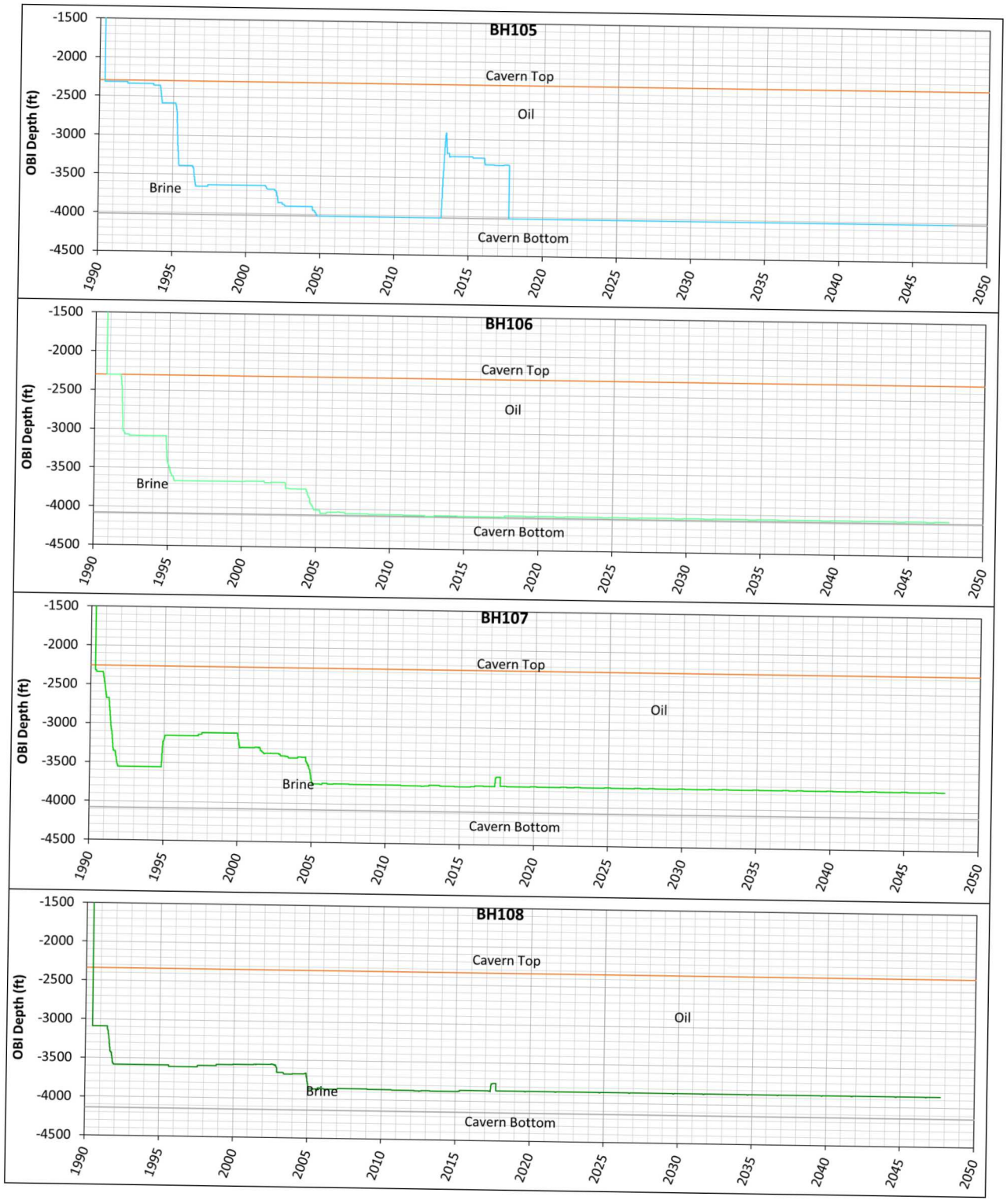
BH105
Cavern Top
Oil
Brine
Cavern Bottom
OBI Depth (ft)
-1500
-2000
-2500
-3000
-3500
-4000
-4500
1990
1995
2000
2005
2010
2015
2020
2025
2030
2035
2040
2045
2050
BH106
Cavern Top
Oil
Brine
Cavern Bottom
OBI Depth (ft)
BH107
Cavern Top
Oil
Brine
Cavern Bottom
OBI Depth (ft)
BH108
Cavern Top
Oil
Brine
Cavern Bottom
OBI Depth (ft)

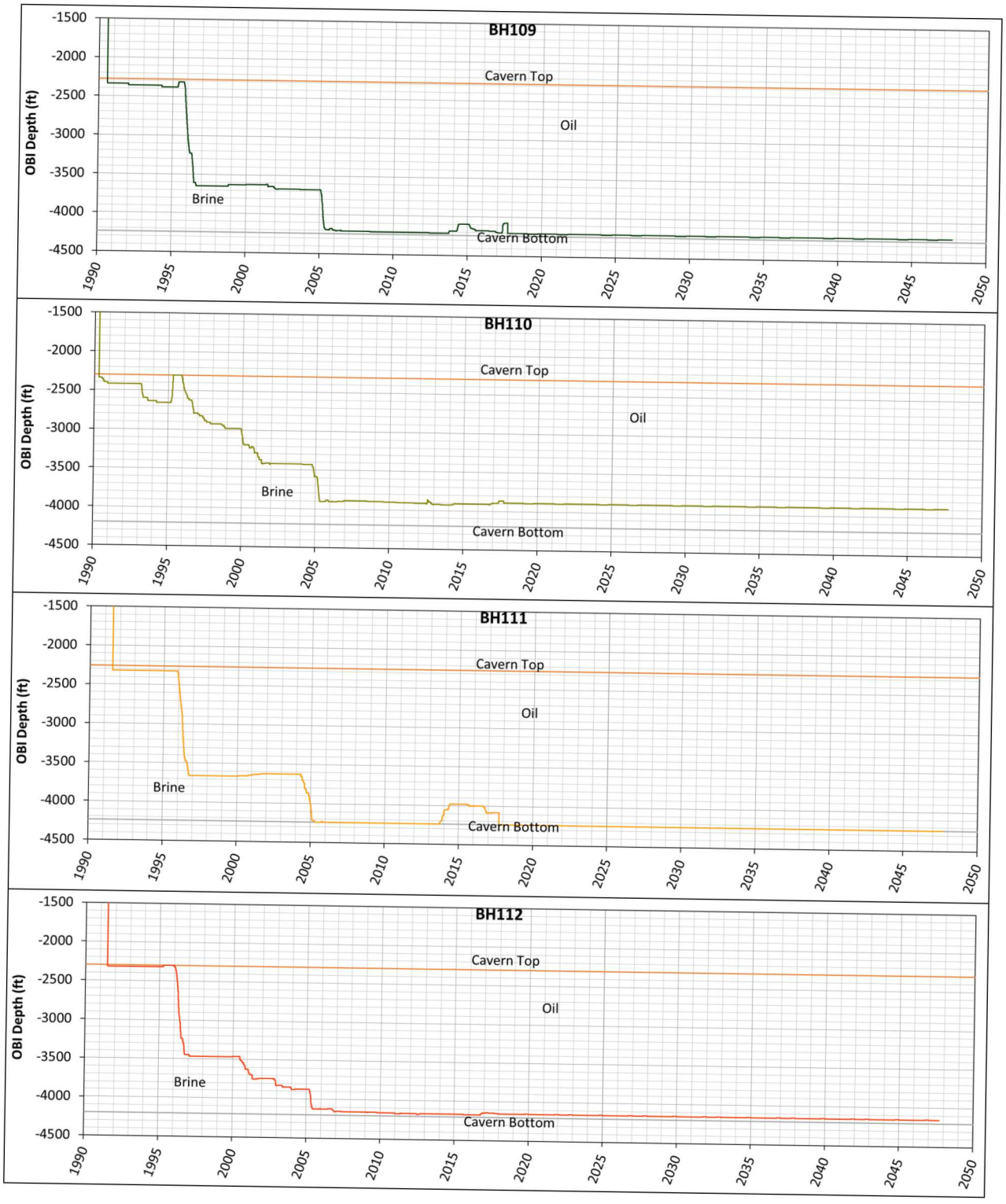
BH109
Cavern Top
Oil
Brine
Cavern Bottom
OBI Depth (ft)
-1500
-2000
-2500
-3000
-3500
-4000
-4500
1990
1995
2000
2005
2010
2015
2020
2025
2030
2035
2040
2045
2050
BH110
Cavern Top
Oil
Brine
Cavern Bottom
OBI Depth (ft)
BH111
Cavern Top
Oil
Brine
Cavern Bottom
OBI Depth (ft)
BH112
Cavern Top
Oil
Brine
Cavern Bottom
OBI Depth (ft)

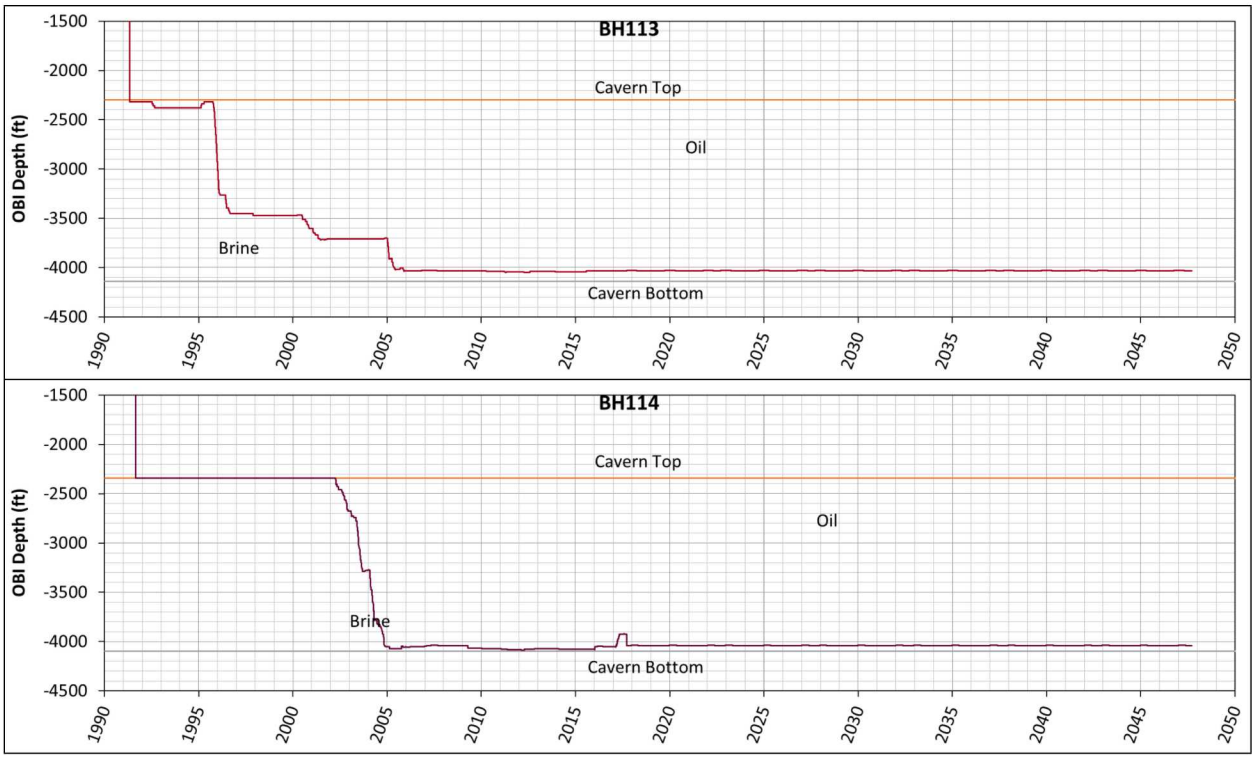

Figure 5. Oil-Brine Interface depth histories to apply into the simulation for 14 Big Hill SPR caverns

3. SALT DAMAGE CRITERIA

Potential damage to or around the SPR caverns was evaluated based on two failure criteria: dilatant damage and tensile failure.

For purpose of these analyses, the tensile strength of the salt is conservatively assumed to be zero in order to check for tensile failure. Tensile cracking in rock salt initiates perpendicular to the largest tensile stress direction. The potential for tensile failure exists if the maximum principal stress (σ_1) is numerically zero or tensile (positive value of σ_1).

Dilatancy is attributed to micro-fracturing or changes in the pore structure of the salt, resulting in an increase in permeability. A dilatancy is considered as the onset of damage to rock salt. A dilatant damage criterion is used to delineate potential zones of damage in the salt formation surrounding the SPR facility. Dilatant damage criterion typically relates two stress invariants to access failure and/or dilation of pressure-dependent materials: the first invariant of the Cauchy stress tensor, I_1, and the second invariant of the deviatoric stress tensor, J_2. These two invariants are defined mathematically as:

$$I_1 = \sigma_1 + \sigma_2 + \sigma_3 \tag{1}$$

$$J_2 = \frac{(\sigma_1 - \sigma_2)^2 + (\sigma_2 - \sigma_3)^2 + (\sigma_3 - \sigma_1)^2}{6} \tag{2}$$

where, σ_1, σ_2, and σ_3 are the maximum, intermediate, and minimum principal stresses, respectively.

Lee et al. [2004] suggested the following strength criterion of BH salt based on a series of quasi-static triaxial compression tests:

$$\sqrt{J_2} = a \cdot e^{n \cdot I_1} + c \tag{3}$$

The values of the parameters are calculated as follows:

a = -1320.5 psi
n = -3.4 x 10^{-4} (1/psi)
c = 1746 psi

A dilatant damage factor (DF) for the BC salt can then be defined by:

$$DF = \frac{a \cdot e^{n \cdot I_1} + c}{\sqrt{J_2}} \tag{4}$$

If $DF \leq 1$, the shear stresses in the salt ($\sqrt{J_2}$) are large compared to the mean stress (I_1) and dilatant behavior is expected. If $DF > 1$, the shear stresses are small compared to the mean stress and dilatancy is not expected. To calculate the dilatancy damage potential in salt, the post-processing code ALGEBRA is used with the output of the FE code ADAGIO to determine spatial locations of dilatant damage.

This page left blank

4. CAVERN INTEGRITY

4.1. BH-101

Modeling of the leaching process of the caverns is performed by deleting a pre-meshed block of elements along the walls of the cavern so that the cavern volume is increased by 16 percent per drawdown. A 15% volume increase is typical for a standard freshwater drawdown, but the BH salt quality is worse than that of other sites. The exact volume increase depends on the insoluble content of salt, so a 16% volume increase is used for a drawdown for the BH salt [Park et al. 2005; Park and Ehgartner, 2011]. Also, typical leaching processes tend to increase a cavern radius more at the bottom of the cavern than at the top, with very little change to the roof and floor of the cavern. For the purposes of this modeling effort for Big Hill, leaching is assumed to add 16% to the volume of the cavern, and is assumed to occur uniformly along the entire height of the cavern, with no leaching in the floor or roof of the caverns. Each leaching layer, or onion skin, is built around the perimeter of the meshed cavern volume using the same rules stated previously.

Figure 6 shows the cavity of BH-101 as developed from sonar data, along with drawdown skins (leaching layers) and extra skins. In this simulation, BH-101 is modeled as having five drawdown layers to be removed to account for the future oil drawdown activities. The thicknesses of five layers and extra skin 1 are calculated to get a 16% cavern volume increase for each drawdown. Five drawdown skins and extra skin 1 are used for examining the analysis results after the initial leach, 1st drawdown, 2nd drawdown, and … 5th drawdown leaches, respectively. Six layers and extra skin 2 of 40 ft thick are used for applying the cavern specific calibrated values of multiplication factors, *A2F* and *K0F* [Park, 2017a].

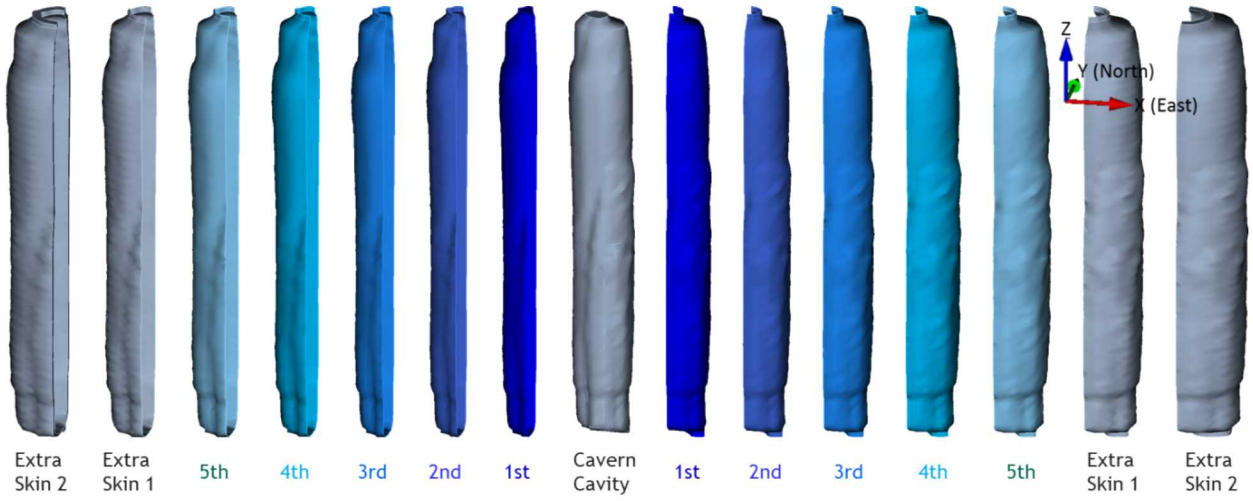

Figure 6. BH-101 cavern cavity with five drawdown skins (leaching layers) and extra skins

Figure 7 shows the predicted maximum σ_1, and minimum *DF* in the salt volume surrounding the cavity of BH-101 over time. In the numerical analysis, σ_1 is calculated in every element in the salt dome at each time step. The maximum σ_1 means the maximum value among all σ_1 values calculated in all elements in a specific volume (in this case, each skin layer) at a specific time. In the plot, a positive value (+) indicates a tensile stress. In the similar manner, *DF* is calculated in every element in the salt dome at each time step. The minimum *DF* means the minimum value

among all *DF* values calculated in all elements in a specific volume at a specific time. As mentioned in Section 3, when $DF \leq 1$, we consider dilatant damage to have occurred. Note that the 1st, 2nd, etc., in the plots indicate the drawdown leach start dates (9/19/2022, 9/19/2027, 9/19/2032, 9/19/2037, and 9/19/2042, respectively) of all SPR caverns.

The maximum σ_1 reaches a positive or tensile value (calculated to be 36 psi) on 1/19/1991 during the first wellhead pressure down (810 psi to 450 psi) (see Figure 4), and keeps the positive value (tensile stress state) until the simulation ends. The minimum *DF* is predicted to be less than 1 (calculated to be 0.7) on 9/20/1991 and return to be larger than 1 right after that. The minimum *DF* fluctuates between larger and smaller than 1 until the simulation ends. The dilatant damage occurs and disappears during $DF \leq 1$ and $DF > 1$, respectively.

Figure 8 and Figure 9 show the locations of the maximum σ_1 and minimum *DF*, respectively, around BH-101 on specific dates. The areas in tensile stressed and dilatant damaged are indicated by the elements in red in the figures. A close examination reveals that the extreme stress state occur at the edge of the floor of the cavern, where there is a sharp corner in the mesh. The mesh geometry at this location is likely creating an numerically high stress concentration that exaggerates the stress at the bottom of the cavern. This occurrence is not believed to be significant enough to cause micro-cracking in the salt of a magnitude that would affect cavern stability. This phenomenon happened also at WH-110 in the West Hackberry [Sobolik, 2016] and BC-101 in the Bayou Choctaw [Park, 2017b] simulations. *Therefore, the salt volume surrounding the cavern cavity excluding the elements at the sharp corners of the cavern roof and floor might be better to predict true tensile stressed and dilatant damaged areas that affect cavern stability*. Because of this, the values of maximum σ_1, and minimum *DF* calculated at the corners of the cavern floor will be removed for every BH SPR cavern in the following sections.

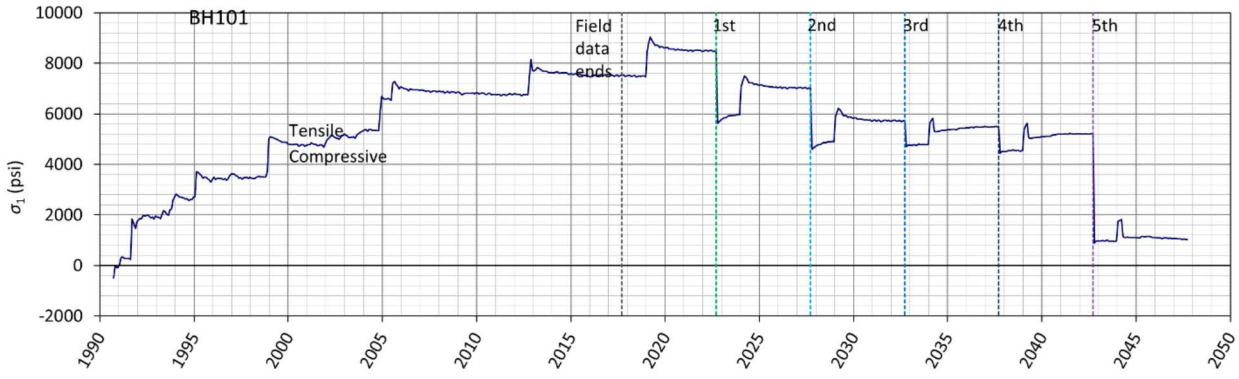

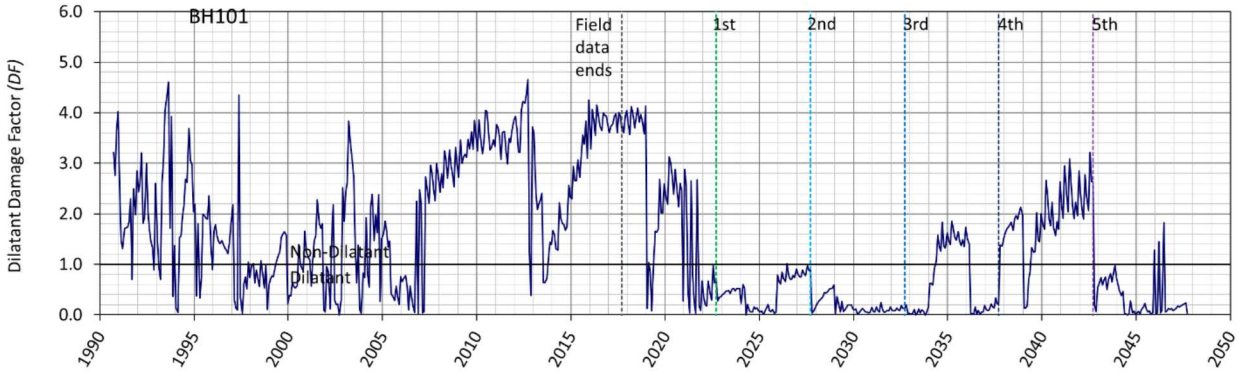

Figure 7. Predicted maximum σ_1 (top) and minimum dilatant damage factor (bottom) in the salt surrounding BH-101 over time

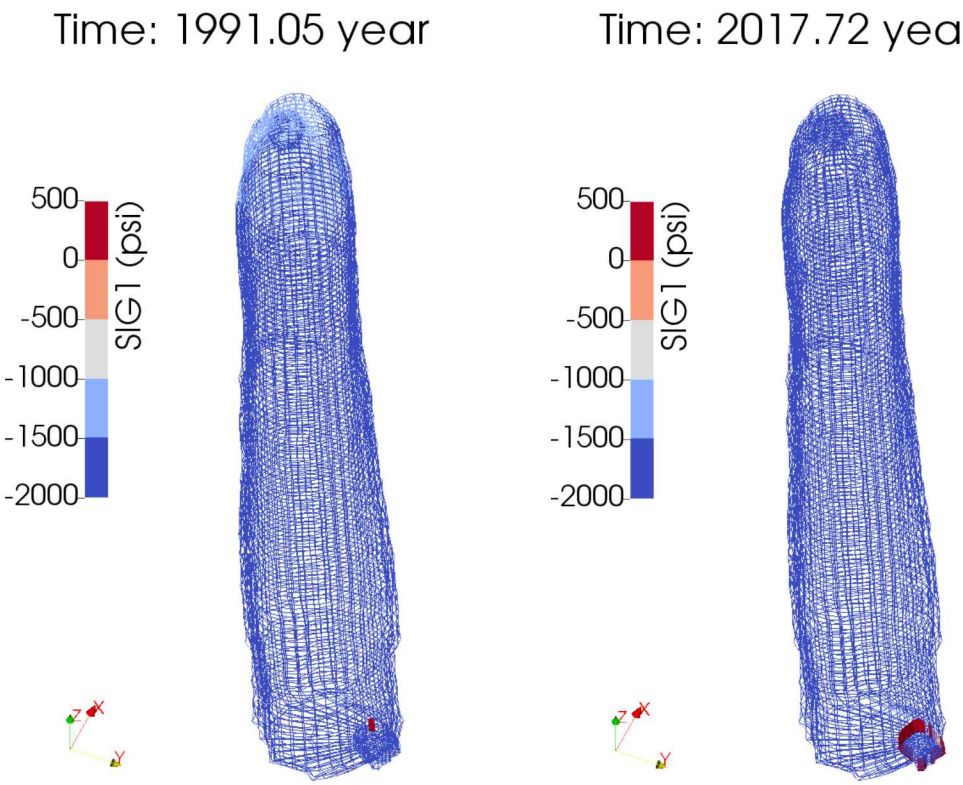

Figure 8. Contour plots of σ_1 on 1/19/1991 and 9/18/2017 (look up view)

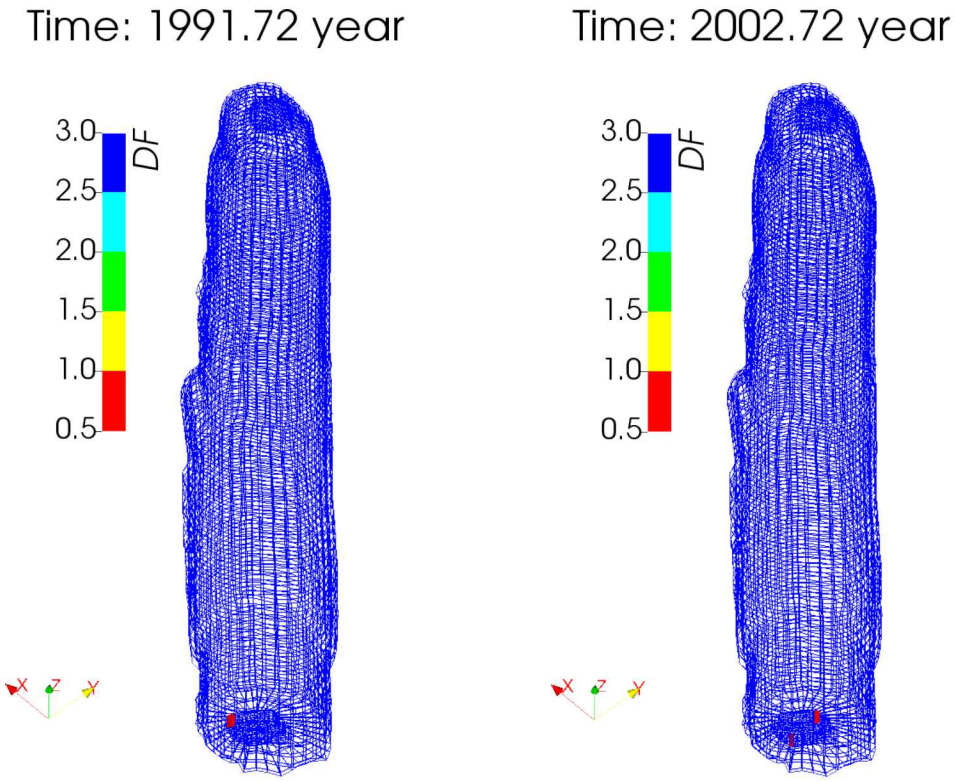

Figure 9. Contour plots of *DF* on 9/20/1991 and 9/20/2002 (look up view)

Figure 10 shows the predicted volumetric change (top), and volumetric closure normalized to initial cavern volume (2nd panel), maximum σ_1 (3rd panel), and minimum *DF* (bottom) in the salt volume surrounding BH-101 excluding elements at the corners of the cavern floor over time. The initial cavern cavity volume was 13.1 MMB on 9/20/1990 and is predicted to be 11.9 MMB on 9/19/2022. The cavern volume is predicted to decrease by 9.1% over 32 years (9/20/1990 - 9/19/2022). The bizarre values of maximum σ_1, and minimum *DF* in Figure 7 are removed through excluding them calculated from the elements at the corners of the cavern roof and floor, thus we can see the true values of them calculated in the volume surrounding the cavern cavity.

The maximum σ_1 reaches a positive (tensile stress state) value during the workovers after the second drawdown leach. The maximum σ_1 are calculated to be 112, 166, 624, and 104 psi at 2029.22, 2034.22, 2039.22, and 2044.22 years, respectively. Figure 11 shows the contour plots of σ_1 on the specific times to show the area in tension in the cavern skin layers during the workovers after each drawdown leach. The areas in tensile state are located in the sloping floor. The tensile state may occur because of the geometry of the relatively horizontal floor, but not vertical wall.

The values of *DF* become less than 1 during every workover as shown in Figure 10. The minimum *DF* are calculated to be 0.92, 0.82, 0.13, and 0.96 at 2029.22, 2034.22, 2039.14, and 2044.22 years, respectively. Figure 12 shows the contour plots of *DF* at specific times to show the areas in dilatant damage state (*DF*<1) in the cavern skin layers after each drawdown leach. The dilatant damaged areas are created during the workovers. This implies there is creation of micro-cracking and increase in porosity/permeability during every workover. The areas in a dilatant damage stress condition disappear when the cavern pressure returns to the normal

operating condition. This implies there is no additional creation of micro-cracking and increase in porosity/permeability during the normal operation. However, there is a possibility of salt fracture and crack propagation under both tensile and dilatant damage states during the workovers after the second drawdown leach. Once a crack is created, the crack will continue to propagate with time because it is in tensile state. Structural failure may occur at the sloping floor, i.e. salt uplift is expected during the four workover periods. However, the salt uplift on the sloping floor may not affect the cavern structural stability.

In conclusion, BH-101 may be structurally stable until the fifth drawdown leach. However, the dilatant damaged areas in tensile stress state are created on the sloping floor of the cavern during the workovers after the second drawdown leach substantially. Therefore, we need to re-examine the cavern stability with a new cavern volume after a drawdown leach in future.

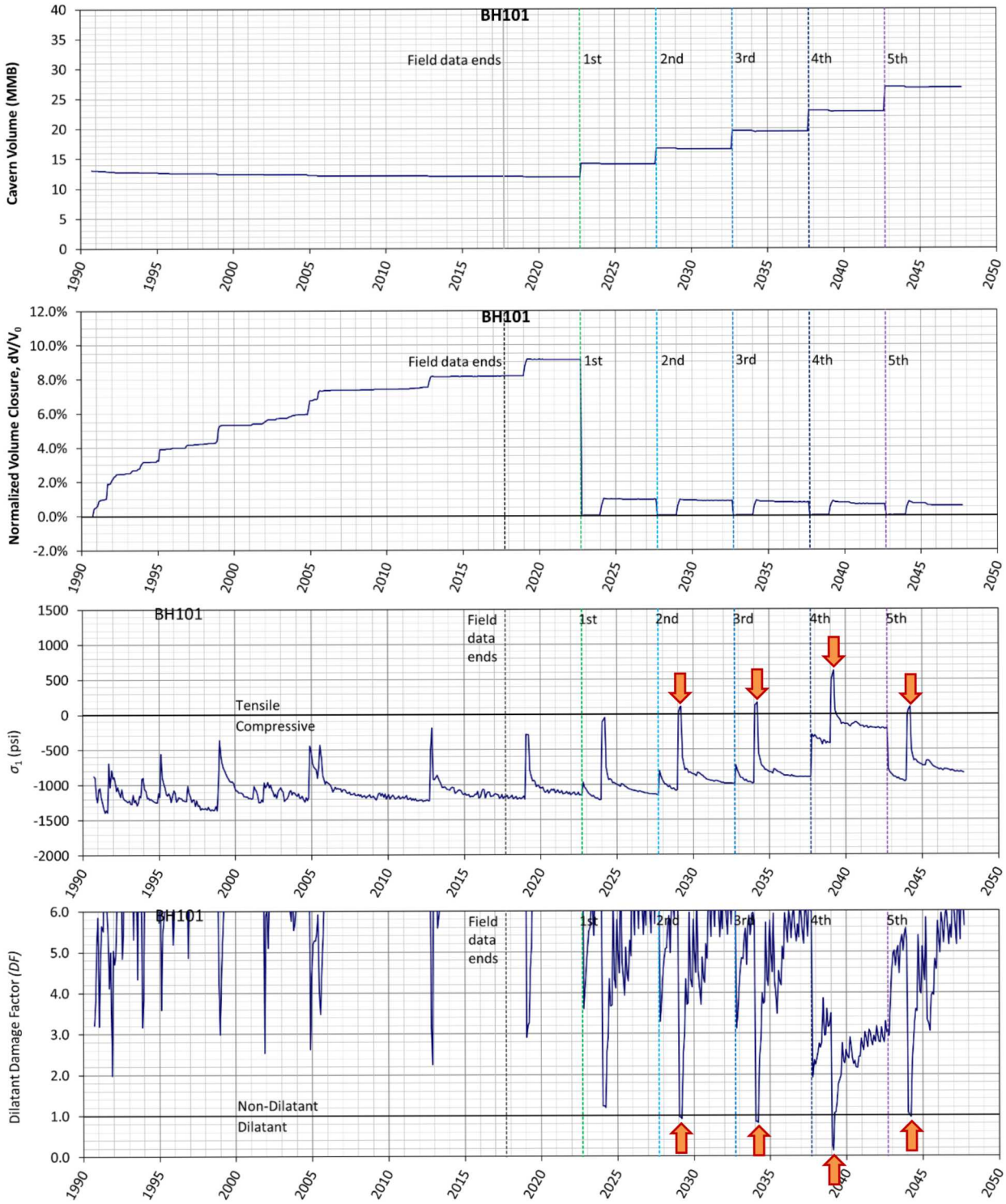

Figure 10. Predicted volumetric change (top), volumetric closure normalized to initial cavern volume of BH-101 (2nd), maximum σ_1 (3rd) and minimum dilatant damage factor (bottom) in the salt surrounding BH-101 over time

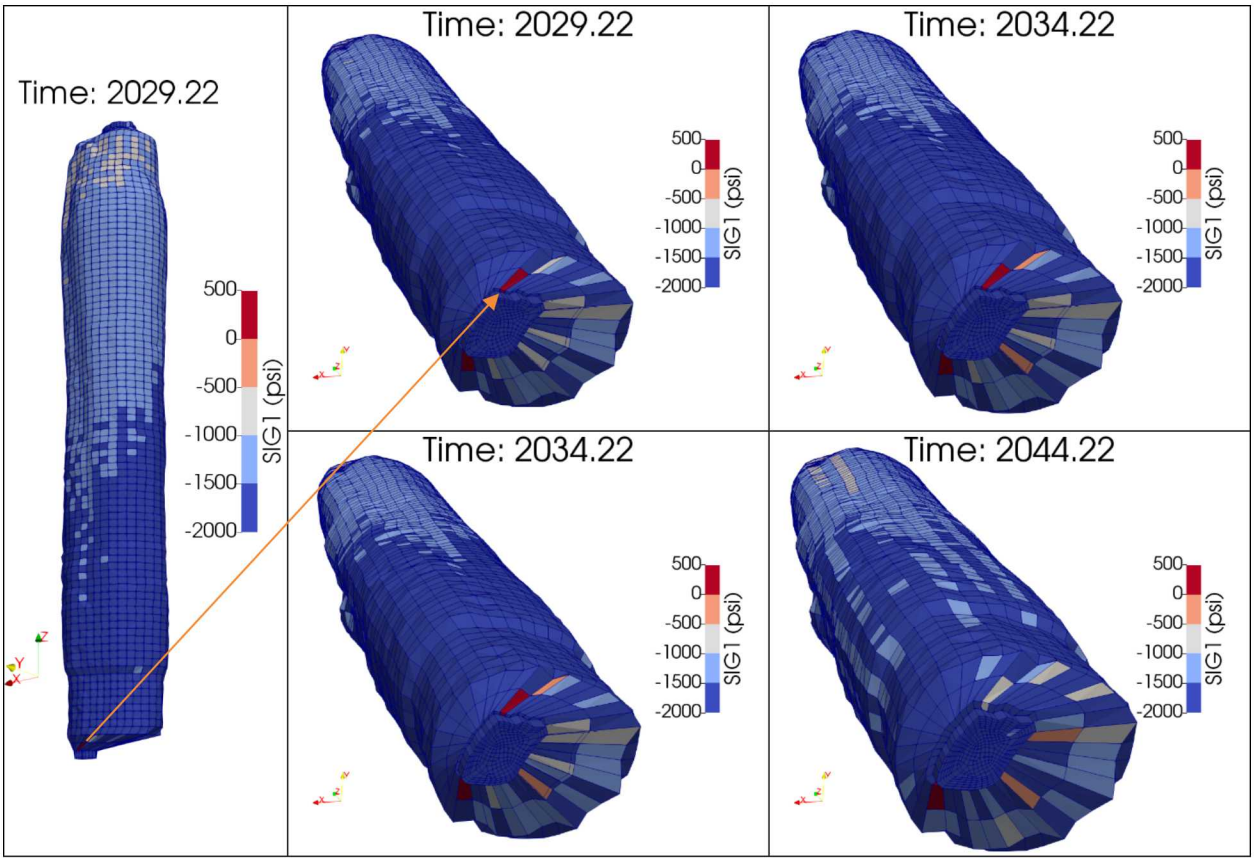

Figure 11. Contour plots of σ_1 on specific dates. Areas in tensile state are shown in red ($\sigma_1 > 0$). Each value of maximum σ_1 are indicated by each arrow at each specific time on the 3rd panel in Figure 10

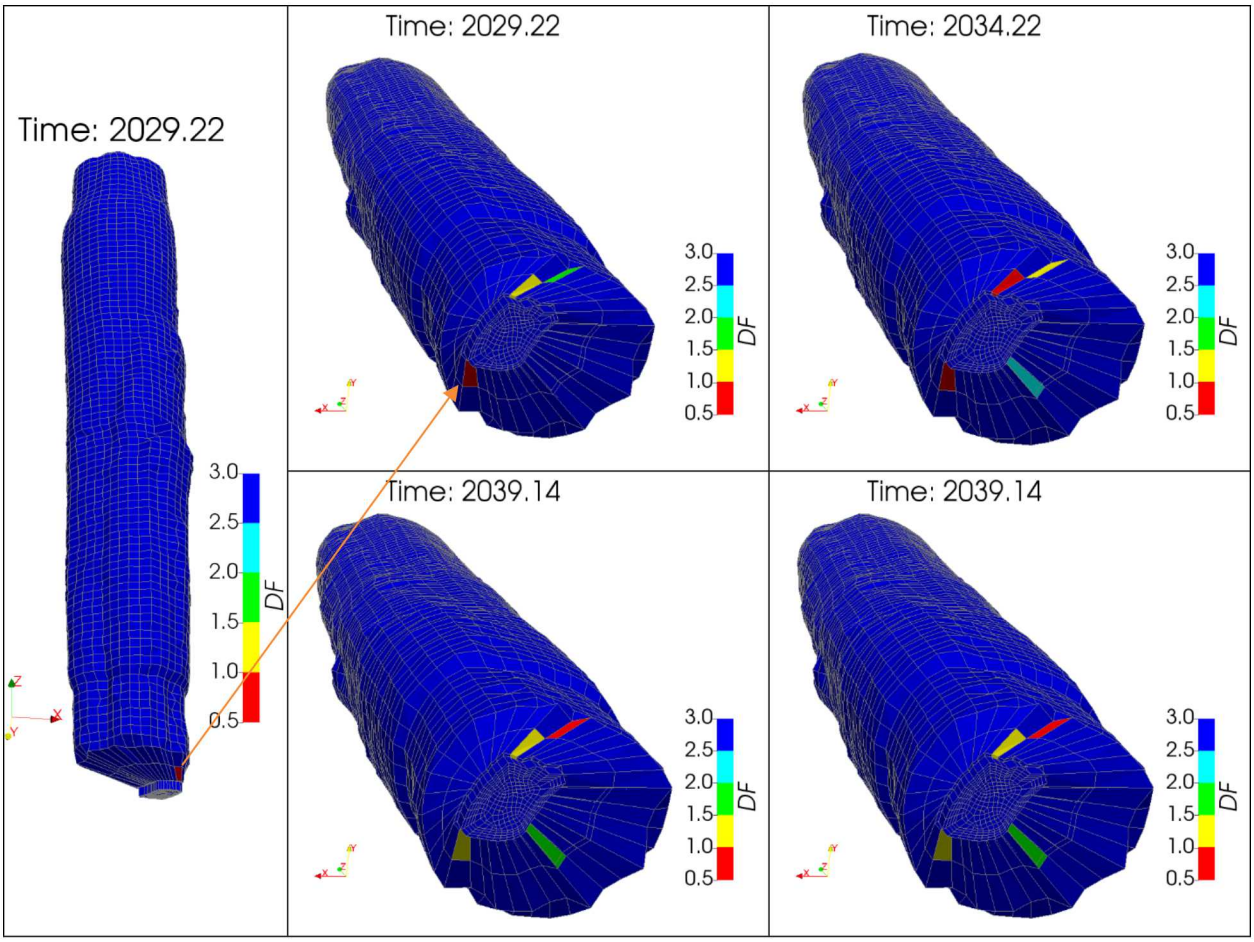

Figure 12. Contour plots of *DF* on specific dates. Areas in dilatant are shown in red (*DF* < 1). Each value of minimum *DF* is indicated by each arrow at each specific time on the bottom panel in Figure 10

4.2. BH-102

Modeling of the leaching process of the caverns is performed by deleting a pre-meshed block of elements along the walls of the cavern so that the cavern volume is increased by 16 percent per drawdown. Figure 13 shows the cavity of BH-102 as developed from sonar data, along with drawdown skins and extra skins. In this simulation, BH-102 is modeled as having five drawdown layers to be removed to account for the future oil drawdown activities as mentioned in the previous section.

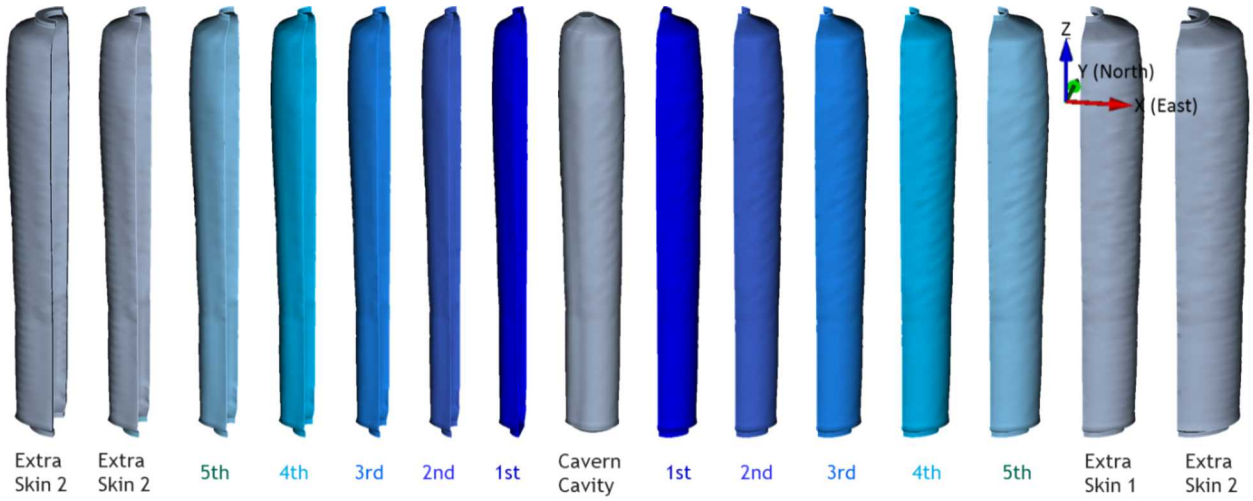

Figure 13. BH-102 cavern cavity with five drawdown skins (leaching layers) and extra skins

Figure 14 shows the predicted volumetric change (top), and volumetric closure normalized to initial cavern volume (2nd panel), maximum σ_1 (3rd panel), and minimum *DF* (bottom) in the salt volume surrounding BH-102 over time. The initial cavern cavity volume was 12.9 MMB on 10/20/1990 and is predicted to be 11.9 MMB on 9/19/2022. The cavern volume is predicted to decrease by 7.7% over 32 years (10/20/1990 - 9/19/2022).

The maximum σ_1 never reaches a positive (tensile stress state) value through five drawdowns, and the minimum *DF* either never reaches to be less than 1 during every workover until the end of simulation. The largest predicted value of the maximum σ_1 is -572 psi on 5/20/2012 during the workover started on 4/10/2012 for 53 days. The smallest predicted value of the minimum *DF* is 1.93 on 8/20/2005 during the workover started on 7/20/2005 for 31 days.

In conclusion, BH-102 is predicted to be structurally stable through the fifth drawdown leach.

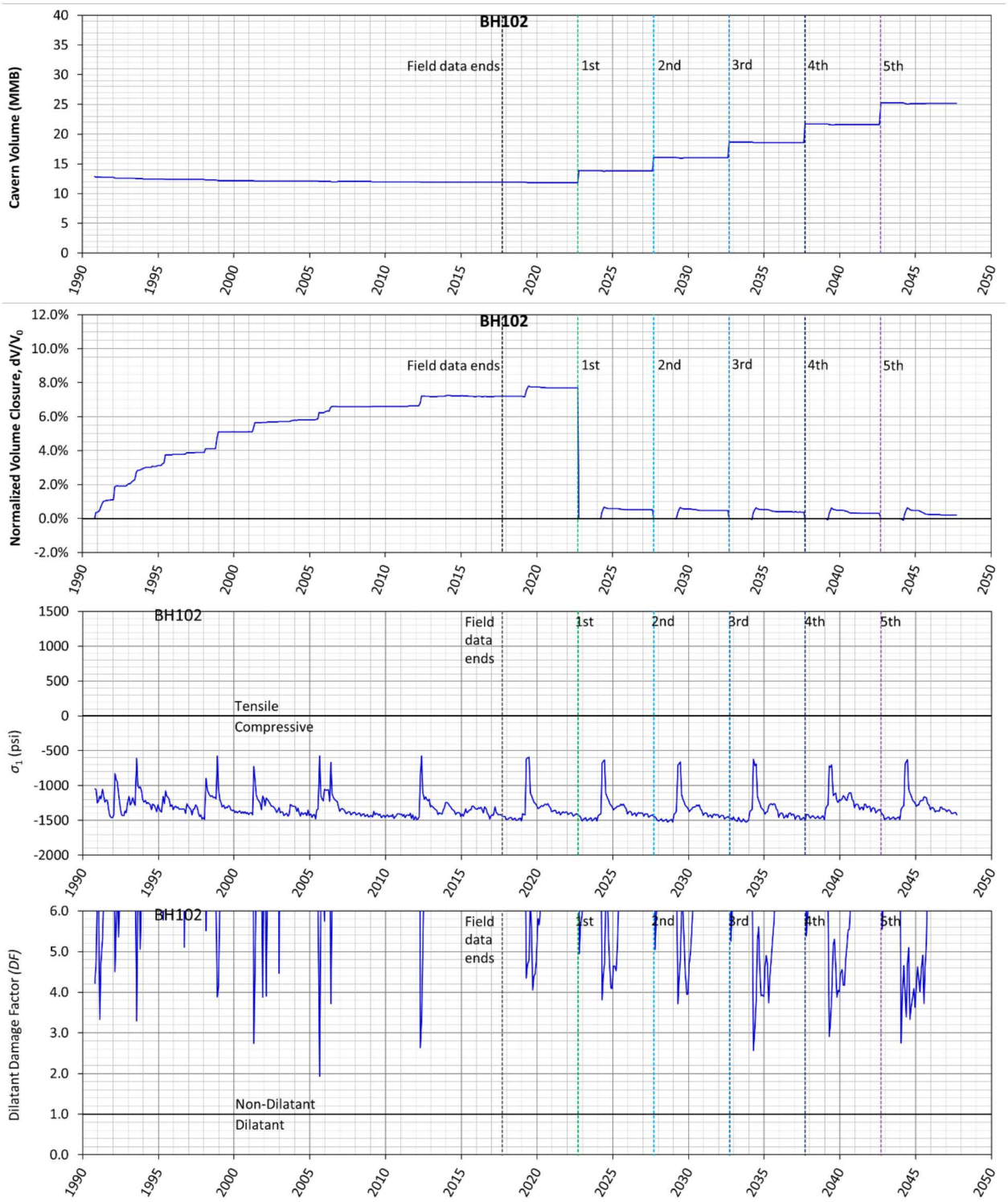

Figure 14. Predicted volumetric change (top), volumetric closure normalized to initial cavern volume of BH-102 (2nd), maximum σ_1 (3rd) and minimum dilatant damage factor (bottom) in the salt surrounding BH-102 over time

4.3. BH-103

Modeling of the leaching process of the caverns is performed by deleting a pre-meshed block of elements along the walls of the cavern so that the cavern volume is increased by 16 percent per drawdown. Figure 15 shows the cavity of BH-103 as developed from sonar data, along with drawdown skins and extra skins. In this simulation, BH-103 is modeled as having five drawdown layers to be removed to account for the future oil drawdown activities.

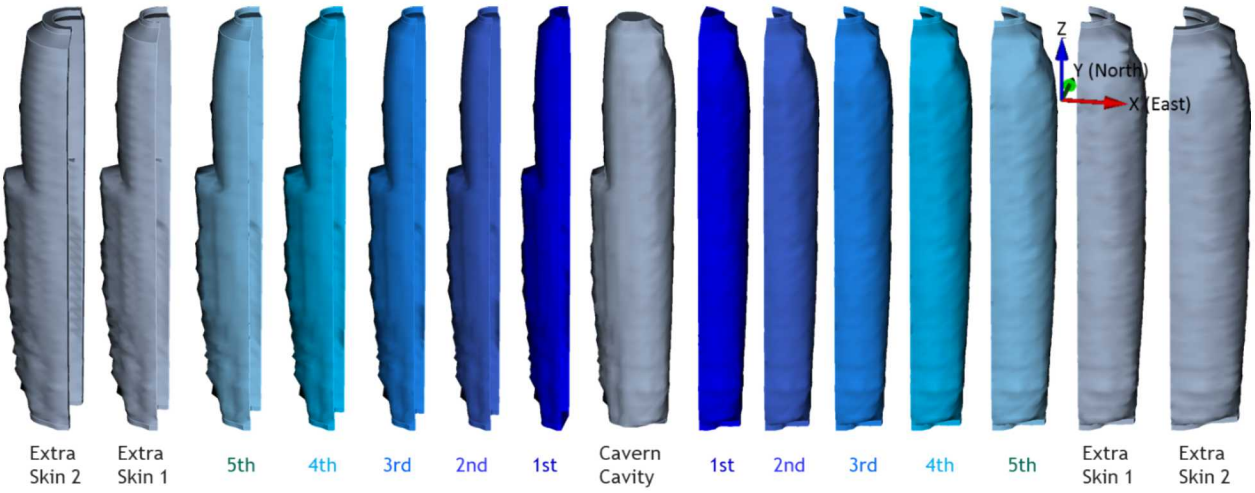

Figure 15. BH-103 cavern cavity with five drawdown skins (leaching layers) and extra skins

Figure 16 shows the predicted maximum σ_1, and minimum *DF* in the salt volume surrounding the cavity of BH-103 over time. The maximum σ_1 reaches a positive or tensile value (calculated to be 9 psi) on 4/20/1998 during the wellhead pressure down (925 psi to 38 psi) (see Figure 4), and return to a negative value. It has been the positive value (tensile stress state) since 5/22/2001 until 9/20/2032. The minimum *DF* is predicted to be less than 1 (calculated to be 0.59) on 5/22/2001 and return to be larger than 1 right after that. The minimum *DF* fluctuates between larger and smaller than 1 until the simulation ends. The dilatant damage occurs and disappears during $DF \leq 1$ and $DF > 1$, respectively.

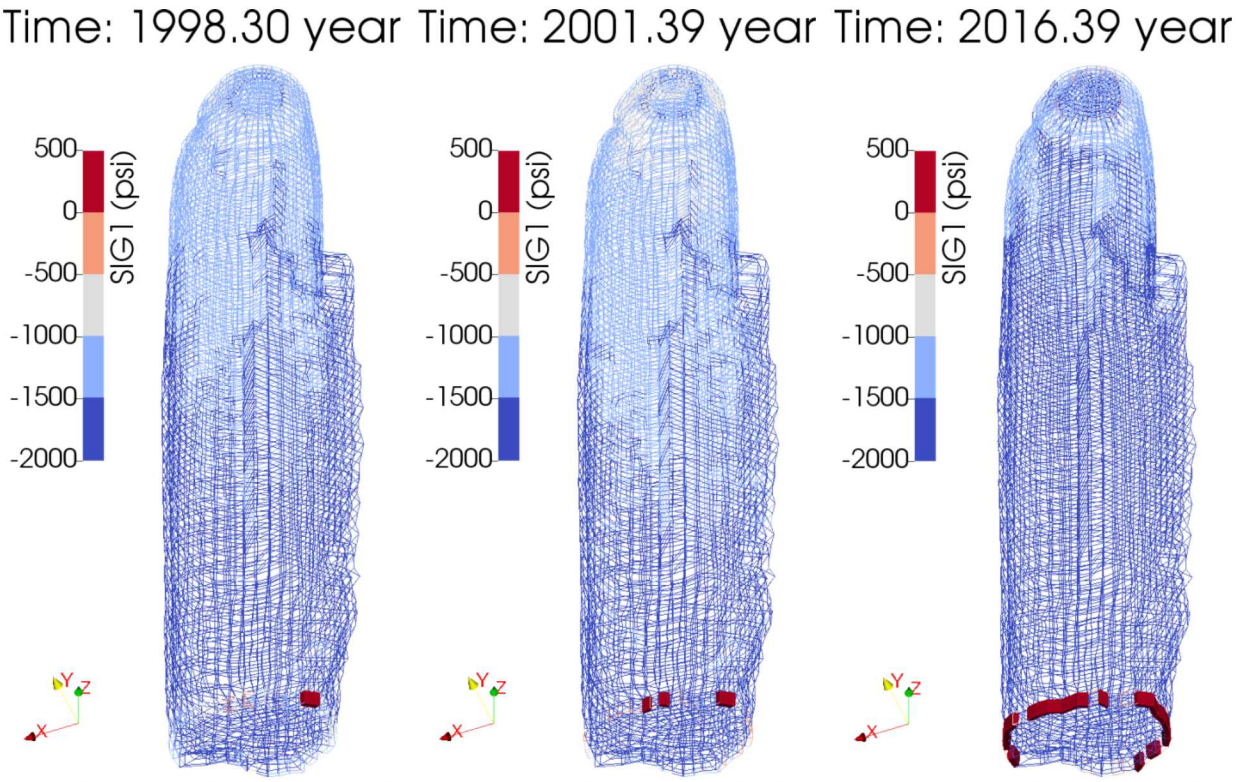

and Figure 18 show the locations of the maximum σ_1 and minimum *DF*, respectively, around BH-103 on specific dates. The areas in tensile stressed and dilatant damaged are indicated by the elements in red in the figures. A close examination reveals that the extreme stress state occur at the edge of the cavern floor, where there is a sharp corner in the mesh. The mesh geometry at this location is likely creating an numerically high stress concentration that exaggerates the stress at the bottom of the cavern. This occurrence is not believed to be significant enough to cause micro-cracking in the salt of a magnitude that would affect cavern stability. Because of this, the values of maximum σ_1, and minimum *DF* calculated at the corners of the cavern floor will be removed as it has been removed in BH-101.

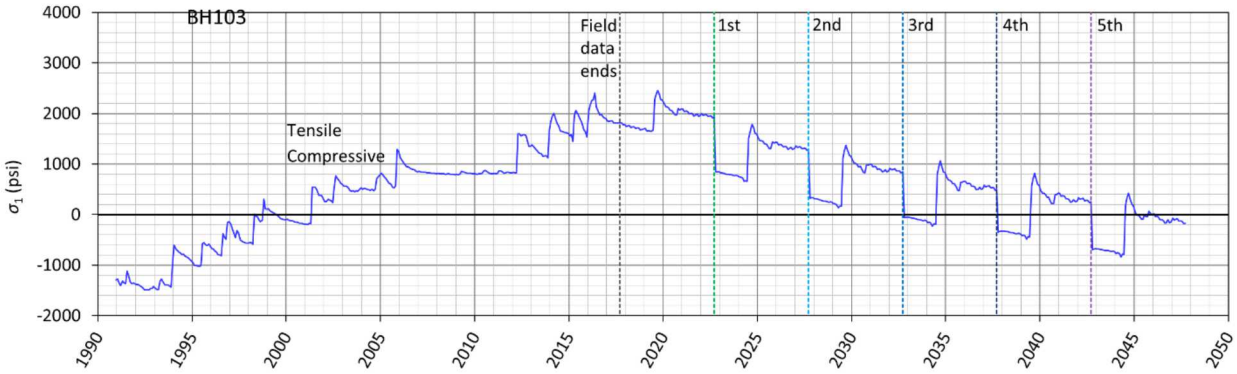

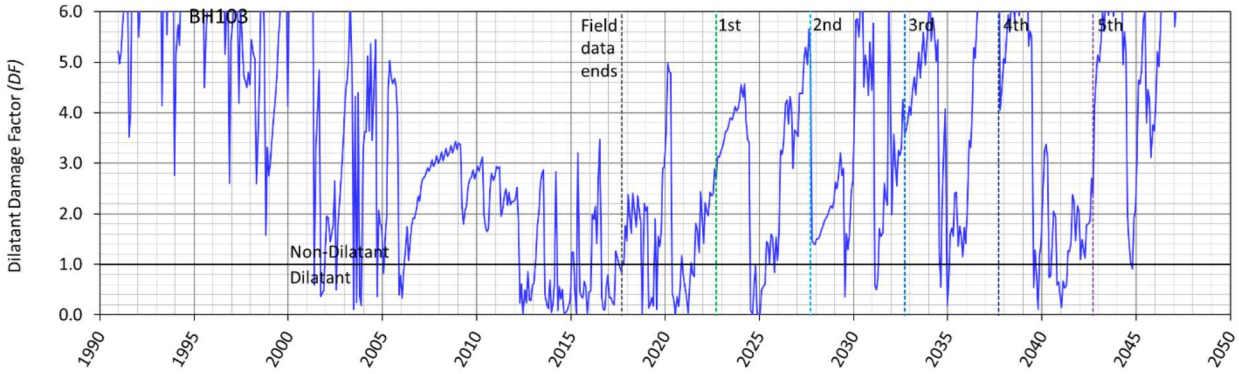

Figure 16. Predicted maximum σ_1 (top) and minimum dilatant damage factor (bottom) in the salt surrounding BH-103 over time

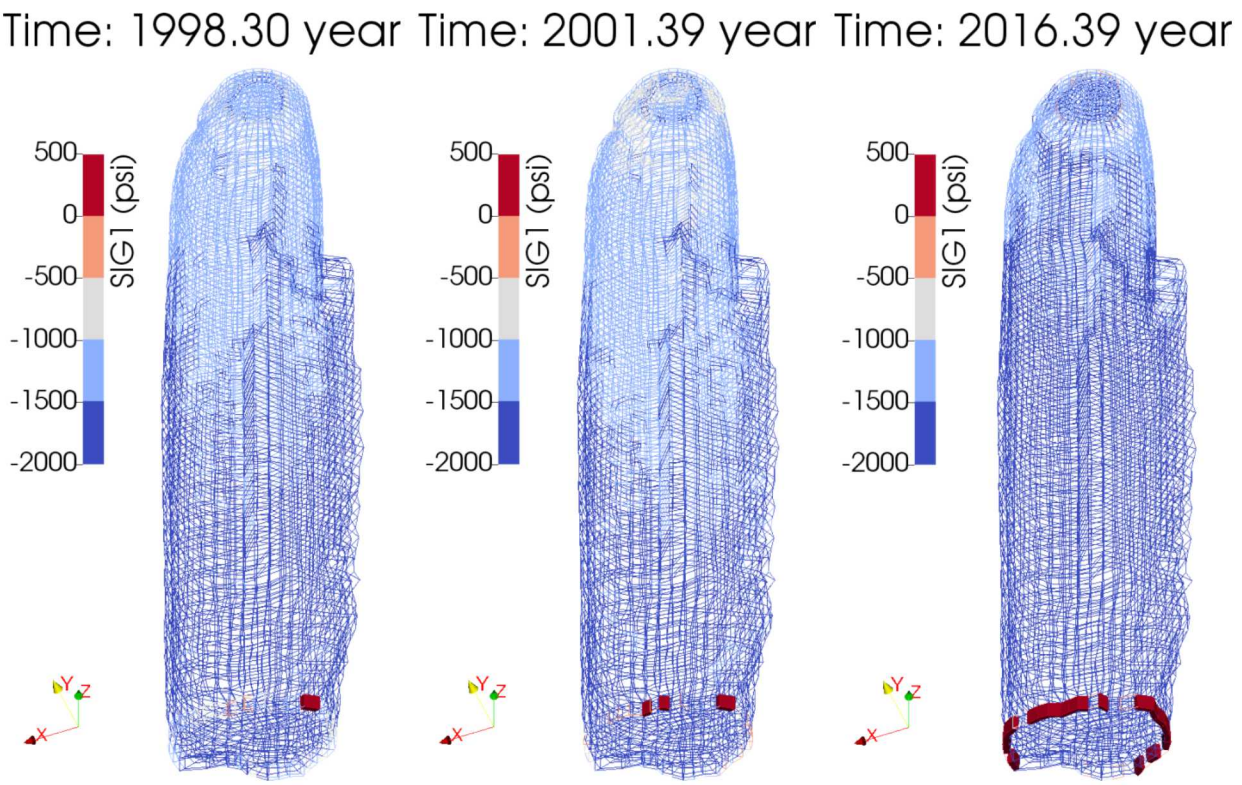

Figure 17. Contour plots of σ1 on 4/20/1998, 5/22/2001, and 5/20/2016 (look up view)

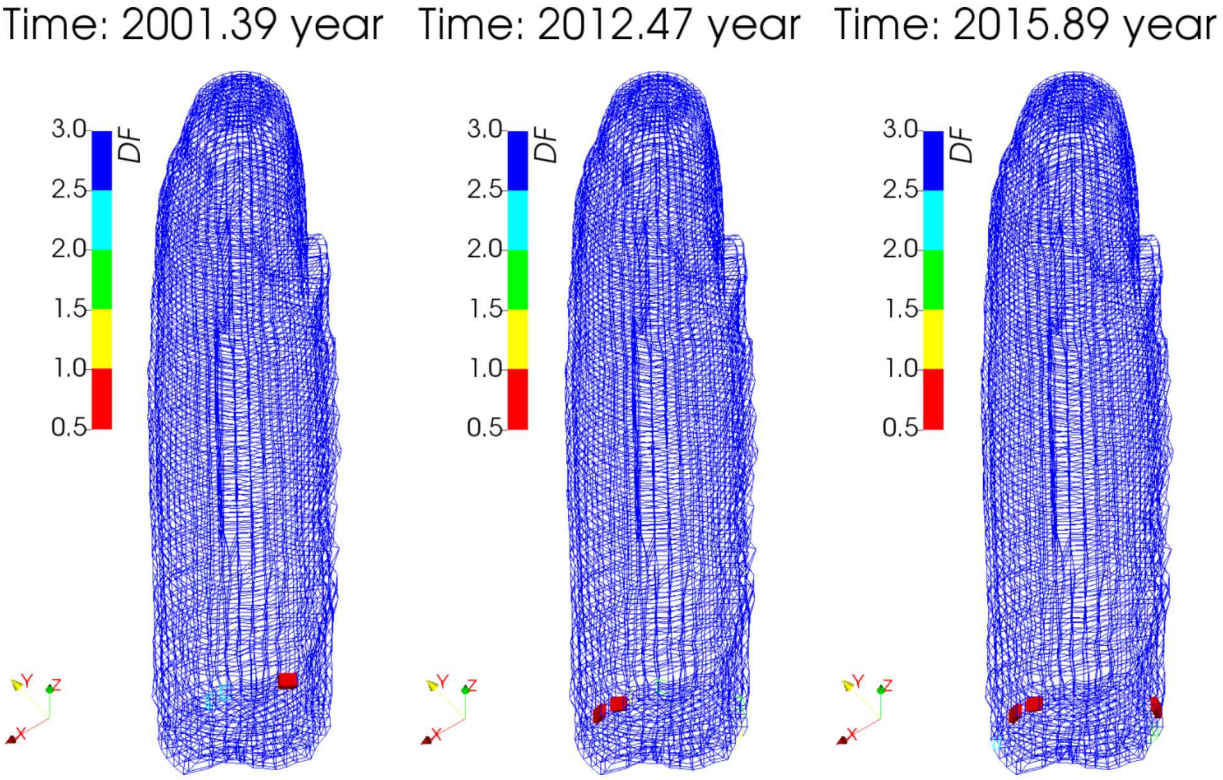

Figure 18. Contour plots of *DF* on 5/22/2001, 6/20/2012, and 11/20/2015 (look up view)

Figure 19 shows the predicted volumetric change (top), and volumetric closure normalized to initial cavern volume (2nd panel), maximum σ_1 (3rd panel), and minimum *DF* (bottom) in the salt volume surrounding BH-103 over time. The initial cavern cavity volume was 13.0 MMB on 11/20/1990 and is predicted to be 11.2 MMB on 9/19/2022. The cavern volume is predicted to decrease by 7.1% over 32 years (11/20/1990 - 9/19/2022).

The maximum σ_1 never reaches a positive (tensile stress state) value through five drawdowns, and the minimum *DF* either never reaches to be less than 1 during every workover until the end of simulation. The maximum σ_1 drops suddenly on 9/18/2017 because the values of that calculated at the corner elements of the cavern floor in the first skin layer were excluded. The largest predicted value of the maximum σ_1 is -148 psi on 8/20/2044 during the workover started on 7/1/2044 for three months. The smallest predicted value of the minimum *DF* is 2.32 on 7/21/2039 during the workover started on 7/1/2039 for three months.

In conclusion, BH-103 is predicted to be structurally stable through the fifth drawdown leach.

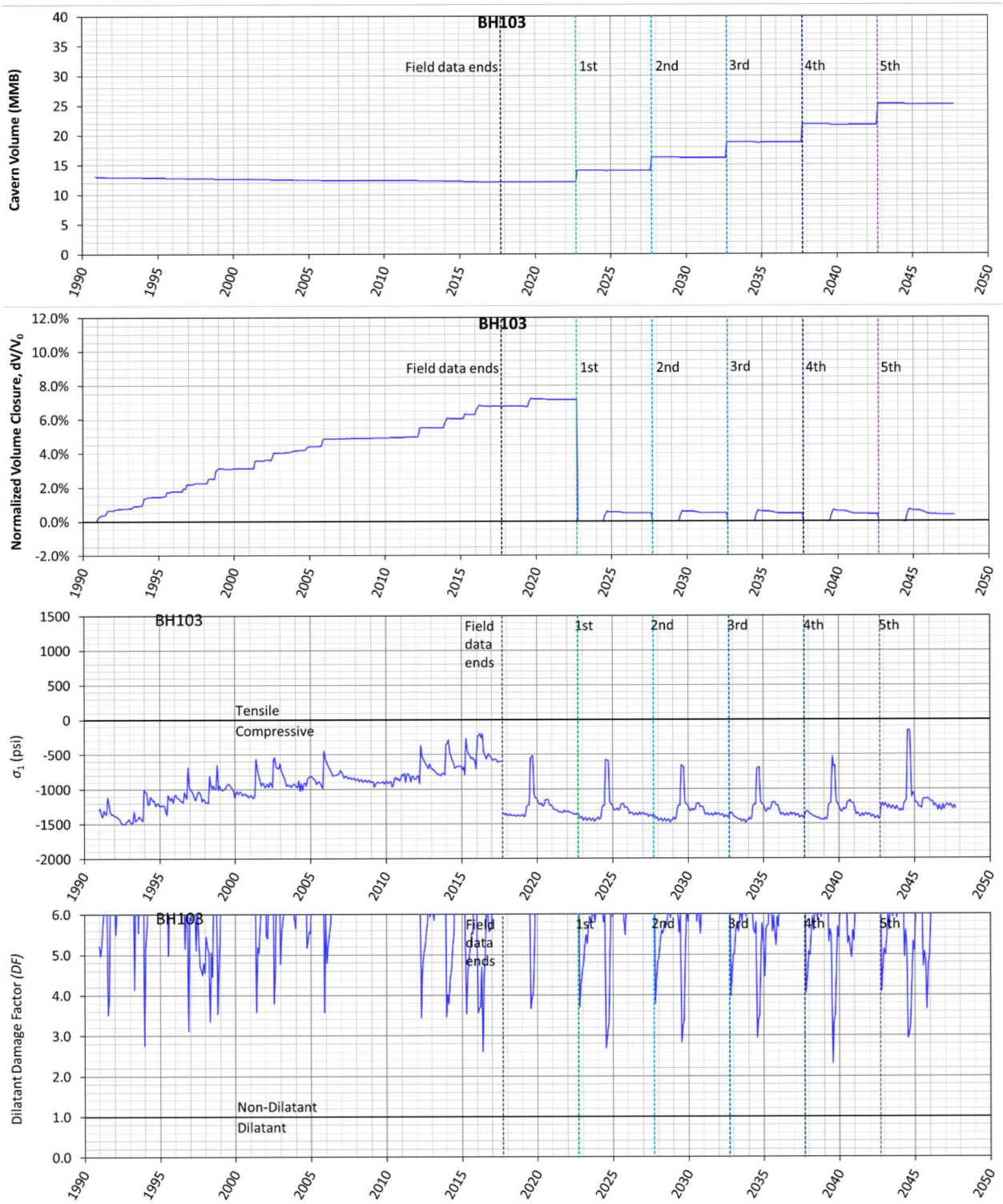

Figure 19. Predicted volumetric change (top), volumetric closure normalized to initial cavern volume of BH-103 (2nd), maximum σ_1 (3rd) and minimum dilatant damage factor (bottom) in the salt surrounding BH-103 over time

4.4. BH-104

Modeling of the leaching process of the caverns is performed by deleting a pre-meshed block of elements along the walls of the cavern so that the cavern volume is increased by 16 percent per drawdown. Figure 20 shows the cavity of BH-104 as developed from sonar data, along with drawdown skins and extra skins. In this simulation, BH-104 is modeled as having five drawdown layers to be removed to account for the future oil drawdown activities.

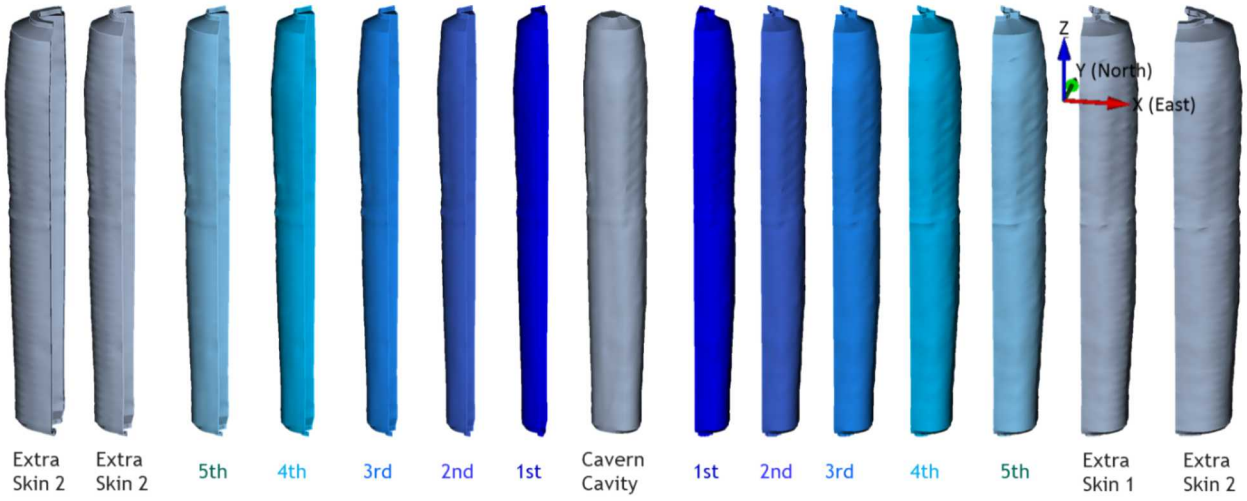

Figure 20. BH-102 cavern cavity with five drawdown skins (leaching layers) and extra skins

Figure 21 shows the predicted volumetric change (top), and volumetric closure normalized to initial cavern volume (2nd panel), maximum σ_1 (3rd panel), and minimum *DF* (bottom) in the salt volume surrounding BH-104 over time. The initial cavern cavity volume was 13.0 MMB on 10/20/1990 and is predicted to be 12.3 MMB on 9/19/2022. The cavern volume is predicted to decrease by 6.7% over 32 years (10/20/1990 - 9/19/2022).

The maximum σ_1 never reaches a positive (tensile stress state) value through five drawdowns, and the minimum *DF* either never reaches to be less than 1 during every workover until the end of simulation. The largest predicted value of the maximum σ_1 is -559 psi on 12/20/2044 during the workover started on 10/1/2044 for 3 months. The smallest predicted value of the minimum *DF* is 2.10 on 1/21/1992 during the workover started on 1/5/1992 for 85 days.

In conclusion, BH-104 is predicted to be structurally stable through the fifth drawdown leach.

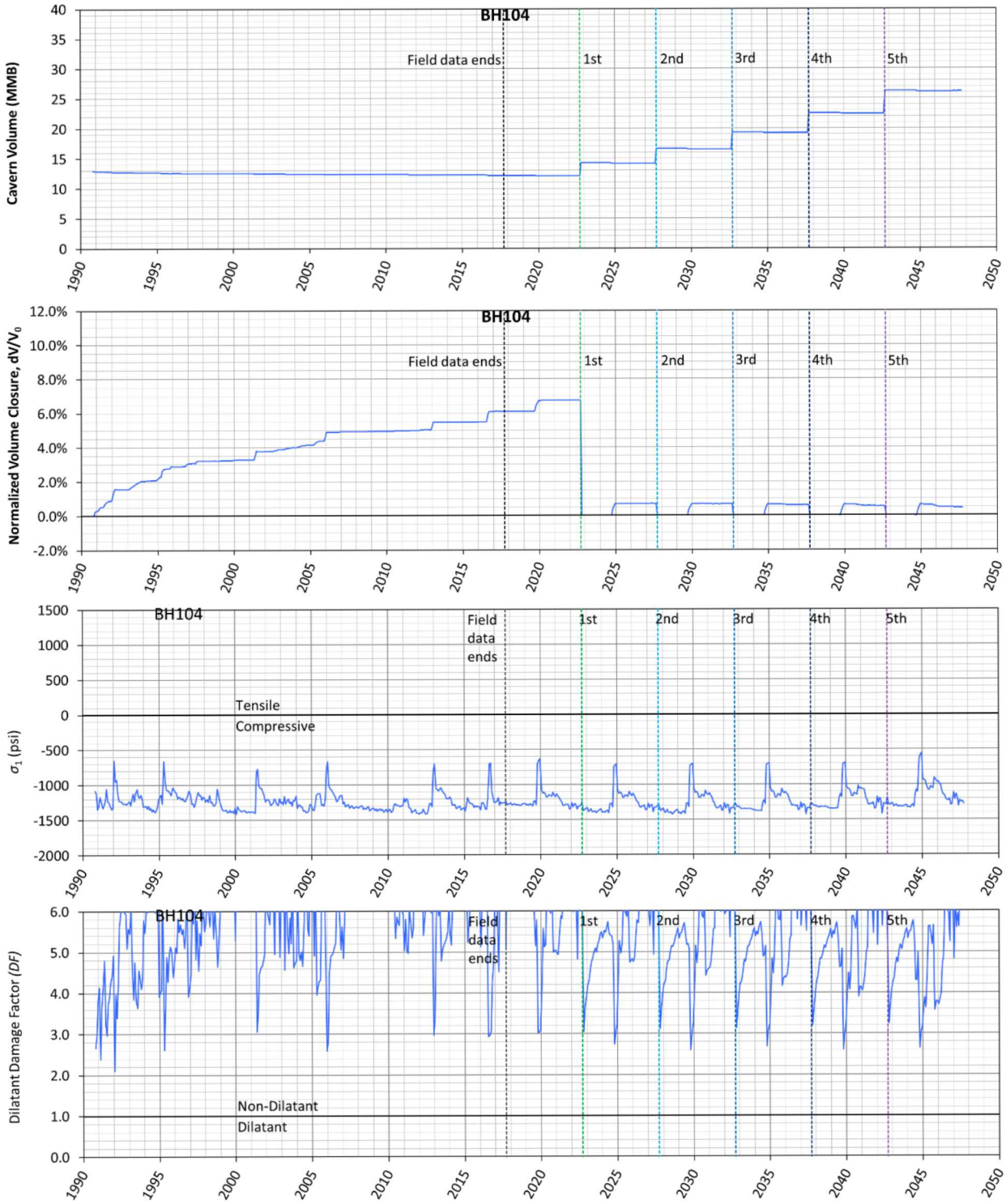

Figure 21. Predicted volumetric change (top), volumetric closure normalized to initial cavern volume of BH-104 (2nd), maximum σ_1 (3rd) and minimum dilatant damage factor (bottom) in the salt surrounding BH-104 over time

4.5. BH-105

Modeling of the leaching process of the caverns is performed by deleting a pre-meshed block of elements along the walls of the cavern so that the cavern volume is increased by 16 percent per drawdown. Figure 22 shows the cavity of BH-105 as developed from sonar data, along with drawdown skins and extra skins. In this simulation, BH-105 is modeled as having five drawdown layers to be removed to account for the future oil drawdown activities.

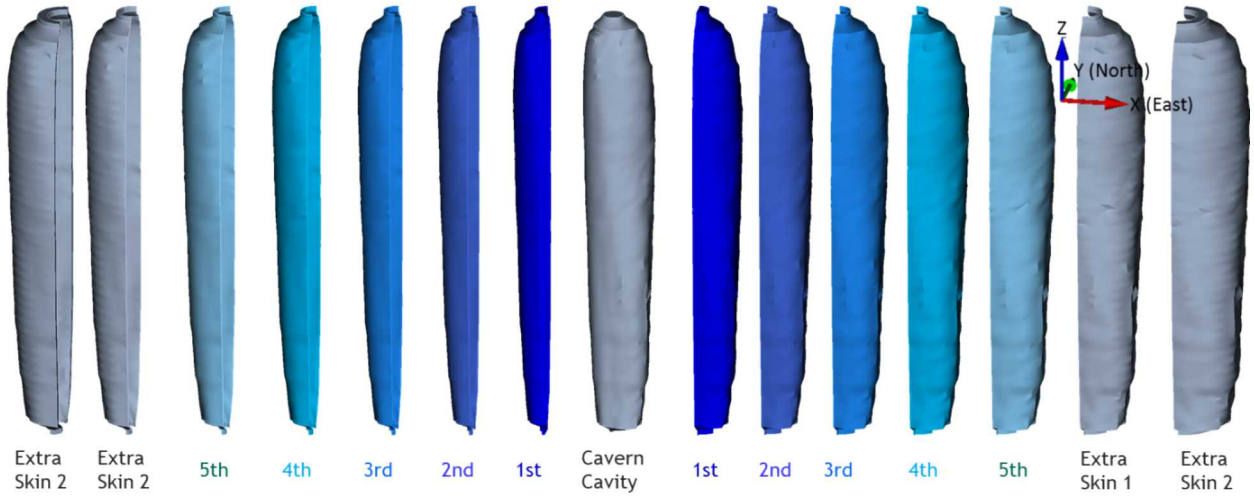

Figure 22. BH-105 cavern cavity with five drawdown skins (leaching layers) and extra skins

Figure 23 shows the predicted volumetric change (top), and volumetric closure normalized to initial cavern volume (2nd panel), maximum σ_1 (3rd panel), and minimum *DF* (bottom) in the salt volume surrounding BH-105 over time. The initial cavern cavity volume was 13.0 MMB on 5/21/1990 and is predicted to be 11.5 MMB on 9/19/2022. The cavern volume is predicted to decrease by 9.3% over 32 years (5/21/1990 - 9/19/2022).

The maximum σ_1 reaches a positive (tensile stress state) value during the workovers started on 5/1/2004 for 65 days. The maximum σ_1 are calculated to be 332 psi on 6/20/2004 (2004.47 year). The value of maximum σ_1 goes up and down with zero until 5/21/2010. The second negative peak appears on 6/22/2011 (2011.47 year) and calculated to be 730 psi. The positive value persists until the first drawdown starts. The positive peaks appear during the workovers after each drawdown leach. The maximum σ_1 are calculated to be 193, 343, 779, 1391, and 2158 psi at 2025.22, 2030.22 2035.22, 2040.22, and 2045.22 years, respectively. Figure 24 shows the contour plots of σ_1 on the specific times to show the area in tension in the cavern skin layers during the workovers at 2004.47, 2011.47, 2020.22, and 2045.22 years. The areas in tensile state are located at the floor edge and on the sloping floor. The tensile state may occur because of the geometry of the edge and floor, but not vertical wall.

The minimum *DF* reaches less than 1 (onset of dilatant damage) during the workovers started on 5/1/2004 for 65 days when the maximum σ_1 reaches a positive (tensile stress state) value simultaneously. The minimum *DF* is calculated to be 0.99 on 6/20/2004 (2004.47 year). The peak values of *DF* appear during every workover as shown in Figure 23. The minimum *DF* are calculated to be 0.13, 0.14, and 0.07 at 2014.05, 2021.80, and 2045.89 years, respectively. Figure 25 shows the contour plots of *DF* at specific times to show the areas in dilatant damage

state (DF<1) in the cavern skin layers after each drawdown leach. The areas in dilatant damaged are located at the floor edge. The dilatant state may occur because of the geometry of the edge of floor, but not vertical wall. This implies it does not affect the cavern structural stability.

In conclusion, BH-105 may be structurally stable until the fifth drawdown leach. However, the dilatant damaged areas in tensile stress state are created on the edge and sloping floor of the cavern during the workovers. Therefore, we need to re-examine the cavern stability with a new cavern volume after a drawdown leach completes in future.

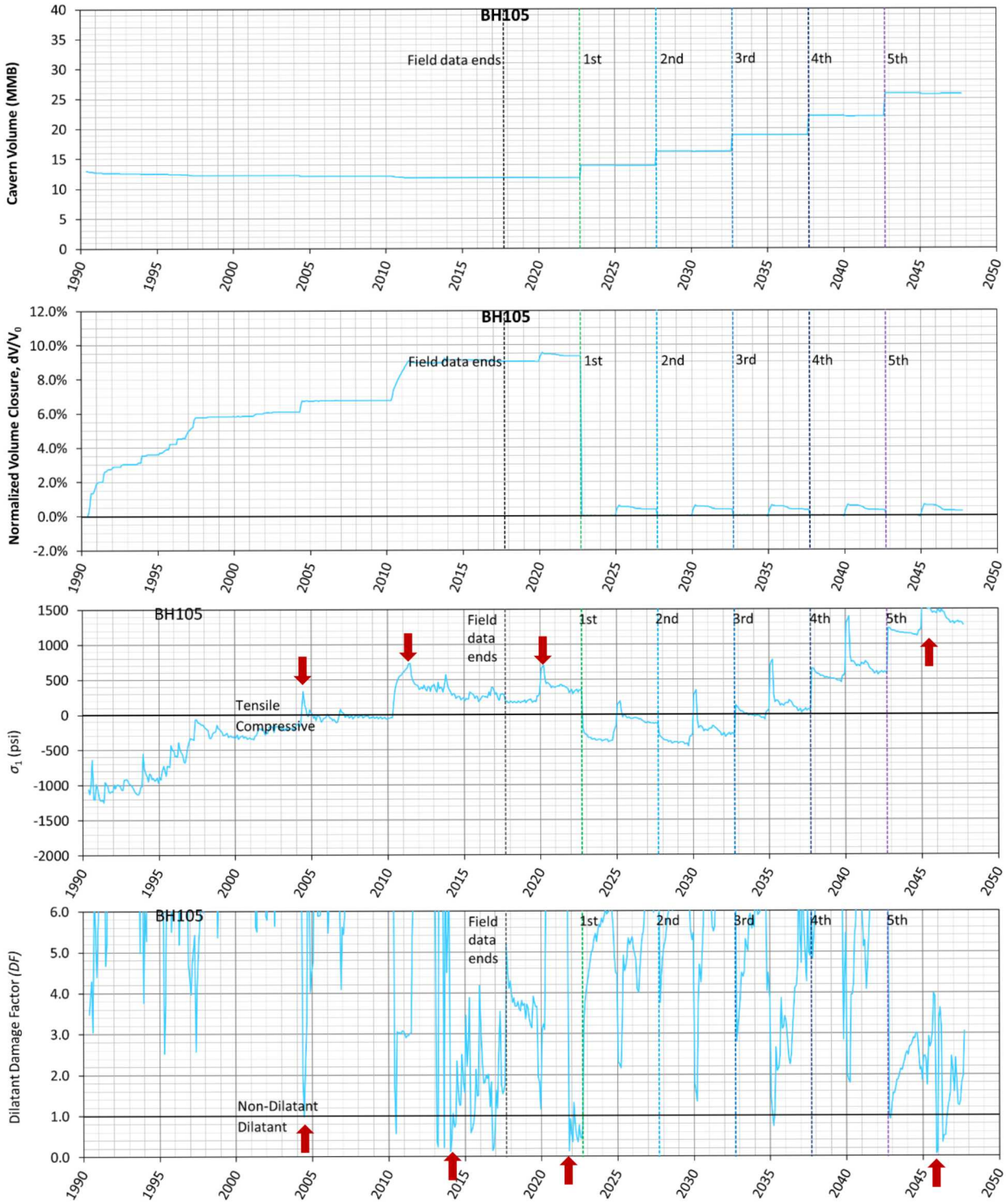

Figure 23. Predicted volumetric change (top), volumetric closure normalized to initial cavern volume of BH-105 (2nd), maximum σ_1 (3rd) and minimum dilatant damage factor (bottom) in the salt surrounding BH-105 over time

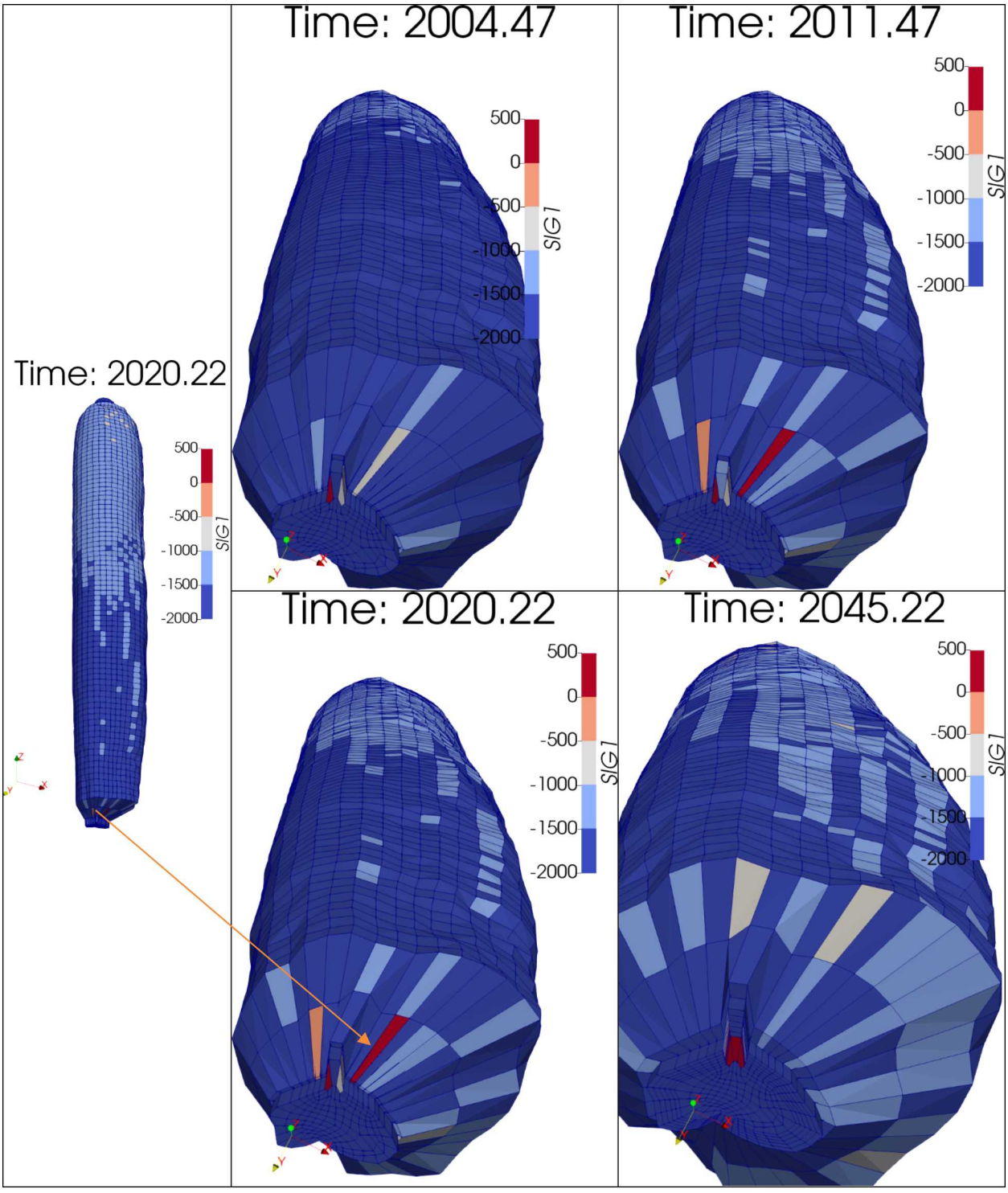

Figure 24. Contour plots of σ_1 on specific dates. Areas in tensile state are shown in red ($\sigma_1 > 0$). Each value of maximum σ_1 are indicated by each arrow at each specific time on the 3rd panel in Figure 23Figure 10

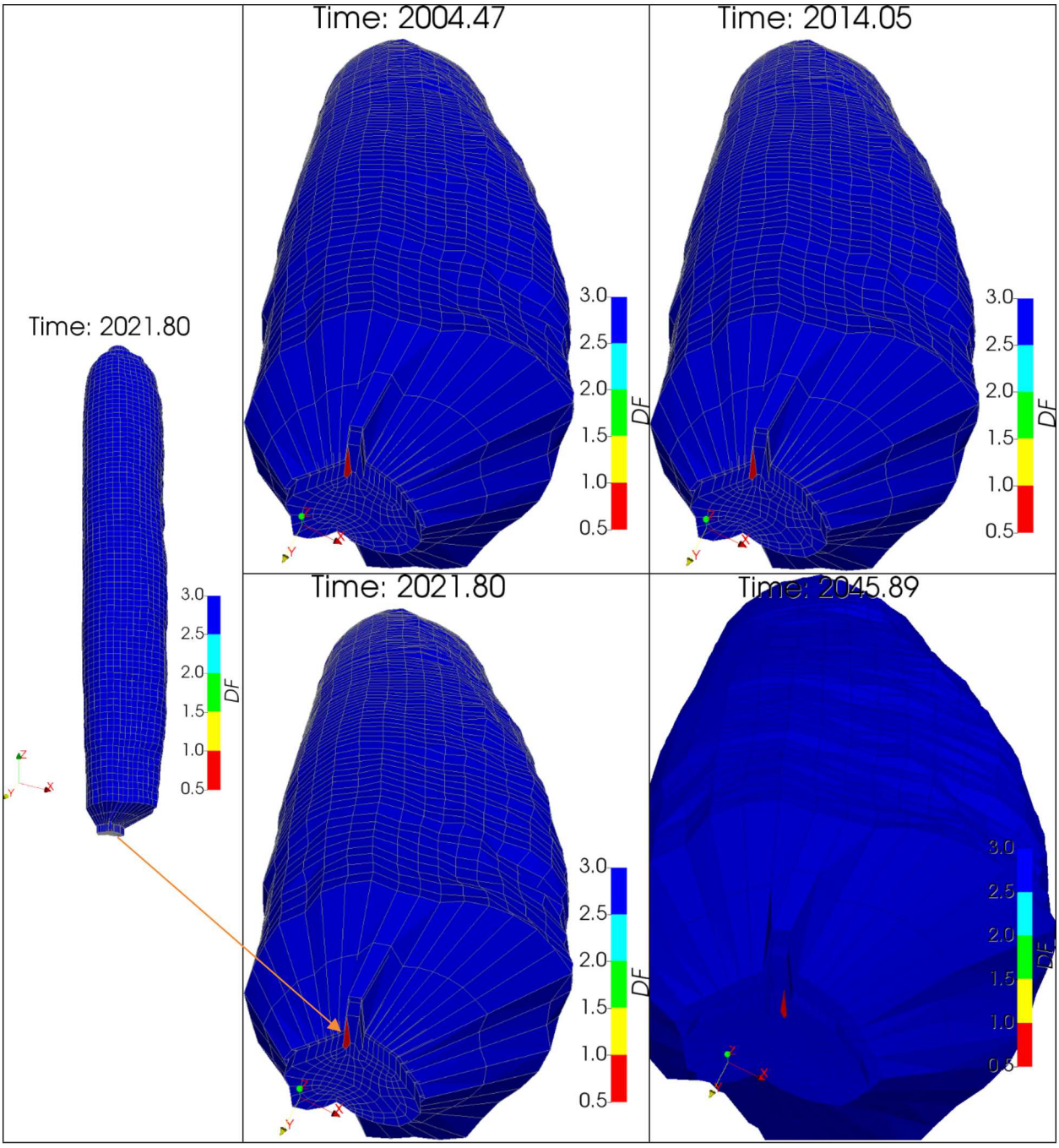

Figure 25. Contour plots of *DF* on specific dates. Areas in dilatant are shown in red (*DF* < 1). Each value of minimum *DF* is indicated by each arrow at each specific time on the bottom panel in Figure 23

4.6. BH-106

Modeling of the leaching process of the caverns is performed by deleting a pre-meshed block of elements along the walls of the cavern so that the cavern volume is increased by 16 percent per drawdown. Figure 26 shows the cavity of BH-106 as developed from sonar data, along with drawdown skins and extra skins. In this simulation, BH-106 is modeled as having five drawdown layers to be removed to account for the future oil drawdown activities.

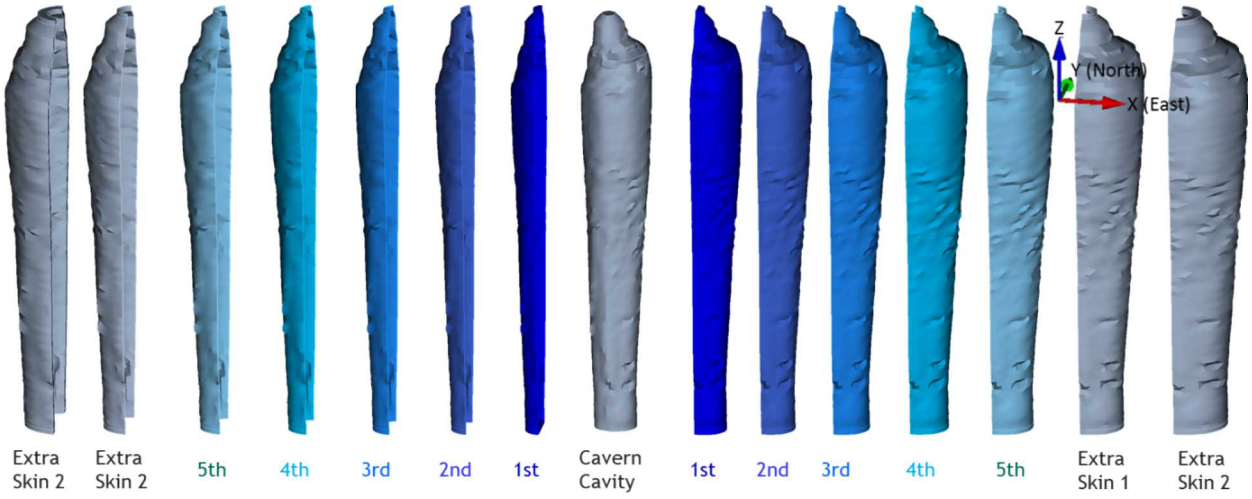

Figure 26. BH-106 cavern cavity with five drawdown skins (leaching layers) and extra skins

Figure 27 shows the predicted volumetric change (top), and volumetric closure normalized to initial cavern volume (2nd panel), maximum σ_1 (3rd panel), and minimum *DF* (bottom) in the salt volume surrounding BH-106 over time. The initial cavern cavity volume was 13.1 MMB on 10/20/1990 and is predicted to be 12.4 MMB on 9/19/2022. The cavern volume is predicted to decrease by 5.2% over 32 years (12/20/1990 - 9/19/2022).

The maximum σ_1 never reaches a positive (tensile stress state) value through five drawdowns, and the minimum *DF* either never reaches to be less than 1 during every workover until the end of simulation. The largest predicted value of the maximum σ_1 is -297 psi on 6/20/2045 during the workover started on 4/1/2045 for three months. The smallest predicted value of the minimum *DF* is 2.16 on 4/22/1991 during the workover started on 4/15/1991 for 20 days.

In conclusion, BH-106 is predicted to be structurally stable through the fifth drawdown leach.

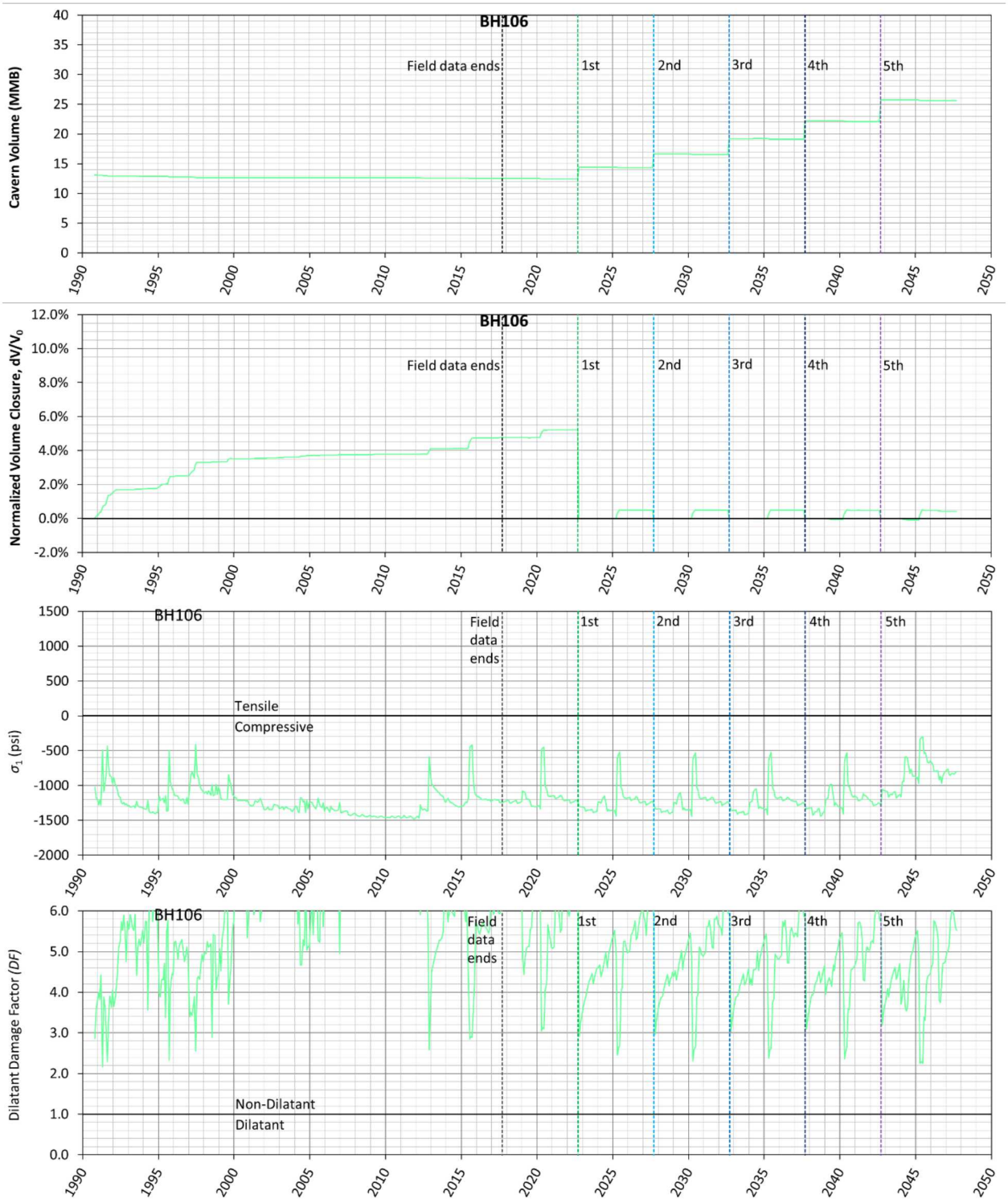

Figure 27. Predicted volumetric change (top), volumetric closure normalized to initial cavern volume of BH-106 (2nd), maximum σ_1 (3rd) and minimum dilatant damage factor (bottom) in the salt surrounding BH-106 over time

4.7. BH-107

Modeling of the leaching process of the caverns is performed by deleting a pre-meshed block of elements along the walls of the cavern so that the cavern volume is increased by 16 percent per drawdown. Figure 28 shows the cavity of BH-107 as developed from sonar data, along with drawdown skins and extra skins. In this simulation, BH-107 is modeled as having five drawdown layers to be removed to account for the future oil drawdown activities.

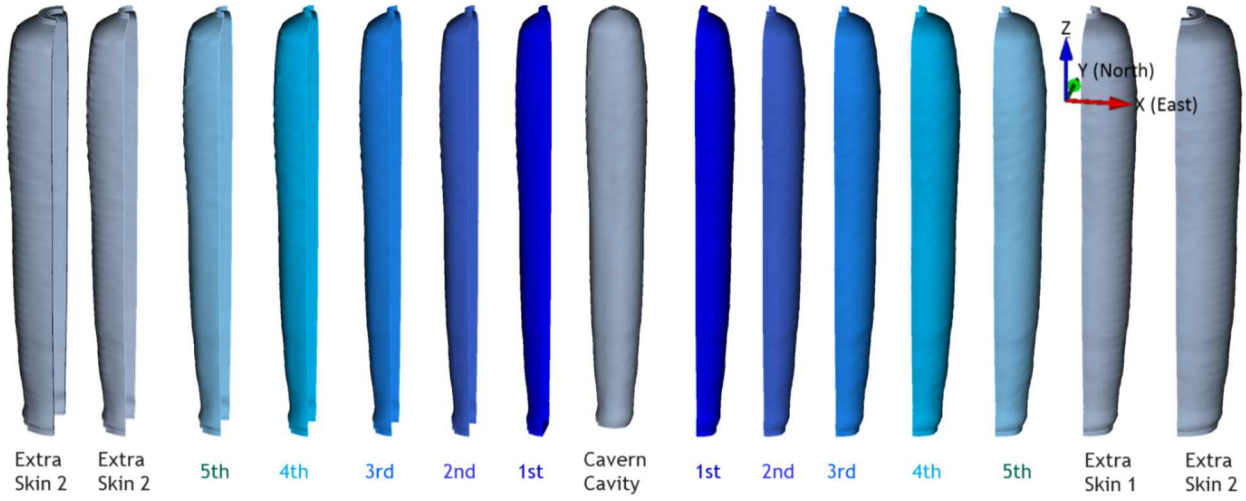

Figure 28. BH-107 cavern cavity with five drawdown skins (leaching layers) and extra skins

Figure 29 shows the predicted volumetric change (top), and volumetric closure normalized to initial cavern volume (2nd panel), maximum σ_1 (3rd panel), and minimum *DF* (bottom) in the salt volume surrounding BH-107 over time. The initial cavern cavity volume was 12.9 MMB on 4/20/1990 and is predicted to be 11.9 MMB on 9/19/2022. The cavern volume is predicted to decrease by 6.7% over 32 years (4/20/1990 - 9/19/2022).

The maximum σ_1 never reaches a positive (tensile stress state) value through five drawdowns, and the minimum *DF* either never reaches to be less than 1 during every workover until the end of simulation. The largest predicted value of the maximum σ_1 is -691 psi on 8/21/1991 during the workover started on 7/22/1991 for 60 days. The smallest predicted value of the minimum *DF* is 2.66 on 7/21/2035 during the workover started on 7/1/2035 for three months.

In conclusion, BH-107 is predicted to be structurally stable through the fifth drawdown leach.

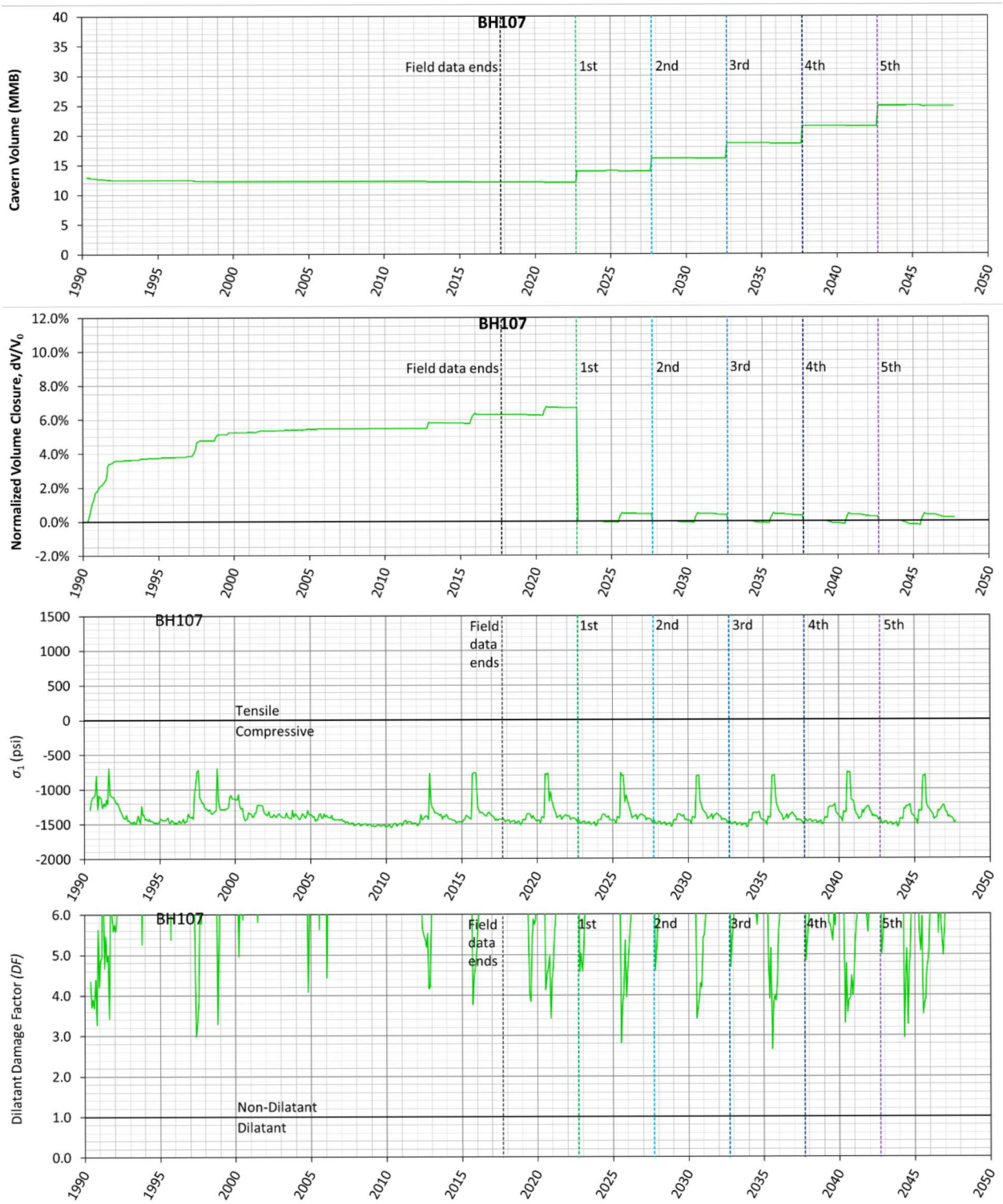

Figure 29. Predicted volumetric change (top), volumetric closure normalized to initial cavern volume of BH-107 (2nd), maximum σ_1 (3rd) and minimum dilatant damage factor (bottom) in the salt surrounding BH-107 over time

4.8. BH-108

Modeling of the leaching process of the caverns is performed by deleting a pre-meshed block of elements along the walls of the cavern so that the cavern volume is increased by 16 percent per drawdown. Figure 30 shows the cavity of BH-108 as developed from sonar data, along with drawdown skins and extra skins. In this simulation, BH-108 is modeled as having five drawdown layers to be removed to account for the future oil drawdown activities.

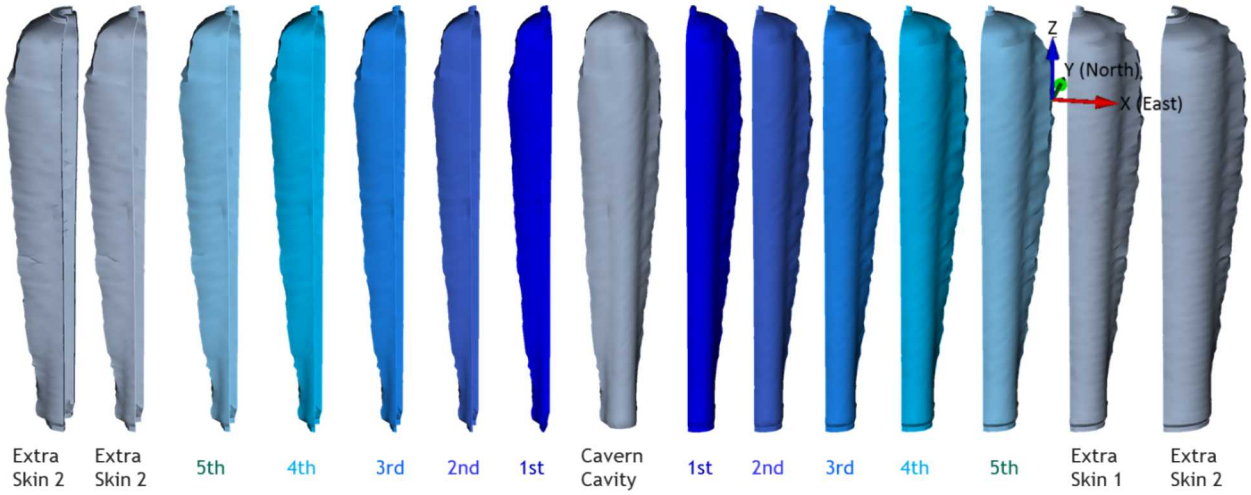

Figure 30. BH-108 cavern cavity with five drawdown skins (leaching layers) and extra skins

Figure 31 shows the predicted volumetric change (top), and volumetric closure normalized to initial cavern volume (2nd panel), maximum σ_1 (3rd panel), and minimum *DF* (bottom) in the salt volume surrounding BH-108 over time. The initial cavern cavity volume was 12.4 MMB on 6/20/1990 and is predicted to be 11.7 MMB on 9/19/2022. The cavern volume is predicted to decrease by 6.0% over 32 years (6/20/1990 - 9/19/2022).

The maximum σ_1 never reaches a positive (tensile stress state) value through five drawdowns, and the minimum *DF* either never reaches to be less than 1 during every workover until the end of simulation. The largest predicted value of the maximum σ_1 is -254 psi on 12/20/2020 during the workover started on 10/1/2020 for three months. The smallest predicted value of the minimum *DF* is 2.66 on 9/20/1998 during the workover started on 9/3/1998 for 88 days.

In conclusion, BH-108 is predicted to be structurally stable through the fifth drawdown leach.

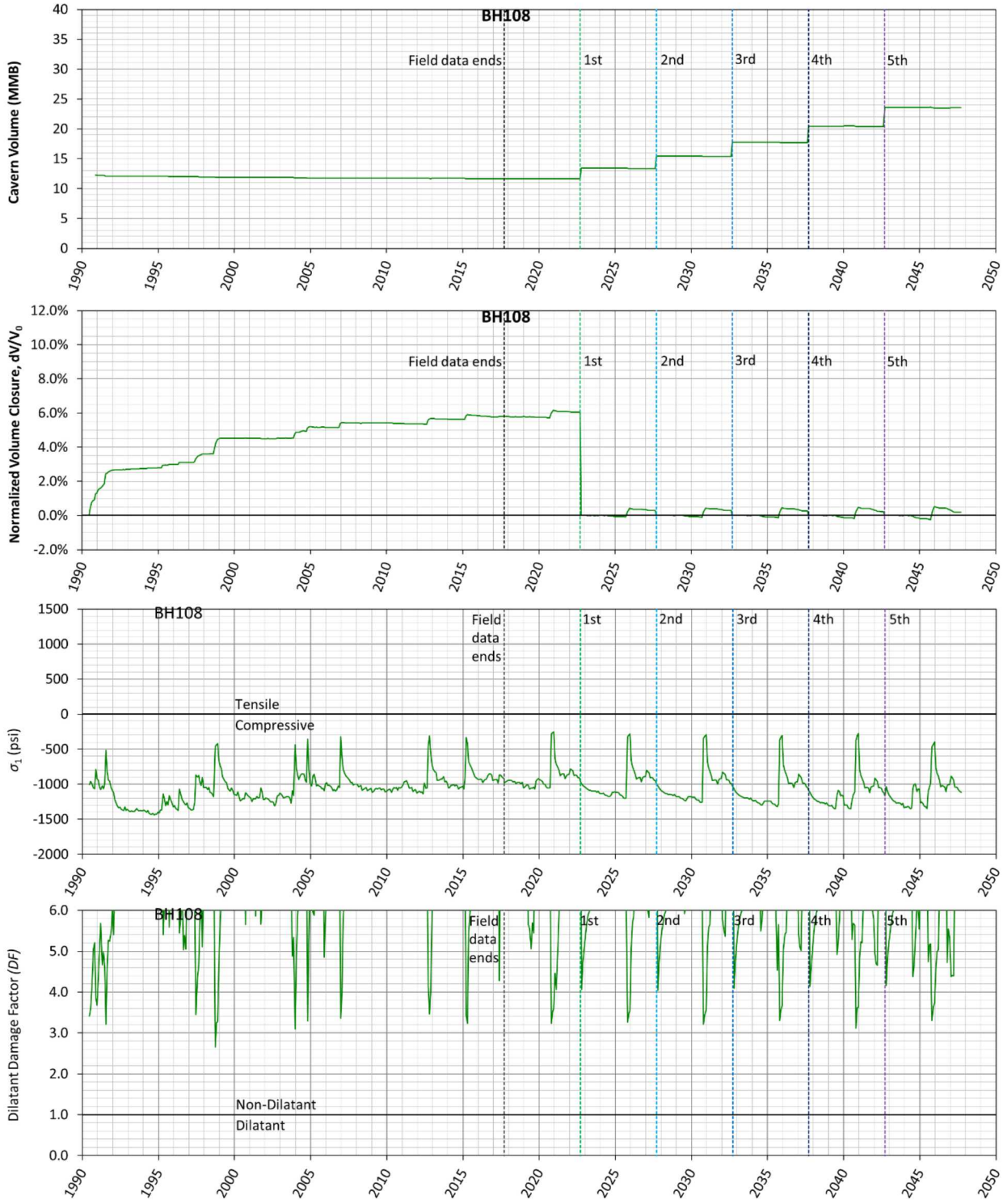

Figure 31. Predicted volumetric change (top), volumetric closure normalized to initial cavern volume of BH-108 (2nd), maximum σ_1 (3rd) and minimum dilatant damage factor (bottom) in the salt surrounding BH-108 over time

4.9. BH-109

Modeling of the leaching process of the caverns is performed by deleting a pre-meshed block of elements along the walls of the cavern so that the cavern volume is increased by 16 percent per drawdown. Figure 32 shows the cavity of BH-109 as developed from sonar data, along with drawdown skins and extra skins. In this simulation, BH-109 is modeled as having five drawdown layers to be removed to account for the future oil drawdown activities.

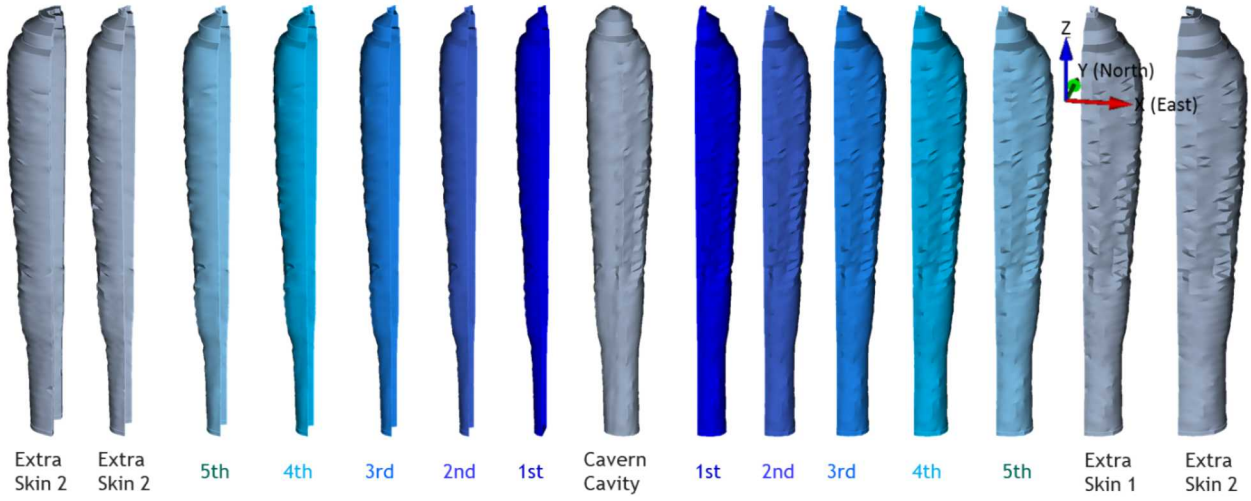

Figure 32. BH-109 cavern cavity with five drawdown skins (leaching layers) and extra skins

Figure 33 shows the predicted volumetric change (top), and volumetric closure normalized to initial cavern volume (2nd panel), maximum σ_1 (3rd panel), and minimum *DF* (bottom) in the salt volume surrounding BH-109 over time. The initial cavern cavity volume was 13.4 MMB on 7/21/1990 and is predicted to be 12.5 MMB on 9/19/2022. The cavern volume is predicted to decrease by 6.8% over 32 years (7/21/1990 - 9/19/2022).

The maximum σ_1 never reaches a positive (tensile stress state) value through five drawdowns, and the minimum *DF* either never reaches to be less than 1 during every workover until the end of simulation. The largest predicted value of the maximum σ_1 is -455 psi on 3/22/2046 during the workover started on 1/1/2046 for three months. The smallest predicted value of the minimum *DF* is 2.47 on 1/20/2046 during the workover started on 1/1/2046 for three months.

In conclusion, BH-109 is predicted to be structurally stable through the fifth drawdown leach.

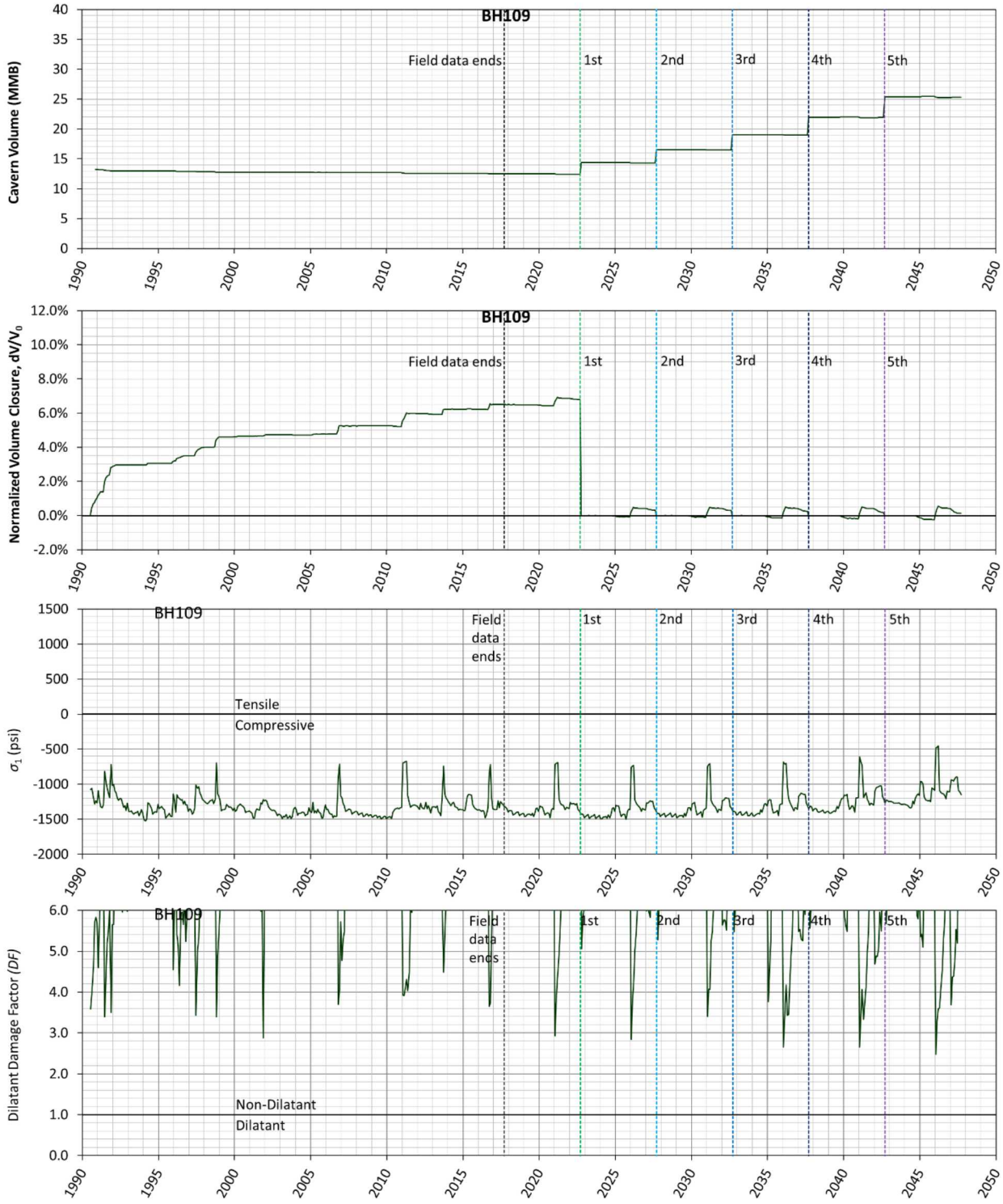

Figure 33. Predicted volumetric change (top), volumetric closure normalized to initial cavern volume of BH-109 (2nd), maximum σ_1 (3rd) and minimum dilatant damage factor (bottom) in the salt surrounding BH-109 over time

4.10. BH-110

Modeling of the leaching process of the caverns is performed by deleting a pre-meshed block of elements along the walls of the cavern so that the cavern volume is increased by 16 percent per drawdown. Figure 34 shows the cavity of BH-110 as developed from sonar data, along with drawdown skins and extra skins. In this simulation, BH-110 is modeled as having five drawdown layers to be removed to account for the future oil drawdown activities.

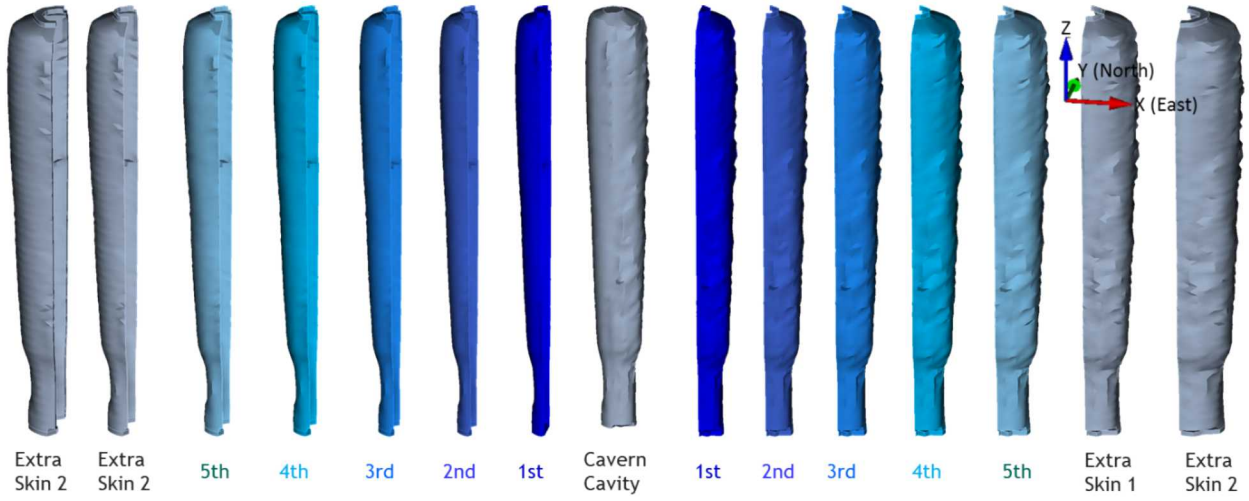

Figure 34. BH-110 cavern cavity with five drawdown skins (leaching layers) and extra skins

Figure 35 shows the predicted volumetric change (top), and volumetric closure normalized to initial cavern volume (2nd panel), maximum σ_1 (3rd panel), and minimum *DF* (bottom) in the salt volume surrounding BH-110 over time. The initial cavern cavity volume was 13.1 MMB on 4/20/1990 and is predicted to be 12.1 MMB on 9/19/2022. The cavern volume is predicted to decrease by 8.0% over 32 years (4/20/1990 - 9/19/2022).

The maximum σ_1 reaches a positive (tensile stress state) value during the workovers started on 4/1/2026 for three months. The maximum σ_1 are calculated to be 466 psi on 6/20/2026 (2026.47 year). The value of maximum σ_1 goes up and down with zero between 10/21/2022 and 4/20/2026. Figure 36 shows the contour plots of σ_1 on the specific times to show the area in tension on the cavern skin layer. Each value of maximum σ_1 are indicated by each arrow at each specific time on the 3rd panel in Figure 35. The area in tensile state is located at the floor edge. The tensile state may occur because of the geometry of the floor edge, but not vertical wall. This implies it does not affect the cavern structural stability. The minimum *DF* either never reaches to be less than 1 during every workover until the end of simulation.

In conclusion, BH-110 may be structurally stable until the fifth drawdown leach. However, the areas in tensile stress state are created on the floor edge of the cavern during the workovers. Therefore, we need to re-examine the cavern stability with a new cavern volume after a drawdown leach completes in future.

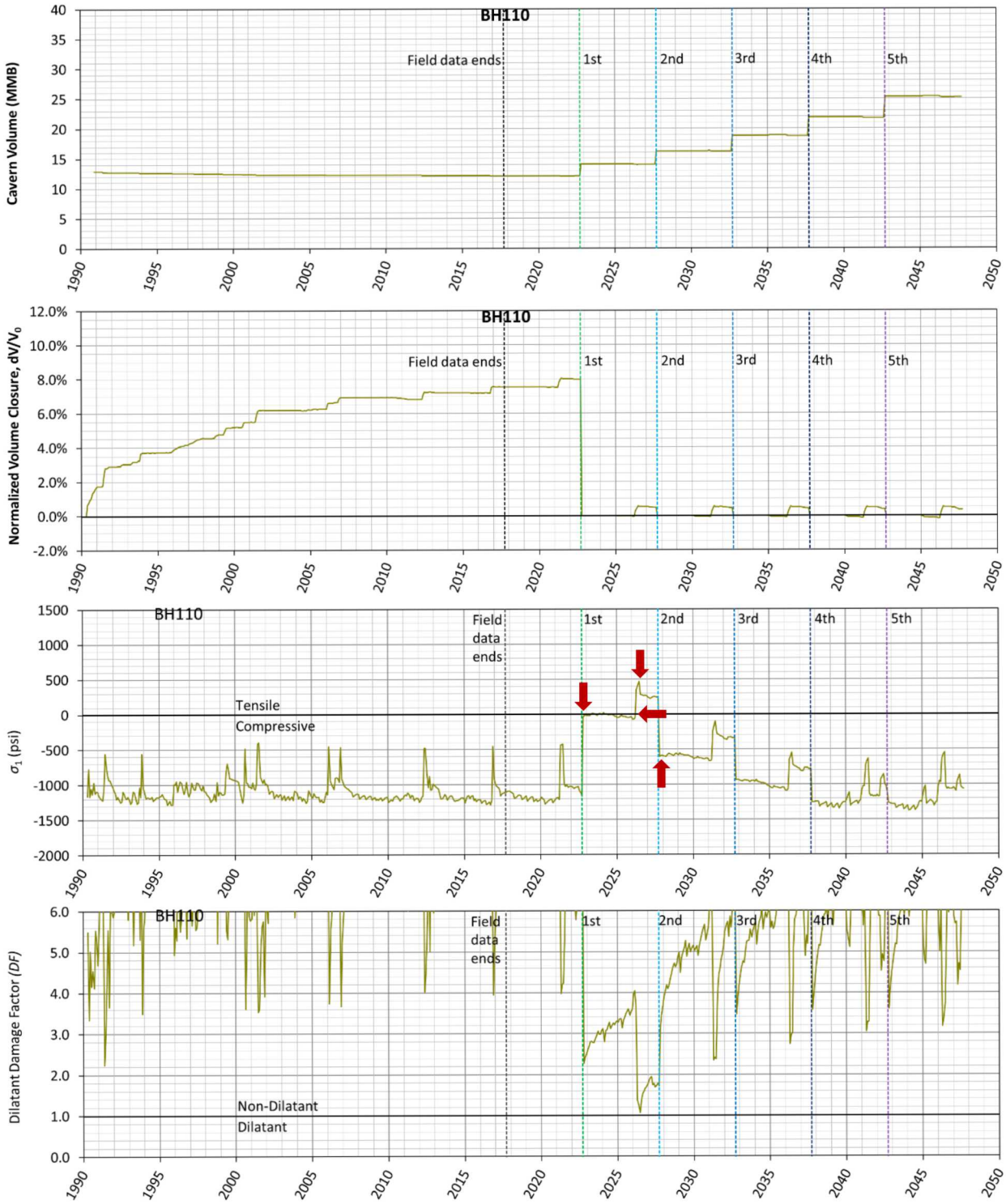

Figure 35. Predicted volumetric change (top), volumetric closure normalized to initial cavern volume of BH-110 (2nd), maximum σ_1 (3rd) and minimum dilatant damage factor (bottom) in the salt surrounding BH-110 over time

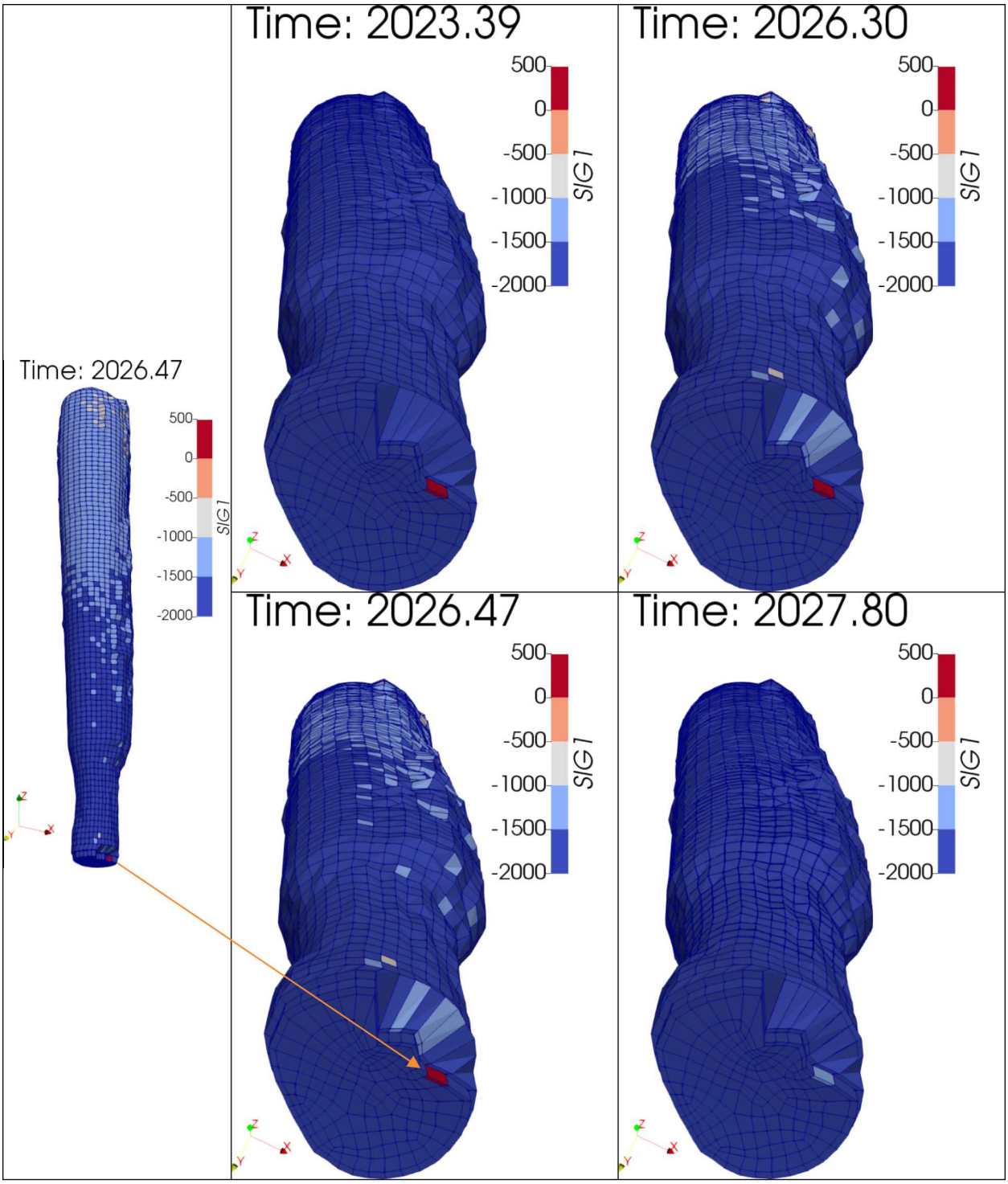

Figure 36. Contour plots of σ_1 on specific dates. Areas in tensile state are shown in red ($\sigma_1 > 0$). Each value of maximum σ_1 are indicated by each arrow at each specific time on the 3rd panel in Figure 35Figure 10

4.11. BH-111

Modeling of the leaching process of the caverns is performed by deleting a pre-meshed block of elements along the walls of the cavern so that the cavern volume is increased by 16 percent per drawdown. Figure 37 shows the cavity of BH-111 as developed from sonar data, along with drawdown skins and extra skins. In this simulation, BH-111 is modeled as having five drawdown layers to be removed to account for the future oil drawdown activities.

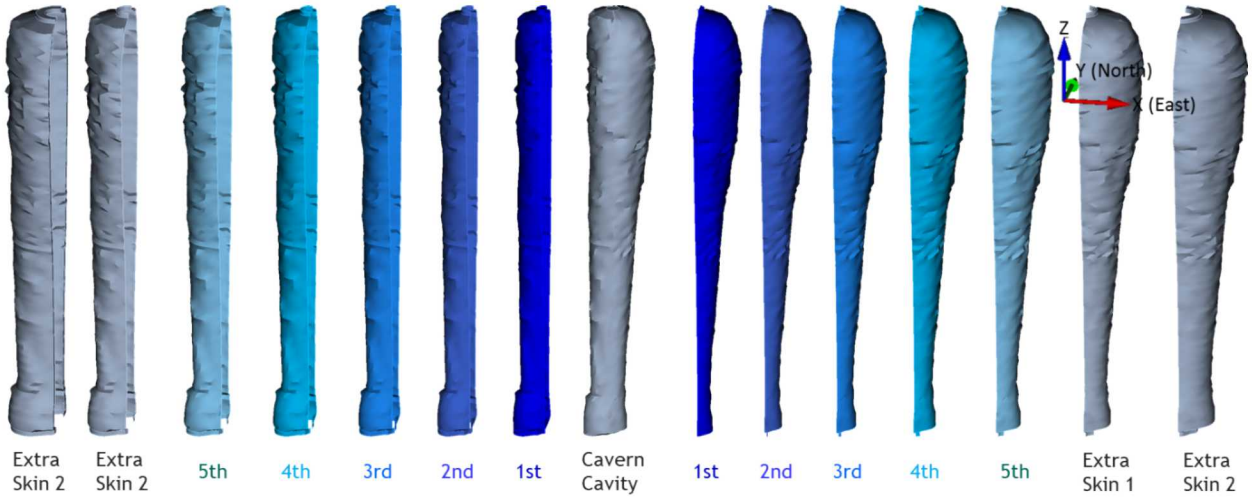

Figure 37. BH-111 cavern cavity with five drawdown skins (leaching layers) and extra skins

Figure 38 shows the predicted volumetric change (top), and volumetric closure normalized to initial cavern volume (2nd panel), maximum σ_1 (3rd panel), and minimum *DF* (bottom) in the salt volume surrounding BH-111 over time. The initial cavern cavity volume was 13.2 MMB on 7/21/1991 and is predicted to be 13.0 MMB on 9/19/2022. The cavern volume is predicted to decrease by 1.9% over 31 years (7/21/1991 - 9/19/2022). The amount of volume closure is smaller than that of other SPR caverns because the lower volume of cavity is relatively small. The creep closure rate increases with depth because the difference between lithostatic and cavern internal pressures increases.

The maximum σ_1 never reaches a positive (tensile stress state) value through five drawdowns, and the minimum *DF* either never reaches to be less than 1 during every workover until the end of simulation. The largest predicted value of the maximum σ_1 is -416 psi on 9/20/2021 during the workover started on 7/1/2021 for three months. The smallest predicted value of the minimum *DF* is 1.36 on 7/22/2036 during the workover started on 7/1/2036 for three months.

In conclusion, BH-111 is predicted to be structurally stable through the fifth drawdown leach.

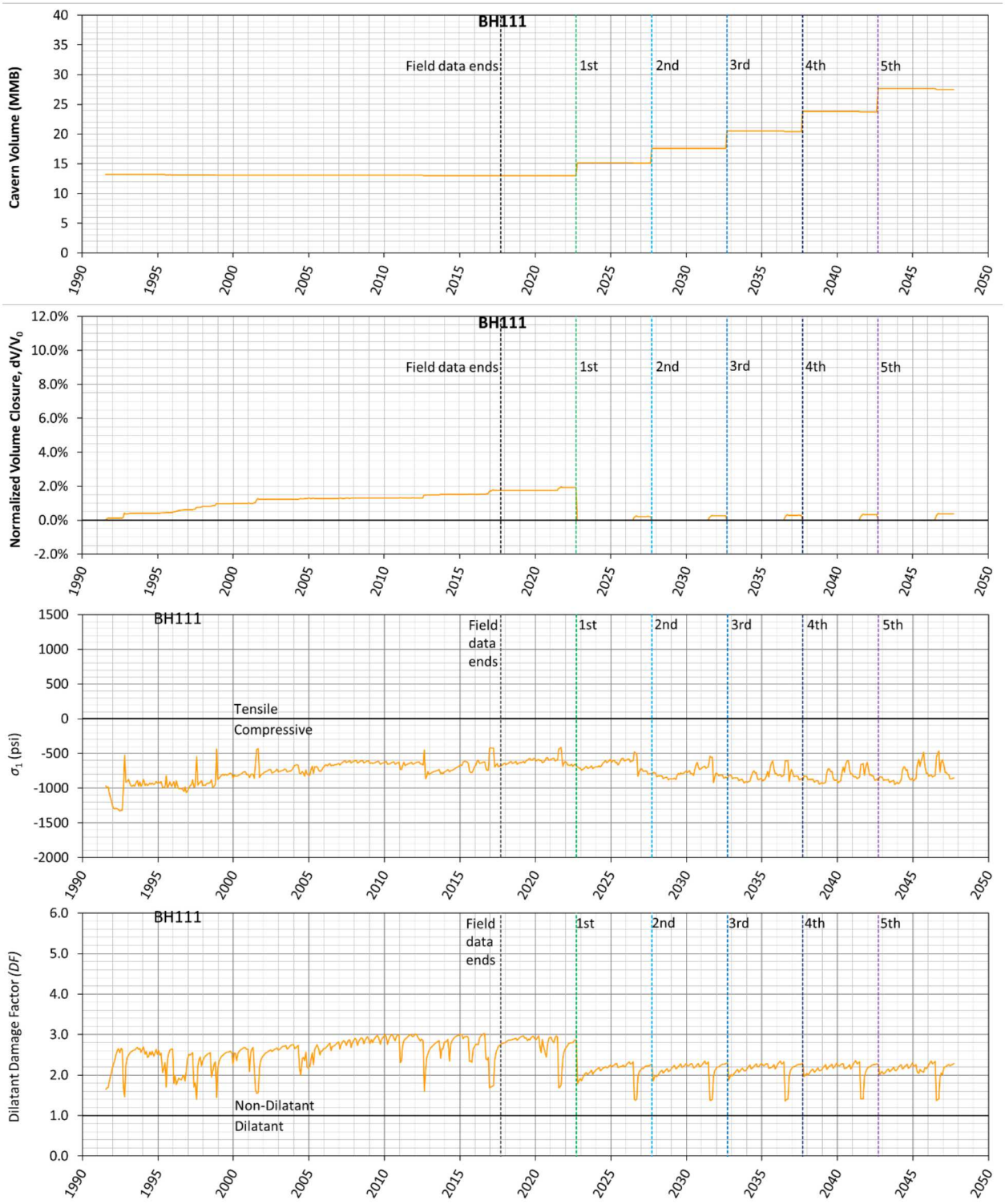

Figure 38. Predicted volumetric change (top), volumetric closure normalized to initial cavern volume of BH-111 (2nd), maximum σ_1 (3rd) and minimum dilatant damage factor (bottom) in the salt surrounding BH-111 over time

4.12. BH-112

Modeling of the leaching process of the caverns is performed by deleting a pre-meshed block of elements along the walls of the cavern so that the cavern volume is increased by 16 percent per drawdown. Figure 39 shows the cavity of BH-112 as developed from sonar data, along with drawdown skins and extra skins. In this simulation, BH-112 is modeled as having five drawdown layers to be removed to account for the future oil drawdown activities.

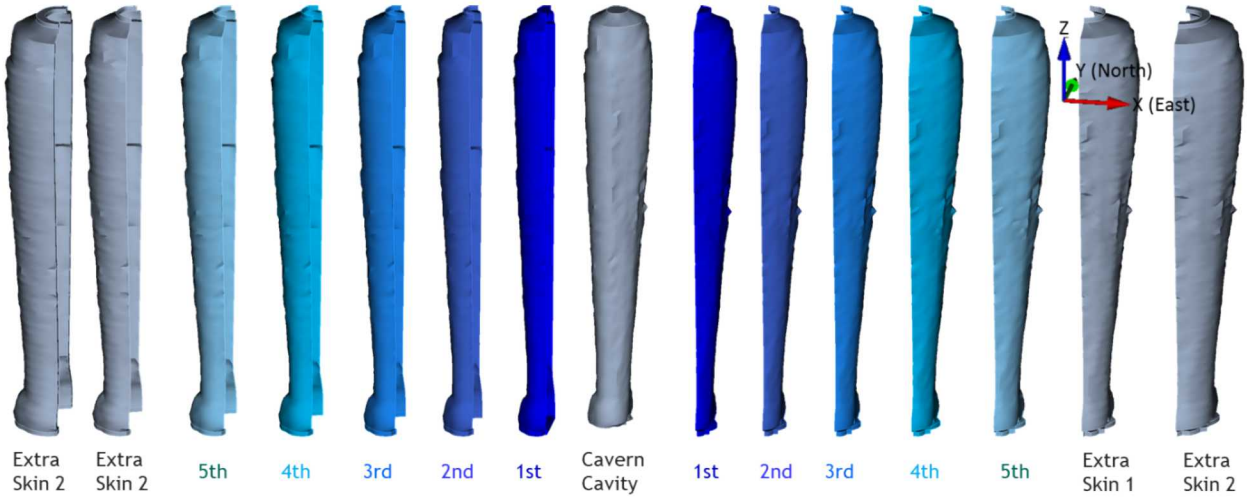

Figure 39. BH-112 cavern cavity with five drawdown skins (leaching layers) and extra skins

Figure 40 shows the predicted volumetric change (top), and volumetric closure normalized to initial cavern volume (2nd panel), maximum σ_1 (3rd panel), and minimum *DF* (bottom) in the salt volume surrounding BH-112 over time. The initial cavern cavity volume was 13.1 MMB on 6/21/1991 and is predicted to be 12.6 MMB on 9/19/2022. The cavern volume is predicted to decrease by 3.8% over 31 years (6/21/1991 - 9/19/2022). The amount of volume closure is relatively small because the lower volume of cavity is small like BH-111.

The maximum σ_1 never reaches a positive (tensile stress state) value through five drawdowns, and the minimum *DF* either never reaches to be less than 1 during every workover until the end of simulation. The largest predicted value of the maximum σ_1 is -170 psi on 12/21/2021 during the workover started on 10/1/2021 for three months. The smallest predicted value of the minimum *DF* is 1.56 on 10/21/2026 during the workover started on 10/1/2026 for three months.

In conclusion, BH-112 is predicted to be structurally stable through the fifth drawdown leach.

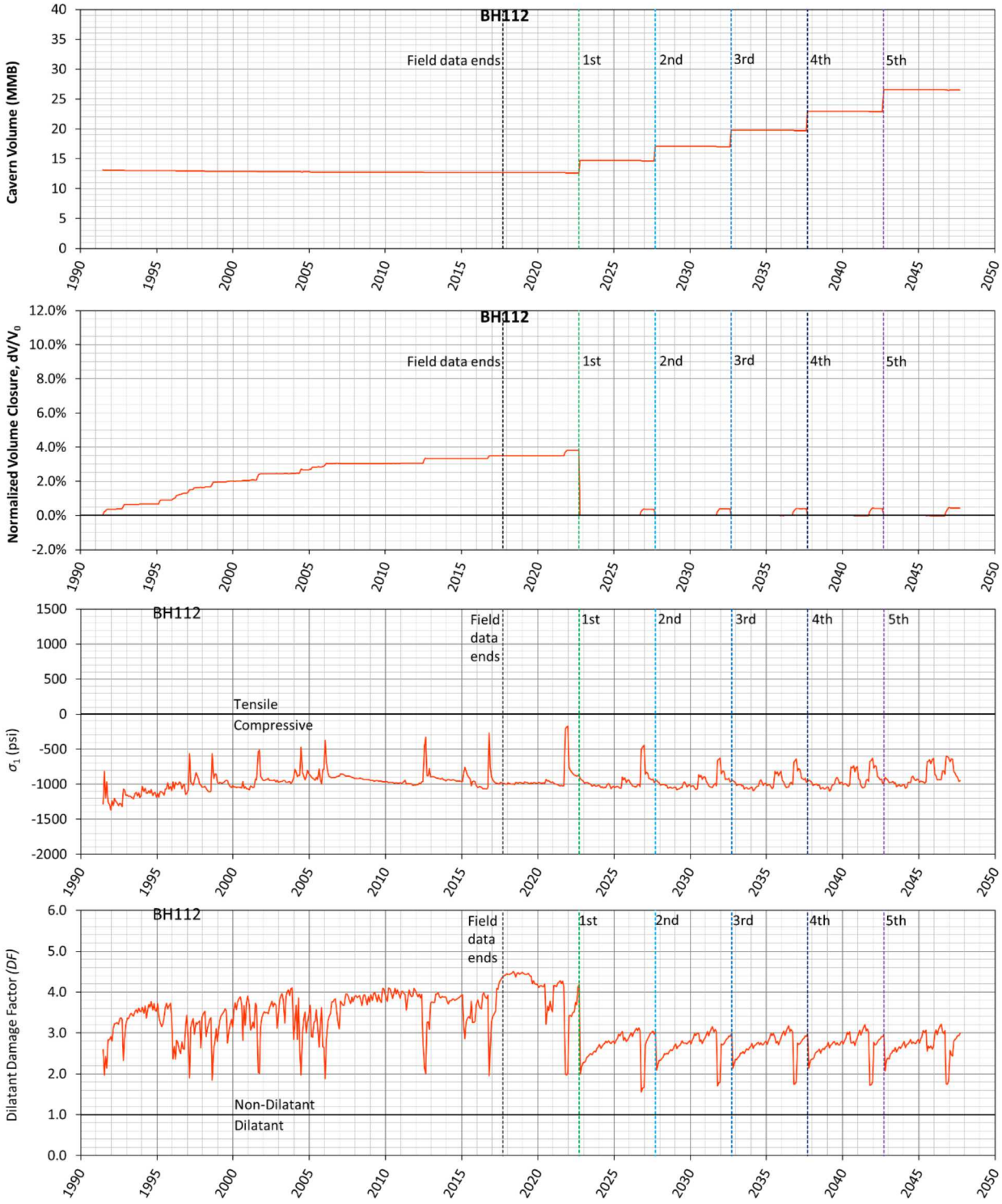

Figure 40. Predicted volumetric change (top), volumetric closure normalized to initial cavern volume of BH-112 (2nd), maximum σ_1 (3rd) and minimum dilatant damage factor (bottom) in the salt surrounding BH-112 over time

4.13. BH-113

Modeling of the leaching process of the caverns is performed by deleting a pre-meshed block of elements along the walls of the cavern so that the cavern volume is increased by 16 percent per drawdown. Figure 41 shows the cavity of BH-113 as developed from sonar data, along with drawdown skins and extra skins. In this simulation, BH-113 is modeled as having five drawdown layers to be removed to account for the future oil drawdown activities.

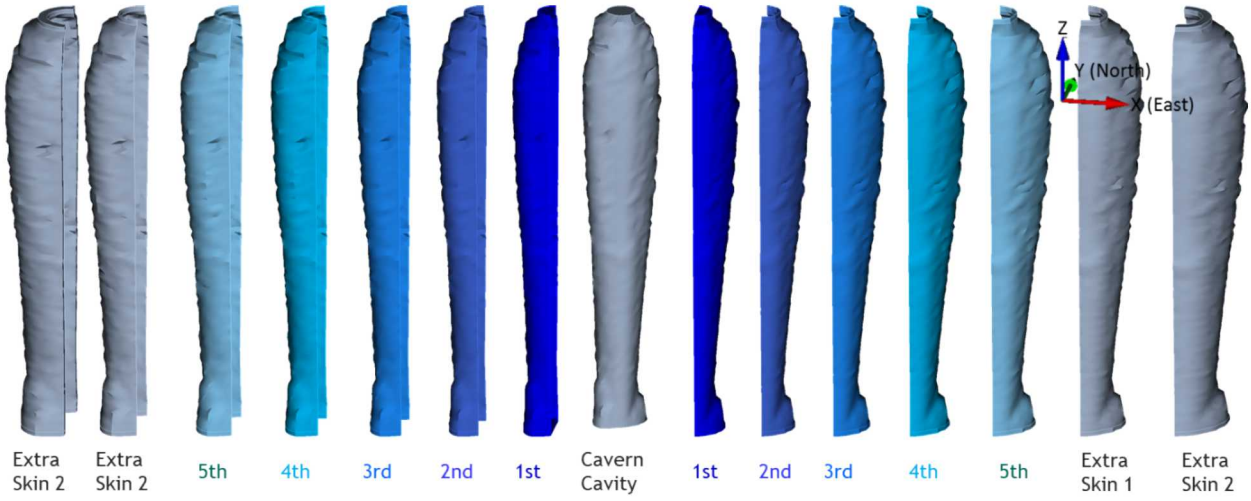

Figure 41. BH-113 cavern cavity with five drawdown skins (leaching layers) and extra skins

Figure 42 shows the predicted volumetric change (top), and volumetric closure normalized to initial cavern volume (2nd panel), maximum σ_1 (3rd panel), and minimum *DF* (bottom) in the salt volume surrounding BH-113 over time. The initial cavern cavity volume was 13.1 MMB on 5/21/1991 and is predicted to be 12.0 MMB on 9/19/2022. The cavern volume is predicted to decrease by 8.1% over 31 years (5/21/1991 - 9/19/2022).

The maximum σ_1 never reaches a positive (tensile stress state) value through five drawdowns, and the minimum *DF* either never reaches to be less than 1 during every workover until the end of simulation. The largest predicted value of the maximum σ_1 is -522 psi on 6/22/2015 during the workover started on 2/10/2015 for 173 days. The smallest predicted value of the minimum *DF* is 2.51 on 2/20/2015 during the workover started on 2/10/2015 for 173 days.

In conclusion, BH-113 is predicted to be structurally stable through the fifth drawdown leach.

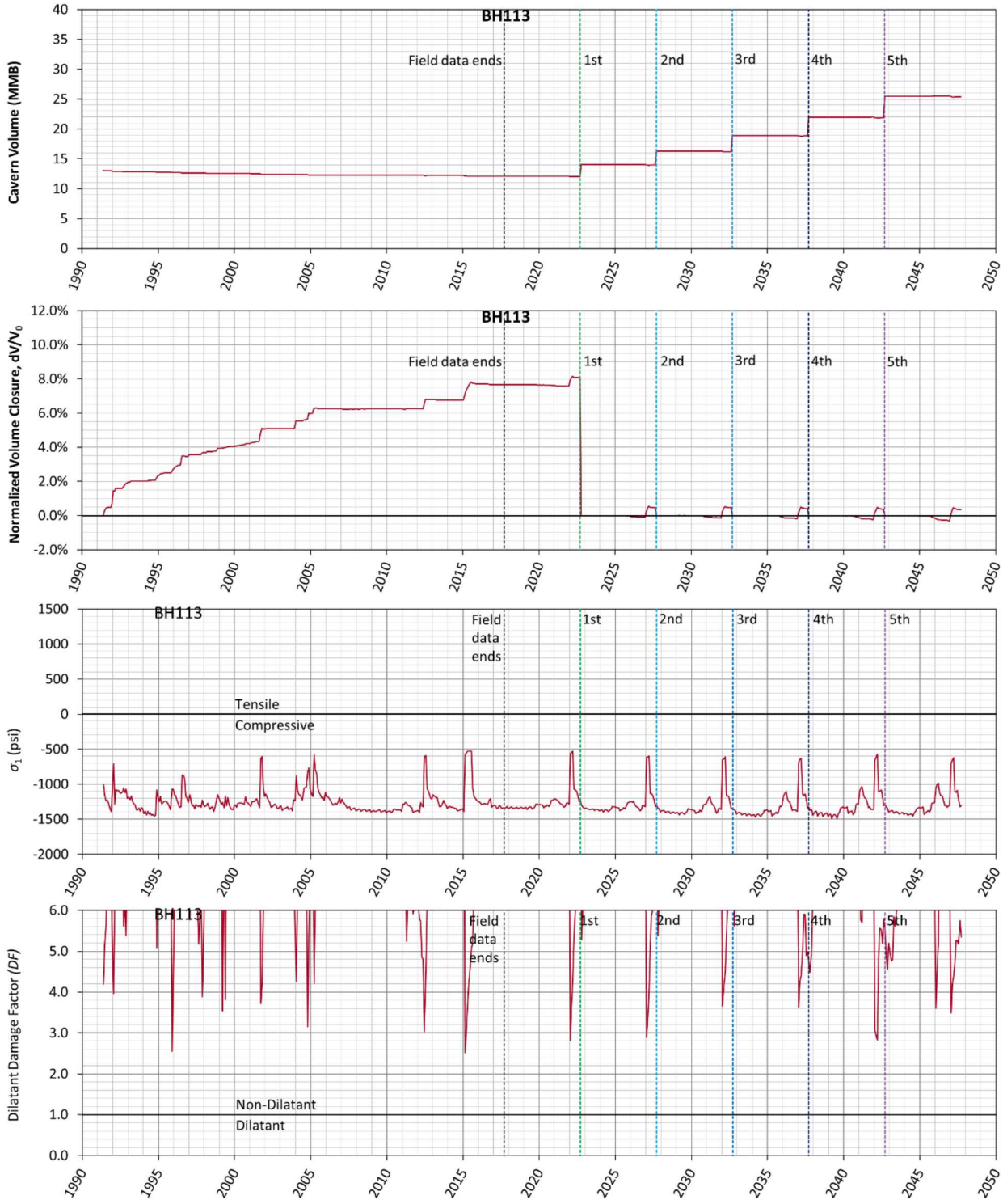

Figure 42. Predicted volumetric change (top), volumetric closure normalized to initial cavern volume of BH-113 (2nd), maximum σ_1 (3rd) and minimum dilatant damage factor (bottom) in the salt surrounding BH-113 over time

4.14. BH-114

Modeling of the leaching process of the caverns is performed by deleting a pre-meshed block of elements along the walls of the cavern so that the cavern volume is increased by 16 percent per drawdown. Figure 43 shows the cavity of BH-114 as developed from sonar data, along with drawdown skins and extra skins. In this simulation, BH-114 is modeled as having five drawdown layers to be removed to account for the future oil drawdown activities.

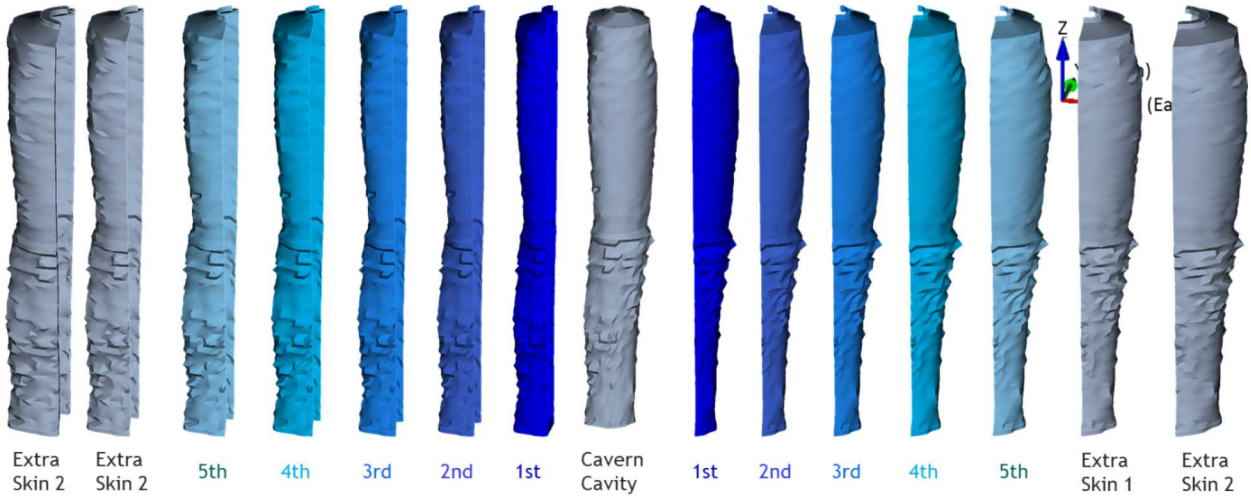

Figure 43. BH-114 cavern cavity with five drawdown skins (leaching layers) and extra skins

Figure 44 shows the predicted volumetric change (top), and volumetric closure normalized to initial cavern volume (2nd panel), maximum σ_1 (3rd panel), and minimum *DF* (bottom) in the salt volume surrounding BH-114 over time. The initial cavern cavity volume was 13.5 MMB on 8/20/1991 and is predicted to be 12.5 MMB on 9/19/2022. The cavern volume is predicted to decrease by 7.1% over 31 years (8/20/1991 - 9/19/2022).

The maximum σ_1 never reaches a positive (tensile stress state) value through five drawdowns, and the minimum *DF* either never reaches to be less than 1 during every workover until the end of simulation. The largest predicted value of the maximum σ_1 is -158 psi on 4/20/2013 during a series of workovers started on 9/8/2012 for 224 days. The smallest predicted value of the minimum *DF* is 1.62 on the same day of predicting the largest value of the maximum σ_1.

In conclusion, BH-114 is predicted to be structurally stable through the fifth drawdown leach.

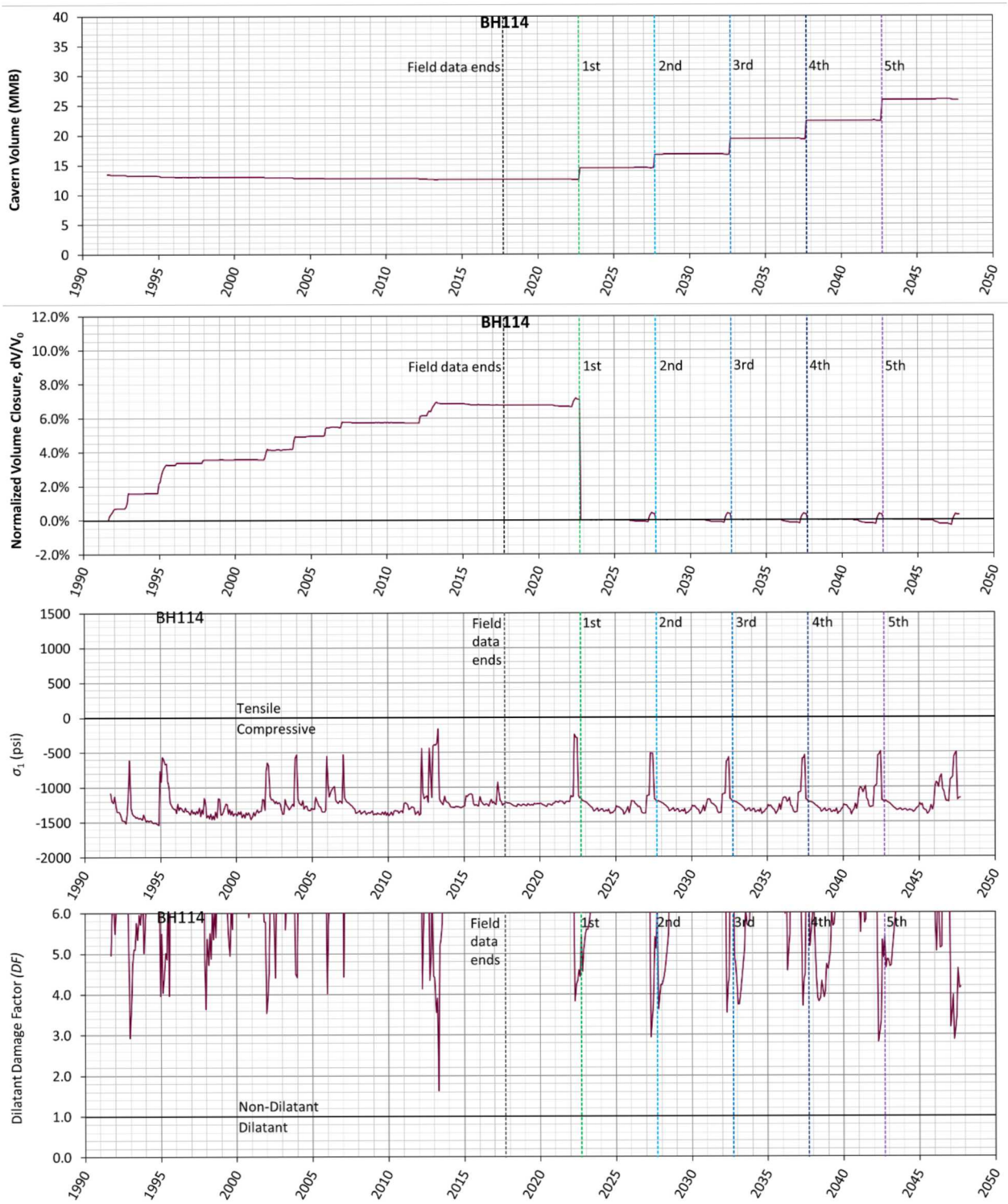

Figure 44. Predicted volumetric change (top), volumetric closure normalized to initial cavern volume of BH-114 (2nd), maximum σ_1 (3rd) and minimum dilatant damage factor (bottom) in the salt surrounding BH-114 over time

5. CONCLUSIONS - AVAILABLE DRAWDOWNS

The estimates for the baseline available drawdowns for each of the Big Hill caverns have been updated based on the recently upgraded Big Hill geomechanical model [Park, 2017a]. The new estimates for Big Hill are summarized in Table 2. All caverns are predicted to have five baseline available drawdowns remaining from a geomechanical perspective. The values for the baseline available drawdowns for the Big Hill caverns presented here were not completed in time to be implemented in the 2019 annual report on the number of available drawdowns for each SPR cavern [Sobolik et al., 2019]; however, they will be included in the next annual report. In those annual reports, the number of available drawdowns for a particular cavern is defined by the difference between number of baseline available drawdowns for a cavern based on geomechanics and cavern geometry (such as presented in Table 2), and the number of drawdowns spent due to the cumulative volume of raw water injections into that cavern.

BC-101, 105, and 110 have a region of concern at the floor edge and/or on the sloping floor, where tensile and dilatant stresses are predicted to occur during each workover. The tensile state is predicted to occur because of the geometries of the edge and floor. Therefore, geomechanical examination for three caverns would be recommended after a drawdown leach.

The well integrity of each cavern is not investigated in this report. The structural integrity of caverns is examined at this time. The number of available drawdowns in Table 2 is not the final. The numbers will be updated after the examination of the well integrity is completed through the upgraded BH geomechanical model next fiscal year.

Table 2. 2019 Updated number of available drawdowns – Big Hill

Cavern	Basis in 2014				Updated Geomechanics in 2019	Remarks
	2D P/D < 1	3D P/D < 1	Geomechanics	Best Estimate		
BH-101	3	3	5	3	5	Re-examine after a drawdown
BH-102	4	4	5	4	5	
BH-103	2	4	5	4	5	
BH-104	3	3	5	3	5	
BH-105	4	4	5	4	5	Re-examine after a drawdown
BH-106	4	4	5	4	5	
BH-107	3	4	5	4	5	
BH-108	2	5	5	5	5	
BH-109	4	5	5	5	5	
BH-110	4	5	5	5	5	Re-examine after a drawdown
BH-111	3	4	5	4	5	
BH-112	3	3	5	3	5	
BH-113	3	3	5	3	5	
BH-114	3	5	5	5	5	

This page left blank

REFERENCES

Lee, M.Y., Ehgartner, B.L., and Bronowski, D.R. (2004) *Laboratory Evaluation of Damage Criteria and Permeability of Big Hill Salt*, SAND2004-6004, Sandia National Laboratories, Albuquerque, NM 87185.

Park, B.Y., B.L. Ehgartner, M.Y. Lee, and S.R. Sobolik (2005) *Three Dimensional Simulation for Big Hill Strategic Petroleum Reserve (SPR)*, SAND2005-3216, Sandia National Laboratories, Albuquerque, NM.

Park, B.Y. and B.L. Ehgartner (2011) *Allowable Pillar to Diameter Ratio for Strategic Petroleum Reserve Caverns*. Unlimited Release SAND2011-2896, Sandia National Laboratories, Albuquerque, NM 87185. U.S. Strategic Petroleum Reserve.

Park, B.Y. (2017a) *Geomechanical Simulation of Big Hill Strategic Petroleum Reserve – Model Calibration*, SAND2018-13783, Sandia National Laboratories, Albuquerque, New Mexico.

Park, B.Y. (2017b) Assessment of the Available Drawdowns for Oil Storage Caverns at the Bayou Choctaw SPR Site, Unlimited Release SAND2017-12757, Sandia National Laboratories, Albuquerque, NM.

Rudeen, D.K. and D.L. Lord (2013) *SPR Cavern Pillar-to-Diameter 2013 Update*, Letter Report to Gilbert Shank, DOE PMO dated October 1, 2013. Geotechnology & Engineering, Sandia National Laboratories. U.S. Strategic Petroleum Reserve.

Sobolik S.R., B.Y. Park, D.L. Lord, B. Roberts, and D.K. Rudeeen (2014) *Current Recommendations Regarding ECP PM-00449, Baseline Remaining Drawdowns for all SPR Caverns*. FY14 Sandia Geotechnical Support for U.S. Strategic Petroleum Reserve, Letter Report to Lisa Nicholson dated May 9, 2014., Sandia National Laboratories, Albuquerque, NM.

Sobolik, S.R. (2016) *Assessment of the Available Drawdowns for Oil Storage Caverns at the West Hackberry SPR Site*. Unlimited Release SAND2016-3077, Sandia National Laboratories, Albuquerque, NM 87185.

Sobolik, S.R., D. Hart, B.Y. Park, and K. Chojnicki (2018) *Proposed Methodology for Assessing Available Drawdowns for Each Oil Storage Cavern in the Strategic Petroleum Reserve*, Unlimited Release SAND2018-4518, Sandia National Laboratories, Albuquerque, NM 87185.

Sobolik, S.R., D. Hart, K. Chojnicki, and B.Y. Park (2019) *2019 Annual Report of Available Drawdowns for Each Oil Storage Cavern in the Strategic Petroleum Reserve*, Unlimited Release SAND2019-3673, Sandia National Laboratories, Albuquerque, NM 87185.

This page left blank

DISTRIBUTION

Hardcopy—Internal

Number of Copies	Name	Org.	Mailstop
5	Carolyn L. Kirby	8862	MS0750
10	Byoung Y. Park	8862	MS0751

Email—External (encrypt for OUO)

Name	Company Email Address	Company Name
Wayne Elias	wayne.elias@hq.doe.gov	U.S. Department of Energy Office of Fossil Energy Washington, DC
Diane Willard	diane.willard@spr.doe.gov	U.S. Department of Energy SPR Project Management Office New Orleans, LA

Email—Internal

Name	Org.	Sandia Email Address
Erik K. Webb	8860	ekwebb@sandia.gov
Kirsten Chojnicki	8862	kchojni@sandia.gov
Donald M. Conley	8862	dconley@sandia.gov
Dylan Michael Moriarty	8862	dmmoria@sandia.gov
Anna C. Snider Lord	8862	acsnide@sandia.gov
Barry L. Roberts	8862	blrober@sandia.gov
Steven R. Sobolik	8862	srsobol@sandia.gov
David Hart	8865	dbhart@sandia.gov
David Lord	8865	dllord@sandia.gov
Giorgia Bettin	8866	gbettin@sandia.gov
Technical Library	01177	libref@sandia.gov

This page left blank

Sandia National Laboratories is a multimission laboratory managed and operated by National Technology & Engineering Solutions of Sandia LLC, a wholly owned subsidiary of Honeywell International Inc. for the U.S. Department of Energy's National Nuclear Security Administration under contract DE-NA0003525.